Universidade de Aveiro Departamento de Química

2018

Diogo Tavares

Antão Folhas Ferreira

Amostragem e caraterização estrutural de matéria orgânica natural de lagos de termocarso

Sampling and structural characterization of natural organic matter of thermokarst lakes

Dissertação apresentada à Universidade de Aveiro para cumprimento dos requisitos necessários à obtenção do grau de Mestre em Química, realizada sob a orientação científica do Doutor Armando da Costa Duarte, Professor Catedrático do Departamento de Química da Universidade de Aveiro, Professor João Alfredo Vieira Canário (Co-orientador) do Departamento de Engenharia Química do Instituto Superior Técnico, e Professor Warwick F. Vincent do Departamento de Biologia da Universidade Laval, Canadá.

Aos meus pais e irmão.

O Júri:

Presidente **Prof. Helena Isabel Seguro Nogueira**

Professora Auxiliar do Departamento de Química da Universidade de Aveiro

Drª. Alexandra Maria Moita Antunes

Investigadora Principal do Centro de Química Estrutural do Instituto Superior Técnico

Prof. Armando da Costa Duarte

Professor Catedrático do Departamento de Química da Universidade de Aveiro

Agradecimentos: A realização desta dissertação não teria sido possível sem a colaboração e ajuda de diversas pessoas, às quais estou profundamente grato, nomeadamente:

Ao meu orientador, Professor Armando da Costa Duarte, e Doutora Regina Maria Brandão de Oliveira Duarte, pela disponibilidade, paciência, ajuda e compreensão demonstrada ao longo da realização desta dissertação.

Aos meus co-orientadores, Professor João Canário e Professor Warwick Vincent, pelo tempo que disponibilizaram para me ajudar,bem como ao Dr. Martin Pilote, sem o qual este trabalho não teria sido possível. Ao Professor Gonçalo Vieira do Instituto de Geografia e Ordenamento de Território, pela ajuda prestada durante a realização deste trabalho.

À Fundação para a Ciência e Tecnologia, através do PROPOLAR por me fornecer apoio financeiro pelo projeto PERMACHEM II, permitindo a minha participação no trabalho de campo no subártico canadiano, bem como ao Centre d'Études Nordiques (Universidade Laval) e ao Environment and Climate Change Canada por fornecer e assegurar toda a logística necessária para a execução do trabalho de campo.

À minha família, que me deu apoio incondicional durante toda esta jornada, nos bons e nos maus momentos. Aos meus amigos e colegas, que sempre me ajudaram e apoiaram ao longo deste ano.

A todas as pessoas que direta ou indiretamente possibilitaram a realização desta dissertação.

Muito Obrigado

Palavras-Chave: Matéria orgânica natural; matéria orgânica dissolvida; lagos de termocarso; permafrost; caracterização estrutural; regiões subárcticas

Resumo:

Lagos de termocarso, resultantes da degradação do permafrost, estão dispersos nas regiões árticas e subárticas, tendo revelado uma crescente contribuição para o ciclo global de carbono ao longo dos últimos 40 anos. O degelo do permafrost resulta na libertação de grandes quantidades de matéria orgânica natural (NOM) para sistemas aquáticos, estando também associado a fenómenos de metanogénese e à consequente libertação de metano para a atmosfera. Matéria orgânica dissolvida (DOM) é uma mistura altamente complexa, estando presente em todos os sistemas naturais aquáticos, apresentando uma composição variável consoante a origem. A pesquisa apresentada neste trabalho tem como objetivo fornecer novas informações relativamente à caracterização estrutural de DOM proveniente de lagos de termocarso em regiões subárticas. Para tal, técnicas de caracterização como espectroscopia de fluorescência, espectroscopia de infravermelho por transformada de Fourier (FTIR), espectroscopia de ressonância magnética nuclear (NMR) e análise elementar (CNHS) foram utilizadas.

As amostras de águas foram recolhidas a diferentes profundidades em três lagos diferentes (SAS-1A, SAS-1B e SAS-2A) no vale Sasapimakwananisikw (SAS), perto da comunidade de Kuujjuarapik-Whapmagoostui (Nunavik, Canadá). Os lagos SAS-1A e SAS-1B estão localizados na margem sul do rio SAS, estando associados à mesma palsa (embora a distâncias diferentes), enquanto que o lago SAS-2A está localizado na margem norte do rio SAS.

As amostras de águas foram filtradas, acidificadas, submetidas a um processo de fixação da matéria orgânica e caracterizadas de modo a

tentar obter o máximo de informação estrutural. A extrema complexidade das amostras dificultou a obtenção de informação estrutural relativamente às amostras, no entanto, foi possível verificar diferenças entre amostras a diferentes profundidades e de diferentes lagos.

Todas as amostras tenham revelado uma forte componente terrestre, com SAS-1B a demonstrar possivelmente o maior grau de humificação. Os dados de fluorescência pareceram indicar a presença de DOM recente na superfície do lago SAS-1A (ao contrário dos restantes lagos), sugerindo uma nova fonte de matéria orgânica na superfície do lago. Contrariamente ao esperado, o lago SAS-1B, embora mais próximo geograficamente do lago SAS-1A, revelou maiores semelhanças com a composição do lago SAS-2A (com base nos dados de FTIR, RMN e espectroscopia de fluorescência).

Atualmente, verifica-se uma falta de estudos relativamente à caracterização estrutural de DOM proveniente de lagos de termocarso. Assim sendo, os resultados apresentados nesta dissertação fornecem o primeiro passo para uma caracterização mais aprofundada de DOM de lagos de termocarso, com o objectivo de melhor compreender a biogeoquímica destes sistemas.

Keywords: Natural organic matter; Dissolved organic matter; Thermokarst lakes; Thaw lakes; Permafrost; Structural characterization; Subarctic regions

Abstract:

Thermokarst lakes, a result of the thawing of ice-rich permafrost, are widespread in subarctic and Arctic regions, displaying over the last decades a continuously higher contribution to the global carbon cycle. Thawing of permafrost not only enables the delivery of considerable amounts of natural organic matter (NOM) to aquatic systems, but is also linked to methanogenesis of organic matter, resulting in substantial releases of methane (CH_4) into the atmosphere. Higher concentrations of NOM also impact geochemical processes and speciation of trace metal in aquatic ecosystems, including the methylation of mercury, a highly toxic species. Dissolved organic matter (DOM) is a highly complex mixture of chemical species present in all natural aquatic systems, with a widely variable composition depending on its source. This research aimed to provide insight into the structural characterization of DOM from thermokarst lakes in the subarctic region. Several analytical techniques were applied, including fluorescence spectroscopy, Fourier-transform infrared spectroscopy (FTIR), nuclear magnetic resonance spectroscopy (NMR), and elemental analysis (CNHS).

Samples were collected at different depths from three different thermokarst lakes (SAS-1A, SAS-1B and SAS-2A) in the Sasapimakwananisikw (SAS) river valley near the community of Kuujjuarapik / Whapmagoostui (Nunavik, Canada). Thaw lakes, SAS-1A and SAS-1B, are located south of the SAS river and associated with the same palsa zone (with different proximities), and thaw lake SAS-2A, is located north of the SAS river. Thereafter, water

samples were filtered, extracted and characterized to obtain structural information.

All of the samples displayed a high level of complexity in molecular composition, which limited the extent of deep structural characterization, and precluded a clear separation of NOM components. Nevertheless, there was pronounced variation in NOM structure among sites, and significant differences were detected among the different thaw lakes and depths.

All of the DOM samples displayed a terrestrial derived origin, however lake SAS-1B had a particularly low hydrogen to carbon (H:C) ratio. The fluorescence data obtained from the excitation-emission matrices suggested a significant presence of “fresh” DOM at the surface of lake SAS-1A, contrary to the other samples, suggesting an input of recently fixed carbon, for example from the emergent aquatic macrophytes that surround the lake. Contrary to expectation, the SAS-1B sample appeared to display closer similarities to SAS-2A, clearly noticeable in both fluorescence EEMs and FTIR spectra, despite being geographically located near lake SAS-1A; neither of these samples showed a conspicuous “fresh” carbon content

Since there is currently very limited research on the organic composition of thermokarst lakes, these results provide an important first step in DOM characterization, in order to better understand the biogeochemistry of these waters. Structural DOM characterization will also contribute towards models of greenhouse gas production and metal dynamics in subarctic aquatic ecosystems.

Table of contents

List of Figures

List of Tables

List of Abbreviations

β:α – Freshness Index

ATR – Attenuated total reflectance

BIX – Biological index

CP – Cross-polarization

COSY - Two dimensional correlation spectroscopy

CRAM - Carboxyl-rich alicyclic molecules

DOC – Dissolved organic carbon

DOM – Dissolved organic matter

EEMs – Excitation-emission matrices

FA – Fulvic acids

FI – Fluorescence index

FT-ICR-MS – Fourier-transform ion cyclotron resonance mass spectrometer

FTIR – Fourier-transform infrared spectroscopy

GC – Gas chromatography

GHG – Greenhouse gases

HA – Humic acids

HETCOR - Heteronuclear shift correlation

HI – Humification indices

HIX – Humification Index

HS – Humic substances

HMQC – Heteronuclear multiple quantum correlation

HSQC – Heteronuclear single quantum correlation

NMR – Nuclear magnetic resonance

NOM – Natural organic matter

MAS – Magic angle spinning

SAS – Sasapimakwananisikw

S/N – Signal-to-noise

SRFA – Suwannee river fulvic acid

SRHA – Suwannee river humic acid

SOM – Soil organic matter

SUVA – Specific Ultraviolet Absorbance

TOC – Total organic carbon

TOCSY - Two dimensional total correlation

UV - Ultraviolet

1

Objective and Structure of Dissertation

1.1 Introduction and motivation for natural organic matter research

Natural organic matter (NOM) originates from the decay of organisms, generally accumulating in soils, sediments and aquatic systems, and therefore playing a key role in various of environmental processes (Hatcher 2004). It should be noted that the majority of the constituents in NOM have undergone biotic and abiotic reactions, producing an immensely diverse pool of structures (Hertkorn et al. 2007).

It is estimated that the organic carbon in soil organic matter (SOM) in northern circumpolar permafrost regions accounts for approximately half of the global belowground organic carbon pool (Tarnocai et al. 2009). The increasingly rising temperatures in arctic and subarctic regions, have triggered the thawing of ice-rich permafrost, resulting in the formation of permafrost thaw lakes, also known as thermokarst lakes. Thermokarst lakes are widespread in these regions and have had a considerably growing contribution for to the global carbon cycle for the last four decades; as permafrost thaws, sizeable quantities of NOM are transported to these aquatic systems.

The degradation of previously frozen NOM into methane (CH_4) and carbon dioxide (CO_2) in these thermokarst lakes, and its subsequent release into the atmosphere poses a significant environmental problem (Matveev et al. 2016). Obtaining structural information regarding the existing NOM samples in these lakes, may provide greater insight regarding the thermokarst environment, thus allowing for a better understanding of its processes.

1.2 Aim of this work

Considering the growing tendency for the formation of thermokarst lake in subarctic regions as a result of rising temperatures, and the small amount of information on the structural characterization of NOM in thermokarst environments, structural characterization of NOM from permafrost thaw lakes presents itself as a crucial aspect to better understand these thermokarst systems and also to predict their capacity to contribute to the greenhouse gases (GHG) release. Nevertheless, NOM is one of the most complex mixtures in existence, posing

considerable analytical challenges not only in its structural characterization, but also to the understanding of the myriad of processes NOM undergoes. Thus, the first objective was to review NOM characterization studies and identify the limitations associated with the study of these highly complex mixtures.

An additional objective in this study was to assess differences in NOM among lake sites and depths. This would allow for a better understanding of NOM distribution in these lakes, assess its origin, and obtain further insight into how the different environments affect the NOM content in the different lakes.

1.3 Structure of dissertation

This dissertation is divided into five chapters, beginning with a general description of the thesis, highlighting the general importance of this subject and clearly stating the main objectives of the research work, as well as my personal motivations (Chapter 1). The second chapter provides an introduction to permafrost regions, thermokarst lakes and NOM, also reviewing a wide range of analytical characterization techniques. Chapter 3 focuses on the specific study area, reporting accurately the employed sampling processes and the measured physicochemical parameters in each of the sampled thermokarst lakes. In Chapter 4, the analytical procedures are summarized and described during the DOM treatment, including the filtration of the water samples, their dissolved organic carbon (DOC) quantification, and the employed solid-phase extraction method; this chapter also exhibits the obtained results from the characterization of DOM from the collected water samples, establishing comparisons between samples from different lakes and depths. Finally, Chapter 5 displays the main conclusions resulting from this study and provides suggestions for future work.

2

Introduction

2.1 Permafrost Regions and Thermokarst Lakes

2.1.1 Permafrost regions: general characteristics and importance

Permafrost, also referred to as perennially frozen ground, consists in gravel, soil, and sand, bound together by ice that remains at least two years at a temperature equal to or below 0ºC, underlying up to a quarter of the Northern Hemisphere's landmass (Brown et al. 1998) and approximately 50% of Canada's land area (French et al. 1988). Based on the percentage of permafrost underlying a landmass, four different zones have been defined: continuous (90–100%), discontinuous (50–90%), sporadic (10–50%) and isolated (<10%) (Vonk et al. 2015). The area of continuous permafrost extends northward of 58ºN, whereas the area of discontinuous permafrost occurs between latitude 56º and 58ºN. Sporadic permafrost is primarily associated with peatlands as a result of the thermal offset associated with peat's thermal properties (it cools easily when frozen during winter and acts as a good insulator preventing its warming in summer) (Burn & Smith 1988).

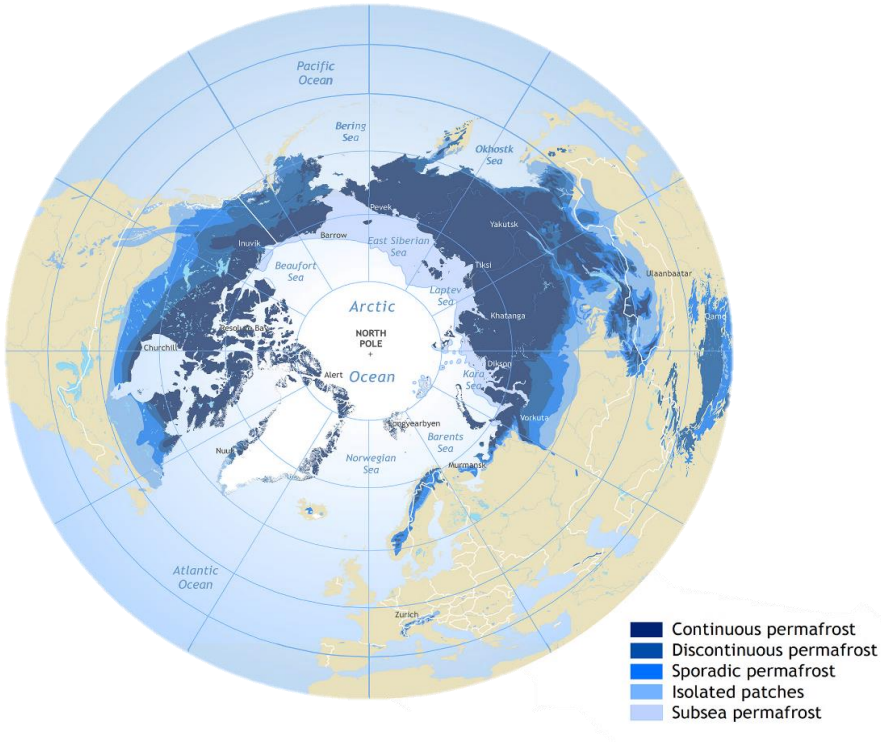

Figure 1 – Scheme portraying the global permafrost distribution map in the north hemisphere – reproduced from (Brown, J., O.J. Ferrians, Jr., J.A. Heginbottom 1997).

A global permafrost distribution map is shown in Figure 1, highlighting the greater areal extent of permafrost at higher latitudes. In permafrost regions, the ground is mainly characterized by two layers: the active layer and the underlying permafrost layer. The active layer, ranging from a few centimeters to 2 meters (in continuous permafrost zones), thaws during summer and refreezes during autumn. Increased snowfall and increased air temperatures cause the active layer thickness to increase (Zhang 2005). Permafrost contains between 1140 and 1476 Pg (1 Pg = 10^{15} g) of soil organic carbon (Hugelius et al. 2014).

Thawing of permafrost exposes organic matter, that in some cases was biogeochemical unavailable for thousands of years, to a oxidation process to CO_2 in aerobic conditions via microbial decomposition, resulting in a gas flux of CO_2 into the atmosphere (Walter et al. 2007). However, anaerobic conditions prompt methanogenesis of organic matter into CH_4, a greenhouse gas (GHG) (Zimov 1997). The flux of these gases into the atmosphere, enhancing the GHG effect, ultimately increases the air temperature, promoting even further permafrost degradation. In this vicious cycle, the thawing of permafrost has a positive feedback in climate warming (Schuur et al. 2008). The temperature rise affects the permafrost-carbon cycle by increasing the thickness of the active layer, thus prompting the increase of soil carbon stock in the seasonal cycle, and by causing a shift in the balance of the CO_2 consumed by Arctic vegetation and the released CO_2 and CH_4 (Streletskiy et al. 2015). In recent decades, there has been an increase in permafrost ground temperature (Romanovsky et al. 2010) due to the surface warming of the Arctic regions. The thawing of ice-rich permafrost enables the transport of organic matter and minerals into aquatic systems, thus producing a variety of landscape features by three main processes (Kokelj & Jorgenson 2013): 1) hillslope processes; 2) wetland processes; and, 3) thermokarst lake processes. Hillslope processes can cause thermoerosional features and their scale depends on the nature of the landscape. However, the transport of sediments, organic matter, and nutrients into aquatic ecosystems may be very large, promoting the formation of such features in a matter of hours, and maintaining a slow growth over several years. Wetland processes involve the collapse of peatland and the formation of bogs and fens. Thermokarst lake processes, associated with lake and pond formation, expansion and drainage, are not only the most recognizable, but also the most common form of thermokarst (Kokelj & Jorgenson 2013). Thermokarst lakes usually form in high latitude environments, at sub-zero temperatures during winters that can last for over 8 months, and short summers with temperatures well

above 10ºC, common in the subarctic landscapes of Canada, Alaska, and Siberia (Vonk et al. 2015).

2.1.2 Thermokarst Lakes: formation and general characteristics

Depending on the two types of thawing that occur, different rates of relocation can be expected: a) thaw of ice-rich permafrost, also known as thermokarst (Van Everdingen 2005), and b) thaw of permafrost with a low ground-ice content. In the circumpolar Arctic region, the total area of thermokarst lakes is estimated to exceed 200 000 km^2 (Grosse et al. 2011).

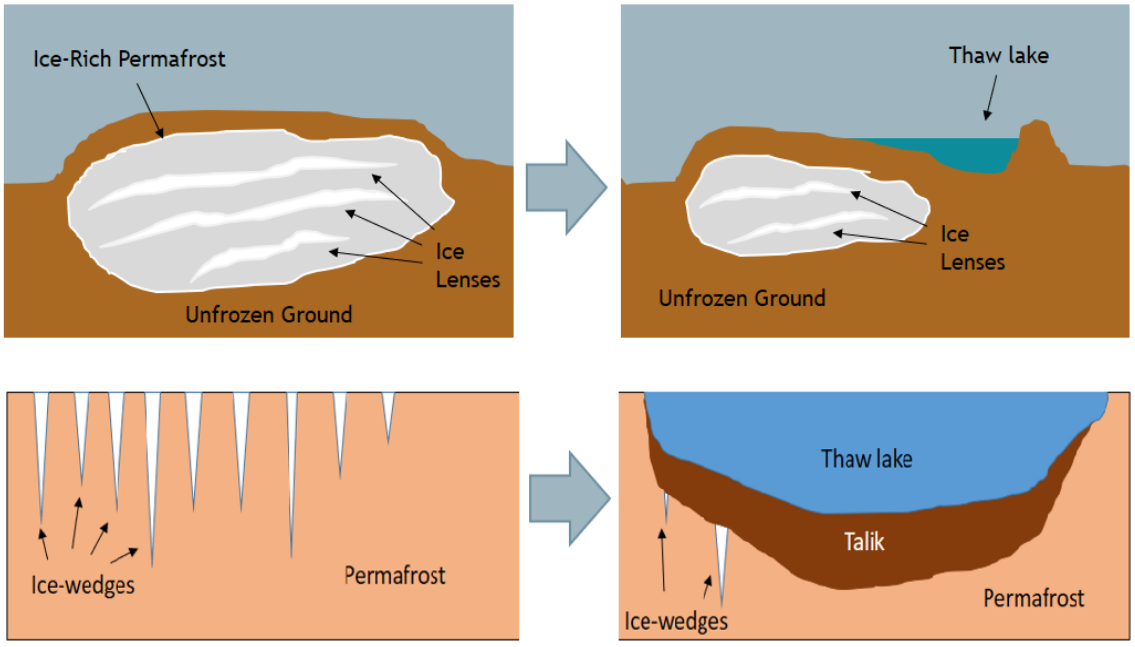

Figure 2a (top) – Scheme of the formation of thaw lakes from the thawing permafrost in a palsa, common in discontinuous permafrost regions. Figure 2b (bottom) - Scheme showing the formation of thaw lakes from melting ice wedges, common in continuous permafrost regions. – adapted from (Bouchard et al. 2016)

The formation of thermokarst lakes is associated with the coalescence of ice-wedges, either through ponds above the melting ice wedge (Figure 2b), or through a surface subsidence of ice-rich ground, resulting in a water impoundment in a growing and coalescing pond (Figure 2a), whose expansion is a result of mechanical and thermal erosion over decades and even centuries (Czudek & Demek 1970). There is also a formation of a thaw bulb, or talik beneath the lake, displaying temperatures equal or above 0ºC (Burn 2002). This thawing displays a more abrupt tendency, manifesting as a pulse disturbance, opposite to the thaw of permafrost

with a lower ground-ice content, which is gradual and manifests itself as a press disturbance (Vonk et al. 2015).

During the summer, the heat energy from the atmosphere is dissipated in the water column and transferred in part to the sediments of the talik and to the permafrost. However, in autumn the lake temperature rapidly decreases from the surface to the bottom, whilst the talik sediments still retain the summer warmth, thus warming the water in the upper zone of the talik (Ling & Zhang 2003). During winter, thermokarst lakes release heat into the atmosphere, whilst maintaining the talik heat transfer into permafrost (Jeffries et al. 1999). These heat fluxes directly affect the permafrost, causing a year-round expansion of the thawed zone; this lateral expansion and the increase in thawing of permafrost, ultimately lead to the drainage of these lakes.

2.2 Analytical approaches to structural characterization of natural organic matter

2.2.1 Introduction to natural organic matter

It is generally considered that natural organic matter (NOM) is a heterogeneous complex mixture of chemical species with different molecular weights, reactivity, and solubility, displaying different optical properties and a widely variable composition depending on its source. The majority of the constituents comprising NOM are transformed via biotic and abiotic processes, ultimately leading to a highly diverse pool of molecular structures (Hertkorn et al. 2007). A number of competing views have different proposed theories to explain NOM formation. Some researchers propose that condensation polymerization of degraded biomolecules leads to these large macromolecular structures (Hatcher 2004), while another view is that the uncharacterized fraction of NOM is a product of the preservation of the most inaccessible and the most structurally robust materials from living organisms, with the remaining biomolecules, labile organic matter, subject to rapid degradation (Hatcher 2004; Hedges et al. 2000).

NOM can be divided into two major fractions: dissolved organic matter (DOM) and non-dissolved organic matter. By definition, DOM is the fraction of organic matter that passes through a filter of 0.45μm pore size, while the retained fraction is defined as particulate organic matter (POM). The distinction between these fractions is vital when analyzing the optical properties of a given sample, considering that some analytical techniques, such as fluorescence spectroscopy, are highly sensitive to suspended particulate matter. In order to obtain reliable optical data, the sample must be filtered through an appropriate filter membrane.

DOM is pervasive throughout all aquatic ecosystems and considered one of the most complex natural mixtures in existence, having proven itself significantly difficult to characterize at a molecular level. The complexity of DOM in natural waters gives rise to numerous analytical problems (Aiken & Leenheer 2006), highlighting the need to use

various analytical approaches in order to obtain relevant data pertaining to its reactivity, but also to its chemical composition. However, characterization techniques such as nuclear magnetic resonance (NMR) spectroscopy and Fourier-transform ion cyclotron resonance-mass spectrometry (FT-ICR-MS), have been cited as some of the most promising techniques to unravel the structural characteristics of DOM (Dittmar & Paeng 2009).

The extremely complex mixture of DOM contains mainly humic substances (HS) and lower amount of protein-like and polysaccharide-like component. The HS can be operationally divided into three major components: humic acids (HA), fulvic acids (FA), and humin. The HA are a complex mixture of acids with phenolic and carboxylic groups (Thurman 1985), behaving functionally mostly as a dibasic acid. Their pK for protonation of carboxyl groups is approximately 4, and approximately 8 for phenolic groups. The HA fraction, containing two or more groups prone to complexation, may enable the formation of chelate complexes (Tipping 1994), and they are capable of forming complexes with major ions, such as Ca^{2+}, Mg^{2+} and ferric ions, such as Fe^{2+}, and Fe^{3+}, usually present in aquatic environments. The HA fractions of larger molecular size are more aliphatic in nature, while smaller size molecules are more aromatic, displaying a higher content in carboxyl groups (Shin et al. 1999). The FA fraction, although similar to HA in terms of the major functional group composition, display differences in acidity, degree of polymerization, color, and both carbon and oxygen content (Thurman 1985). Their average molecular weight is relatively low when compared to HA. Both HA and FA contain aromatic and aliphatic components rich in phenolic, carboxylic, alcoholic, hydroxyl, and keto functional groups (Thurman 1985) . The differences in NOM matrix effects from various aquatic environments, cause the characteristics of both FA and HA to be very source dependent, prompting a “FA-like” and “HA-like” denomination.

Wetland or peat humic matter is formed in wet ecosystems, accumulating in deposits of peat, mucks, and bogs. These types of HS are mainly composed of FA and HA, with the latter increasing from peat to muck, and possibly humin (in considerable amounts). It is not yet clear whether there is variation of properties of humic substance from different types of peat (Tan 2003).

2.2.2 Introduction to elemental analysis of dissolved organic matter

Information about the total carbon, hydrogen, nitrogen and sulphur content in organic matter can be obtained using CHNS elemental analysis. This method displays applicability both in solid and liquid samples. In a furnace at 1000ºC, carbon is converted to CO_2, hydrogen converted to water, nitrogen converted to nitrogen oxides and N_2, and sulphur to SO_2. A wide range of absorbents can be used to remove additional combustion products, resulting from the presence of other elements. The remaining combustion products are carried by an inert gas, such as helium, and passed through high purity copper (at 600ºC), removing the oxygen not consumed during the combustion process and converting any nitrogen oxide to N_2. Absorbent traps are then used to remove any other products, leaving only water, CO_2, N_2, and SO_2. The detection of these gases can be carried out by various methods, including: a gas-chromatography (GC) separation prior to thermal conductivity detection; a partial GC separation (frontal chromatography) prior to thermal conductivity detection (only CHN, excluding Sulphur); a set of separate infrared and thermal conductivity cells, in order to detect individual compounds. An accurate quantification of these elements requires a thorough calibration for each element under study, therefore high-purity micro-analytical standard compounds are used for this purpose.

The lack of information relative to elemental analysis of samples from thermokarst lakes undermines an optimal comparison with the obtained results from this project; therefore, three different types of samples were compiled and compared in Table 1. The elements presented in Table 1 are carbon (C), hydrogen (H), oxygen (O), nitrogen (N), chlorine (Cl) and sulphur (S). Table 1 contains elemental analysis results of Pony Lake (Antarctica) (McKnight et al. 1994), Toolik Lake (Alaska), Island Lake (Alaska) and Campsite Lake (Alaska) (Cory et al. 2007), as well as the Suwannee River (South Georgia) FA standard (Duarte et al. 2007).

The use of atomic elemental ratios allows to establish comparisons between samples and deduct information regarding the nature of the samples. Atomic ratio of hydrogen to carbon (H:C) is mainly associated with the percentage of saturation of carbon atoms; a higher atomic H:C ratio suggests a greater aliphatic content, with more than one hydrogen atom for each carbon atom. For example, a H:C ratio of 1:1 would indicate that there is one degree of

unsaturation, like a double bond between two carbon atoms, a carbon and oxygen/nitrogen atom, or associated with the formation of a cyclic structure. Therefore, a lower H:C ratio prompts the notion of a higher aromatic or carbonyl content.

A nitrogen to carbon atomic ratio (N:C) helps provide some valuable information regarding the possible origin of the DOM under study, as a higher N:C ratio is usually associated with DOM with microbially derived origin, as displayed in Table 1 in the case of Pony lake, while lower N:C ratios are typically associated with terrestrially derived DOM. It should also be noted that upon separating humic and FA from the original DOM sample, HA tend to display a higher atomic N:C ratio than FA (Thurman 1985).

Table 1 – Elemental analysis data of FA from water samples collected from lakes in polar regions (Antarctica ([a]) and Arctic ([b])) as well as FA from Suwanee River ([c]) (standard) – *a*: (McKnight et al. 1994); *b*: (Cory et al. 2007); *c*: (Duarte et al. 2007).

Sample	**C (%)**	**H (%)**	**O (%)**	**N (%)**	**Cl (%)**	**Ash Content (%)**	**N:C ratio**	**S (%)**	**H:C ratio**
Pony Lake (total) [a]	49.1	6.3	36.4	4.7	0.61	14.9	0.082	-	1.52
Pony Lake (dissolved) [a]	48.9	6.2	40.4	4.4	0.45	10.1	0.077	-	1.51
Toolik Lake [b]	53	5.2	41	0.89	-	-	0.015	0.44	1.18
Island Lake [b]	52	5.1	41	1.1	-	-	0.018	0.52	1.18
Campsite Lake [b]	53	5.3	40	1.1	-	-	0.018	0.46	1.2
Suwanee River Standard [c]	52.4	4.3	42.2	0.7		0.5	0.012	-	0.98

Upon comparing the data compiled in Table 1, arctic lakes seem to display a higher carbon and oxygen content, while Antarctic lakes showcase a higher percentage of hydrogen and nitrogen. Chlorine and sulphur contents are not compared, as information regarding their

content is not found for lakes of both environments. The N:C ratio appears to be significantly higher in Arctic lakes, as Pony lake's FA carbon content is associated with algal-derived FAs. Toolik, Island and Campsite lakes were considered oligotrophic kettle lakes, ponds formed in holes in the ground, possessing no hydrological inlet or outlet. The difference in origin may explain the difference in the atomic N:C ratio shown in Table 1.

The atomic H:C ratio of Pony lake FA appears to be higher than Toolik lake FA, Island lake FA, and Campsite lake FA, thus suggesting a higher aliphatic content in Pony lake FA. However, Suwannee River FA displays the lowest of all expressed H:C ratios in Table 1, with an atomic H:C ratio bellow 1.0, suggesting a higher aromatic or carboxylic content.

2.2.3 Introduction to total dissolved organic carbon quantification

There are two main types of methods to process for the quantification of the total concentration of DOC: High-temperature combustion (HTC) and wet chemical oxidation (WCO). Although these two methods have been widely compared and discussed, in an attempt to explain their discrepancies (usually attributed to analytical bias), it should be emphasized that both HTC and WCO methods perform at a relatively satisfactory level and there is no evidence for systematic differences on the DOC content derived from the two methods (Sharp 1993).

The conversion of DOC into CO_2 through a UV-persulphate oxidation is the most common WCO method of DOC quantification. Upon DOC sample oxidation, CO_2 concentration induces a pH change, resulting in a change of color in the phenolphthalein solution, while the color intensity of the solution is measured by spectrometer colorimetry. The use of a dialysis Teflon® membrane ensures that only the CO_2 passes through to the color reagent flux, prompting the change in color and eliminating the possibility of contamination of the color reagent. According to the authors, no interferences were detected in this method when subject to different salinities (Lopes et al. 2006). The detection limit of this method was reported as being 0.26 mg/L (calculated based on Miller and Miller (2010). This WCO methodology is suitable to measure the DOC content of natural waters, displaying a precision and sensitivity for analysis of DOC in a wide range of water samples, including freshwater, estuarine and seawater. This method can be also applied to measure the DOC content of surface waters, pore waters, and the water-soluble organic carbon in atmospheric aerosol samples.

2.2.4 Introduction to nuclear magnetic resonance spectroscopy of dissolved organic matter

The NMR spectroscopy is a characterization technique that relies on the magnetic properties of the nuclei to produce structural information regarding the molecules in a given sample. When placed in a strong magnetic field, the atomic nuclei resonate at distinct frequencies, as the slight variations in the resonance frequency provide insight into the molecular structure in which the atom is inserted (Jacobsen 2007).

Liquid-state NMR spectroscopy is especially suitable for analyzing of DOM, mainly with low MW. The ^{1}H-NMR can provide structural information relative to protons in HS, however the removal of phenolic hydrogens in HS (when using a Sodium deuteroxide (NaOD) solvent solution) may lead to molecule rearrangements (Mikita et al. 1981). As a result, ^{1}H-NMR data should be analyzed with caution. These spectra can be divided into different regions, with each resonance area being assigned to a specific functional group.

Solid-state NMR spectroscopy is also an important tool in DOM characterization, mainly due to the ease of analysis, as there is no need for solvent selection. In solid-state NMR spectroscopy, the primary technique used in NOM studies is the ^{13}C cross polarization-magic angle spinning technique (CP-MAS). Cross-polarization (CP) is a technique to reduce the line broadening. Firstly, the sample is irradiated with a radiofrequency field at ^{1}H resonance frequency, providing a 90º proton pulse and then a 90º phase shift of the field, originating a "spin-lock" condition (maintained during the entire NMR experiment). Once the ^{1}H spin-lock is established, a new radiofrequency pulse is now applied at ^{13}C resonance frequency during "contact time"; the ^{13}C resonance frequency is then turned off, originating a ^{13}C inductive decay. After the "repeat time", the process is restarted, in order to produce a ^{13}C-NMR spectrum with high resolution (Hayes et al. 1989). Magic-angle spinning, also a technique commonly used to reduce line broadening (Andrew 1971), is based on the notion that dipolar ^{13}C-^{1}H interactions can be removed and chemical shift anisotropy effects reduced, when the solid sample is rapidly rotated at a "magic-angle" of 54.7º relative to the applied magnetic field. This magic-angle spinning mimics the natural motions experienced in the liquid state. High-power proton decoupling helps remove the dipole-dipole interactions, helping the reduction of line (Hayes et al. 1989). Generally, chemical shifts are

similar in both solid- and liquid-state NMR spectroscopy, however, slight variations may take place due to solvent and temperature effects.

In solid-state NMR, a greater amount of time is required in the preparation of the sample prior to NMR analysis (ex: lyophilization). One must also take into account that high concentrations of inorganic components may decrease the signal-to-noise (S/N) ratio and that the presence of salts in the DOM sample should be accounted for, due to their hygroscopic nature. However, passing the DOM sample through an ion-exchange resin, would allow for a desalination process of the sample, therefore reducing the previously mentioned risks (Mitchell et al. 2013).

In solution state, ^{1}H NMR spectra displays not only broadened lines relative to the chemical shift range, but also a water peak that requires an adequate solvent suppression technique, in order to obtain a good signal to noise ratio. The use of ^{1}H and ^{13}C NMR in conjunction, can provide complementary information, thus resulting in further knowledge about the nature of the sample (Bortiatynski et al. 1996; Cardoza et al. 2004). The abundance of the isotopes is also an important factor to consider, as the ^{1}H isotope is present with 100% abundance in the sample, while ^{13}C isotope's abundance is only 1.1%. The increased sensitivity factor of the ^{1}H isotope relative to ^{13}C, as well as the relative abundance of each isotope, prompts the notion that not only ^{1}H NMR experiments have shorter acquisition time, but also higher sensitivity when compared to ^{13}C NMR experiments (Preston et al. 1998; Jacobsen 2007).

Studies focusing on ^{13}C NMR characterization of soil organic carbon from drained thaw lake basins in Arctic Alaska have been conducted, shedding light on the composition of soil organic matter in these basins (Pedersen et al. 2011). The nature of the soils in drained thaw lake basins should display considerable similarities to DOM in thaw lake water samples, providing further insight into these types of samples. In the thaw-lake basin soils, alkyl and O-alkyl structures displayed the highest ^{13}C signal intensity, while aromatic, carboxylic and carbonyl carbons were associated with lower signal intensities (Pedersen et al. 2011). Comparing to soils from temperate regions (Simpson and Feng 2008), these soils contained higher alkyl and O-alkyl carbon content, and lower aromatic, carbonyl and carboxylic carbon content. Surface soil samples display the highest relative quantities of O-alkyl carbon, suggesting that SOM had a higher carbohydrate and peptide content. Methoxyl carbon is also associated to the O-alkyl region (50-110 ppm), possibly arising from lignin. However,

lignin is also associated to a phenolic carbon signal (145-160 ppm), a region with lower signal intensity in the obtained spectra. Therefore, as lignin content appears to be a minor component of the superficial SOM samples, the high signal intensity in the O-alkyl region is mainly due to labile organic matter. Also, in surface soils, the anomeric carbon signal (105 ppm) displayed significant intensity, typical of "younger" organic matter. Generally, organic matter in these types of soils tends to be older for greater depths; however, cryoturbation (i.e. frost mixing) may prompt "younger" and more labile organic matter to reach greater depths. The two ancient soil samples from the thaw lake basin contained 50% and 43% of O-alkyl carbon, suggesting that labile organic matter is preserved in Arctic environments. The aromatic component signal may suffer the contribution of black carbon; in some environments with low lignin content, the signal relative to the aromatic component may suffer contributions from other sources (Wilson et al. 1986), namely black carbon. Table 2 contains the different chemical shift regions and respective assignment of ^{13}C NMR spectra of soil organic matter.

Table 2 – Table containing the ^{13}C NMR chemical shift regions and respective assignments for soil organic matter.

^{13}C chemical shift region (ppm)	**Assignment**
0-44	Alkyl carbon
44-64	Methoxyl or N-alkyl carbon
64-93	O-alkyl carbon
93-110	Alkyl O-C-O
110-143	Aromatic carbon
143-159	Aromatic C-O
159-190	Groups carboxyl and N-C=O
190-220	Aldehydes and Ketones

A signal in the alkyl carbon region (0-44 ppm) is commonly associated with lipids and aliphatic chains of amino acids; in the region of 44 to 64 ppm, methoxyl is a part lignin component, while N-alkyl carbons are associated to peptides. O-alkyl carbons, however, are commonly present in polysaccharides, as well as alkyl O-C-O bonds. The aromatic (110-143

ppm) and the aromatic C-O region (143-159 ppm) can be associated not only to lignin, but also to black carbon. A higher alkyl/O-alkyl ratio may indicate a more advanced state of decomposition for the organic matter. Alkyl/O-alkyl ratios for subsurface soils displayed higher values than in surface horizons, indicating a more advanced state of decomposition. With depth, alkyl carbon tends to accumulate, while polysaccharide-like compounds are depleted.

A typical spectrum of aquatic HS in CP-MAS ^{13}C-NMR displays relatively broad peaks located at 30-35 ppm (aliphatic carbon), 75 ppm (carbon bonded to oxygen such as in hydroxyl and ether groups), 130 ppm (aromatic carbon), 140 ppm (carbon bonded to phenolic hydroxyl), 175 ppm (carboxyl and esther) and 210 ppm (carbonyl). The area under each peak is integrated in order to determine the percentage of each functional group. It is currently regarded that HA contains higher percentage of aromatic carbon and phenolic carbons, having lower percentage of carboxyl carbons and aliphatic carbons (Thurman 1985). Figure 3 reveals the solid-state ^{13}C-NMR spectra of the Suwannee River humic acid (SRHA) and Suwannee River fulvic acid (SRFA) standards, which can be divided into four regions: 0-50 ppm (unsubstituted saturated aliphatic carbon), 60-95 ppm (aliphatic carbons bonded to one nitrogen or oxygen atom), 110-160 ppm (aromatic and unsaturated carbons) and 160-190 ppm (ester, amide and carboxyl carbons). The SRFA standard spectrum clearly displays a higher intensity for the 160-190 ppm region than the SRHA standard spectrum. Peak areas were calculated with SRHA displaying higher peak areas than SRFA between 160-140, 140-110, 110-95, 95-60, and 50-60 ppm.

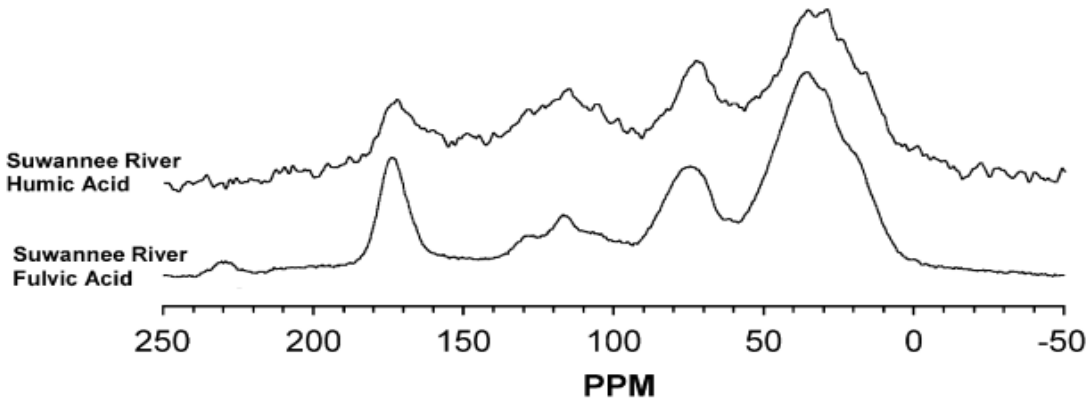

Figure 3 – Solid-state ^{13}C-NMR spectra of SRHA and SRFA standards (adapted with permission from (Duarte et al. 2007), License Number: 4247160239755).

The use of multidimensional NMR experiments has proven to be a powerful tool to unravel the structural characterization of DOM, providing a greater diversity of structural information for HS. These multidimensional NMR applications have resulted in numerous findings linking material derived from protein, lignin, lipids, tannins and carbohydrates to the composition of HS (Hertkorn et al. 2002; Simpson et al. 2001; Simpson et al. 2002)

However, the immense complexity of DOM results in an extensive spectral overlap, hindering the chances of identifying an exact structure, rendering the precise identification of its components, relying solely on one technique, impossible. Therefore, the use of multidimensional NMR experiences and other analytical techniques in conjunction, may help refute or corroborate previously held interpretations of highly complex spectra.

2.2.4.1 Brief overview of two-dimensional NMR experiments

Two-dimensional experiments are always based on one principle: to correlate two nuclei contained in a molecule, either through a bond interaction (*J* coupling) or an interaction through space (Nuclear Overhauser Effect).

Heteronuclear single quantum correlation (HSQC) experiments result in cross-peaks that represent ^{1}H-^{13}C coupling over a single bond (although it can also be used for ^{15}N nuclei). In an HSQC spectrum, the ^{1}H chemical shift scale is located in the horizontal axis, while the ^{13}C chemical shift scale is located in the vertical axis. For example, if proton H_a is directly bound to C_a, there would be an intersection between the ^{1}H chemical shift relative to H_a and the ^{13}C chemical shift associated with C_a (Jacobsen 2007). The use of two dimensions decreases significantly the chance of peak overlaps.

Contrary to the heteronuclear shift correlation (HETCOR), where ^{1}H magnetization is indirectly detected and converted to ^{13}C magnetization to be detected directly, HSQC is an "inverse" experiment, which means ^{13}C magnetization is indirectly detected and the ^{1}H magnetization is directly detected. This results in increased sensitivity and allows the detection of long-range (two and three bonds) interactions between ^{13}C and ^{1}H nuclei, using heteronuclear multiple quantum correlation (HMQC).

An HSQC experiment can be subject to variations, so that the cross-peaks may provide further information regarding the number of protons attached to heteronuclei. Considering ^{1}H-^{13}C experiments, the CH and CH_3 crosspeaks are displayed as positive, while CH_2 crosspeaks are portrayed as negative (Jacobsen 2007).

The HSQC displays great similarities with HMQC, however, HMQC allows the magnetization of both ^{1}H and ^{13}C to evolve, while HSQC only allows the heteronuclei magnetization. As HSQC does not contain proton couplings, its spectra is more resolved in comparison to HMQC (Simpson 2001).

The Heteronuclear Multiple-Quantum Correlation (HMQC) experiment produces a two-dimensional heteronuclear correlation map of the direct-bonded ^{1}H nuclei and the corresponding heteronuclei (usually ^{13}C or ^{15}N). HMQC is based on proton-detection, resulting in higher sensitivity in comparison to conventional 2D HETCOR experiments.

The HMQC requires fewer pulses, displaying lower sensitivity to pulse calibration errors than HSQC. However, the resolution in HMQC is limited in the ^{13}C dimension due to the ^{1}H multiplet pattern, while resolution in HSQC depends solely on the ^{13}C linewidths. As such, in complex mixtures as NOM, when there is a crowded ^{13}C NMR spectra, HSQC presents itself as the method of choice (Cook 2004).

Two dimensional correlation spectroscopy (COSY) is an NMR experiment that is based on the correlation of nuclei of a single isotope (generally ^{1}H) coupled over a single *J*-coupling that may be germinal (2-bond), vicinal (3-bond) or, in rare situations, long-range (4-bond or 5-bond).

A plot, symmetric diagonally, displays the cross-peaks associated with the ^{1}H-^{1}H couplings, with both the horizontal and vertical axis displaying the ^{1}H chemical shift scale. The magnetization transfer produces these cross-peaks, providing information regarding the two coupled nuclei. Generally, a final pulse at 90º is applied in these experiments, however, reducing the angle will prompt the reduction of the intensity of the spectral splitting, simplifying the spectra; an example of this is the COSY45 experiment, which replaces the final 90º pulse with a 45º pulse, a technique better suited for extremely complex spectra, even though a loss in sensitivity is to be expected (Jacobsen 2007).

Two dimensional total correlation (TOCSY) spectroscopy, similarly to COSY, measures the magnetization transfer between ^{1}H-^{1}H. However, while COSY focuses on neighboring ^{1}H spins, TOCSY is associated with the multiple correlations throughout an entire spin network, enabling the detection of all coupled protons contained in a given molecule. The TOCSY experiment transfers the magnetization of one proton along the spin-lock axis, to all other protons in the same spin system (Jacobsen 2007).

2.2.5 Introduction to Fourier-transform infrared spectroscopy of dissolved organic matter

The use of Fourier-transform infrared spectroscopy (FTIR) can complement the information obtained through ^{13}C CP-MAS NMR, providing further insight into the nature of the sample.

The FTIR spectroscopy is a semi-quantitative tool, used to identify what fraction of incident light is absorbed by a particular sample at a particular wavelength, producing a spectrum that characterizes the vibrations of the bonds present in the molecule. Each spectrum can act as a chemical fingerprint for compound identification (Ferraro & Krishnan 1990), being widely used for organic and inorganic compounds, due to the fact that most molecular species absorb infrared radiation, with the exception of some homomolecular species.

Photon energy ranging from 4000 cm^{-1} to 400 cm^{-1}, associated with infrared, although insufficient to excite electrons, can cause vibrational changes between atoms and covalent bonded groups. These vibrations can be classified as stretching (axial deformation) or bending (angle deformation), as the respective frequency of vibration depends on bond forces and the atoms mass. Inducing bending vibration requires less energy than stretching vibrations (Silverstein et al. 2005).

A FTIR spectra of thaw lake basin soils in arctic regions (Pedersen et al. 2011) (using FTIR photoacoustic spectroscopy) displayed several prominent spectra bands: a broad band in the 3500 to 3200 cm^{-1} region; two bands at 2923 and 2850 cm^{-1}; a small peak at 1715 cm^{-1}; a slightly broad band extending from 1660 to 1600 cm^{-1}; an absorption band from 1590 to 1510 cm^{-1}; a small peak at 1160 cm^{-1}; and a broad peak at 1040 cm^{-1}. The assignment corresponding to each of the previously referred peaks can be found in Table 3.

Table 3 – Prominent FTIR spectra bands and corresponding assignments (Pedersen et al. 2011).

Wavenumber (cm^{-1})	**Assignment**
3500-3200	Carboxylic acid, phenol and alcohol ν_{O-H}; possible minor contributions from amine and amides ν_{N-H};
2923; 2850	Aliphatic ν_{C-H} and $_s\nu_{C-H}$ associated with CH_2;
1715	COOH, ketones and aldehydes $\nu_{C=O}$;
1660-1600	Aromatic $\nu_{C=C}$; amides, quinones and H-bonded conjugated ketones $\nu_{C=O}$; $_s\nu_{C=O}$ from COO^-;
1590-1510	δ_{N-H}, $\nu_{C=N}$ and aromatic $\nu_{C=C}$;
1160	Aliphatic ν_{C-OH};
1040	ν_{C-O} from polyssacharides and polyssacharide-like compounds; ν_{Si-O} from silicates

In order to further research the structure of peat organic matter in collapsed palsas, bogs and fens, studies have used FTIR spectroscopy to characterize peat from different depths (Hodgkins et al. 2014). The obtained spectra displayed great similarities between samples, however the relative band intensities showcased considerable differences, providing information relative to changes in peat humification.

Along the thaw progression, the relative intensity of carboxylic acid bands diminishes, attributed to the recognition of organic acids as carboxylate ions, due to the higher pH encountered in fens (Hodgkins et al. 2014). Surface fen peat, when compared to deep fen peat, displayed higher abundance in the polysaccharide band, and lower abundance in lignin (1513 to 1515 cm^{-1}), aromatic and aliphatic bands, suggesting the presence of more cellulose (O-alkyl carbons) in surface fens, and the presence of organic matter in a higher state of decomposition in deep fens. In bogs and collapsed palsas, these differences were more attenuated.

Comparing the spectra of young thaw-lake basin soil (Pedersen et al. 2011) and fens soil at different depths (Hodgkins et al. 2014), one can verify significant similarities, suggesting the possibility of a similar nature. The polysaccharide band in young thaw-lake basin soil appears to display lower relative intensity when compared to the spectra of surface fens,

while the carboxylic acid (COOH), ketone and aldehyde band possesses slightly higher intensity in young thaw lake basin soils than in surface fens.

As an example of FTIR spectra of complex humic samples, Figure 4 exhibits the FTIR-Attenuated total reflectance (ATR) spectra of SRHA and SRFA, two well-known standards for humic matter. The spectra display bands at approximately 3400 cm^{-1}, associated with O-H stretching of carbonyl, phenol and hydroxyl groups; at 2970-2840 cm^{-1}, C-H stretching of methyl and methylene in aliphatic chains; at 1720 cm^{-1}, C=O (unconjugated) stretching of (mainly) carboxyl groups (also ketones and aldehydes, but in a lesser extent); and at 1200 cm^{-1}, C-O stretching and O-H bending vibrations of (mainly) carboxyl groups.

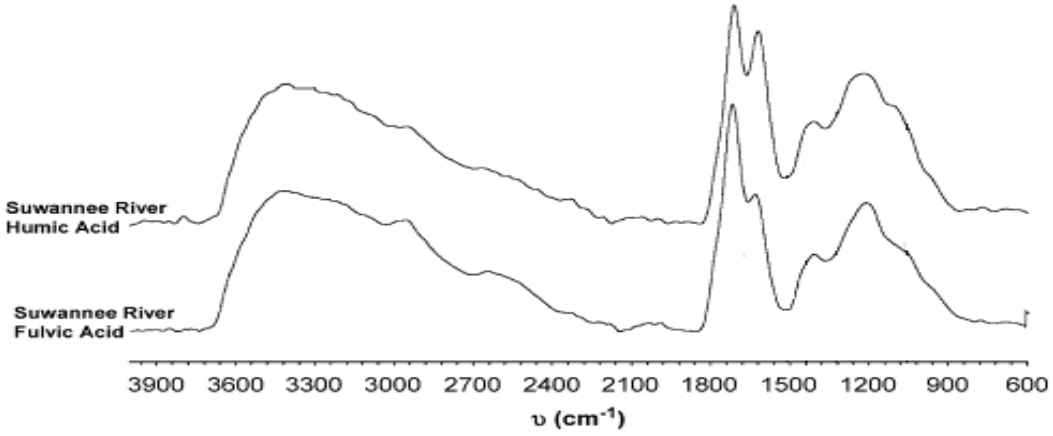

Figure 4 – The FTIR-ATR spectra of SRHA and SRFA standards (adapted with permission of (Duarte et al. 2007), License Number: 4247160239755).

2.2.6 Introduction to fluorescence spectroscopy and specific ultraviolet absorbance of dissolved organic matter

Molecular fluorescence spectroscopy has been increasingly used to study DOM in a wide variety of aquatic systems, as it can be applied to assess its source and also to determine the physical properties of HS, such as diffusion coefficients (Lead et al. 2000) and electrostatic properties (Green et al. 1992). Fluorescence spectroscopy is considered a useful tool to investigate variability within a sub-fraction of DOM. This technique is based on the excitation of molecules within a sample and measuring the resulting emission of light. While sample components excited to a singlet state return to the ground state shortly after, with the emitted energy being typically lower than the absorbed energy (Stokes shift), the obtained excitation and emission spectra might provide insight into the nature of the sample, the surrounding environment, and the fluorophores contained in the sample (Lakowicz 2006). Therefore, variation in peak width, intensity, and wavelength of maximum intensity are interpreted as either a change in the origin of its components or the addition (or removal) of some DOM components, due to biological activity (Coble et al. 2014). However, the comparability of fluorescence signals is difficult due to inherent factors, such as instrumental inefficacies, different environmental conditions (including temperature and pH), and the existence of inner filter effects.

The plot of a range of emission spectra resulting from a range of excitation wavelengths, provides a three-dimensional plot, commonly referred to as excitation-emission matrices (EEMs). The EEMs are widely used in DOM studies, not only due to their increased sensitivity, but also because of the short time of analysis; the deconvolution of these EEMs has enabled researchers to identify different fluorophores within DOM samples with distinct origins (Coble et al. 1990; Coble 1996; Stedmon et al. 2003); however, the introduction of statistical analysis to EEMs (namely parallel factor analysis (PARAFAC)), has been known to provide detailed information regarding the DOM sample (Stedmon et al. 2003). The fluorescence spectra of FA and DOM display characteristic humic peaks, similar in both marine and freshwater environments, even though a wide variability of fluorophores is to be expected for different DOM (Coble et al. 1990), while changes in the source of DOM may

prompt differences in both position and intensity of these humic peaks in the fluorescence spectra.

As previously referred, natural organic fluorophores found in aqueous systems are mostly aromatic compounds with polar functional groups such as hydroxy, carboxyl, and amine groups, being categorized by their central conjugated system (e.g., indoles, and phenols, among others). The adequate interpretation of the spectroscopic data compiled in the EEM spectra is based on a correct pinpointing of the excitation/emission maxima positions for the most common fluorophores associated with DOM or HS. Table 4 displays the most common peaks for different types of fluorophores in EEMs spectra as well as the signal pairs relative to humic matter.

Table 4 – Peak and region locations for different fluorophores in EEMs spectra (for DOM and HS). P1 has a microbial source (autochthonous source), while P8 and P3 have an allochthonous humic terrestrial source. Peak positions were compiled from literature data collected by (Stedmon a. 2003; Stedmon and Markager 2005b; Stedmon and Markager 2005a; Coble et al., Castillo, and Avril 1998; Murphy et al. 2008).

Peak Label	**Excitation maximum (nm)**	**Emission maximum (nm)**	**Type of fluorophore**
B	275	305	Tyrosine-like, protein-like
T	275	340	Tryptophan-like, protein-like
A	260	400-460	Humic-like
M	290-310	370-410	Marine humic-like
P1	240	350-400	Humic-like M
	290-310	370-420	
C	320-360	420-460	Humic-like
P8	260	400-460	Humic-like C
	320-365	420-470	
P3	250	470-504	Humic-like C+
	385-420	470-504	
D	390	509	Soil FA
E	455	521	Soil FA
N	280	370	Plankton derived

Fresh FA showcased two excitation/emission maxima; one located around an excitation wavelength (Ex_{max}) of 250-270 nm and emission wavelength (Em_{max}) ranging from 418 to 504 nm, while the longer excitation maximum is located around Ex_{max} 322-358 nm and Em_{max} 410-456 nm (Klapper et al. 2002), coinciding with the A and C maxima described by Coble. However, the EEMs of the reduced FA displayed considerable differences when compared to the EEMs of fresh FA. The EEM of reduced FA contains only one maximum at Ex_{max} 250-270 nm and Em_{max} ranging from 425 nm to 550 nm (Klapper et al. 2002). In recent times, it has been observed that shifts in FA fluorescence spectra may be a function of redox gradients, either in the field or associated with microbial reduction of FA. It has been asserted that microbial reduction of HS prompts an increase in semiquinones, proportional to the electron-accepting capacity of HS (Scott et al. 1998).

In fluorescence spectroscopy, the light scattering effects are named Rayleigh scatter (most commonly, first and second order) and Raman scatter. First order Rayleigh scatter line centers at the emission wavelength equals the excitation wavelength, while second order Rayleigh scatter line centers at an emission wavelength twice the value of the excitation wavelength (Rinnan et al. 2005).

Recent advances in spectroscopic techniques have prompted an increase in the use of optical properties of DOM, in an attempt to assess or infer information regarding its sources and, to an extent, its composition. The use of fluorescence and absorption optical properties for compositional and origin evaluation of DOM, has proven itself useful in recent times. Table 4 comprises a set of fluorescence optical properties, containing the basis of its calculation, its description and the associated references.

HS are typically associated with fluorescence peaks A, C, D and M, while the protein-like component manifests itself in the fluorescence peaks B, N and T. It should be noted that although the lower UV region is commonly associated with protein-like fractions, studies have shown that other non-protein compounds display fluorescence in that region (Hernes et al. 2009; Hernes 2003), mainly thought to be undegraded polyphenols present in plant leachates (Coble et al. 2014). Considering this, these fluorescence peaks are more appropriately described as “fresh” organic matter, rather than “protein-like”.

Specific peaks in EEM spectra can display shifts to lower or higher emission wavelengths, triggered by the change of the relative separation of the ground electronic state of the

molecules. For example, the protonation of electron withdrawing groups (e.g. carboxyl groups), prompts a shift of the fluorescence peak to longer wavelengths, typically referred to as a red shift; the deprotonation of this functional group will shift the fluorescence peak to shorter wavelengths, generally referred to as blue shift. In electron-donating groups, the opposite effect is verified; the protonation of these groups (e.g. Amide / NH_2) results in a shift to lower emission wavelengths, whereas deprotonation of these functional groups prompts a shift to longer emission wavelengths (Coble et al. 2014).

Table 5 – Set of fluorescence optical properties, indexes and ratios, their respective description and reference.

Fluorescence Measurements	**Parameters**	**Description**	**Reference**
Peak Ratio A:T	Ratio of Peak A to Peak T intensity.	Indicator of the amount of humic-like vs. labile fluorescence in DOM	(Hansen et al. 2016)
Peak Ratio C:A	Ratio of Peak C to Peak T intensity	Indicator of the amount of humic-like vs. fulvic-like fluorescence in DOM	(Baker et al. 2008)
Peak Ratio C:M	Ratio of Peak C to Peak M intensity	Indicator of the amount of humic-like vs. marine-like fluorescence in DOM	(Coble 1996)
Peak Ratio C:T	Ratio of Peak C to Peak T intensity	Indicator of the amount of humic-like vs. freshlike fluorescence in DOM	(Baker et al. 2008)
Fluorescence Index (FI)	Ratio of emission wavelengths at 470 nm and 520 nm, obtained at excitation wavelength of 370 nm	Indicator of relative contribution of terrestrial or microbial sources to DOM	(McKnight et al. 2001; Cory et al. 2010)

Table 5 (Continuation) – Set of fluorescence optical properties, indexes and ratios, their respective description and reference.

Fluorescence Measurements	**Parameters**	**Description**	**Reference**
Humification Index (HIX)	Area under the emission spectra 435–480 nm divided by the peak area 300–345 nm1435–480 nm, at excitation 254 nm	Indicator of humic substance content. Higher values are associated with greater humification	(Zsolnay et al. 1999; Kowalczuk et al. 2013)
Freshness Index	Intensity at 380 nm (emission wavelength) divided by the maximum intensity between 420 nm and 435 nm (emission wavelength) at 310 nm (excitation wavelength)	Indicator of recently produced DOM, with higher values associated with a greater amount of recent DOM	(McKnight et al. 2001)
Biological Index (BIX)	Ratio of emission intensity at 380 nm divided by 430 nm at excitation 310 nm	Indicator of autotrophic productivity. Values greater than 1 correspond to recently produced DOM of autochthonous source.	(Huguet et al. 2009)
Relative Fluorescence Efficacy (RFE)	Ratio of intensity at 380 nm divided by 430 nm (emission wavelength) at excitation 310 nm	Relative indicator of algal vs non-algal DOM	(Downing et al. 2009)

2.2.6.1 Use of fluorescence index for dissolved organic matter characterization

The fluorescence index (FI) is a ratio of emission intensities (450 nm/500 nm) at an excitation wavelength of 370 nm, has been used to distinguish the contribution of microbial versus the plant/terrestrially derived organic matter comprising the DOM pool (McKnight et al. 2001). A study where the microbially derived FA were associated with a FI of 1.9, while plant/terrestrially derived FA displayed a FI between 1.4 and 1.5 on uncorrected emission spectra (McKnight et al. 2001). For corrected spectra, FI is calculated as the is a ratio of emission intensities 470 nm/520 nm at an excitation wavelength of 370 nm (Cory et al. 2010).

The notion that some DOM fluorophores are a function of the redox state has been suggested, indicating a link between some fluorophores and redox active quinones (Klapper et al. 2002). Humic substances have been known to display at least two main excitation-emission maxima in their fluorescence EEMs, providing information about the source of these substances. Biogeochemical transformations to aquatic HS may prompt changes to their electron-accepting capacity. However, one cannot rely solely on electron-accepting capacity to determine the origin of HS, as Lake Fryxell (located in Antarctica and of microbial origin) displays similar capacity to Suwannee River (terrestrial/plant origin) (Scott et al. 1998).

2.2.6.2 Use of humification index for dissolved organic matter characterization

The humification index (HIX) is considered to be an indicator of source, diagenesis and sorptive capacity. This index is based on the notion that as the degree of humification of DOM increases, the ratio of hydrogen to carbon decreases, thus shifting the emission spectra of the fluorescent components towards longer wavelengths (Ohno 2002; Fleck et al. 2014).

There are different approaches to calculating HIX values; one of these approaches consists in dividing the intensity between 435 and 480 nm of emission by the intensity in the 300 to

345 nm (Zsolnay et al. 1999), while another approach consists in using the 390 nm/355 nm, 400 nm/360 nm, 470 nm/360 nm and 470 nm/400 nm ratios of a synchronous fluorescence spectra, with a $\Delta\lambda$ of 18 nm (Kalbitz et al.2000). However, it is important to keep in mind that fluorescence intensity measurements may be subjected to attenuation due to primary-inner filters, the absorption of the excitation beam before it reaches the sample, and secondary inner filters, the absorption of the fluorescence photons emitted from the sample (Kubista et al. 1994). As the fluorescence primary inner filter effect affects all emission wavelengths equally, the use of ratios to determine the HIX value, allows one to ignore the effects of the primary filter on the HIX value. The secondary inner filter however, may require correction in the HIX values, because that organic matter absorbs UV light in monitored fluorescence regions (Ohno 2002).

The HIX can be calculated as expressed in Equation 1 (Zsolnay et al. 1999; Cox et al. 2000), where WI is the wavelength (in nanometers), and I_{WI} is the fluorescence intensity at the WI wavelength.

$$HIX = \frac{\sum_{WI=435}^{480} I_{WI}}{\sum_{WI=300}^{345} I_{WI}} \quad (1)$$

However, an alternative HIX formula (expressed in equation 2) emerged based on Equation 1, where the HIX value would range from 0 to 1 with increasing degree of humification (Ohno 2002).

$$HIX = \frac{\sum_{WI=435}^{480} I_{WI}}{\sum_{WI=300}^{345} I_{WI} + \sum_{WI=435}^{480} I_{WI}} \quad (2)$$

Considering HIX as an indicator of humification/humic content, higher index values are associated with higher degrees of humification. Table 6 expresses the intervals of HIX values and their characteristics.

Table 6 – Intervals of humidification index (HIX) values and their associated dissolved organic matter (DOM) characteristics - (adapted with permission (Huguet et al. 2009), License Number: 4434880980266).

HIX values	DOM characteristics
<4	Biological or aquatic bacterial origin
4-6	Weak humic content and important recent autochtonous component
6-10	Important humic content and weak recent autochtonous component
>16	Strong humic content

2.2.6.3 Use of freshness index and biological index for dissolved organic characterization

The freshness index (β:α) is mainly considered to be an indicator of newly produced marine DOM (Parlanti et al. 2000; Wilson and Xenopoulos 2009), where β represents the newly derived DOM, while α represents the highly degraded DOM portion. Peak C (Coble's nomenclature) was renamed as peak α and peak M as peak β, under a different nomenclature (Parlanti et al. 2000).

Changes to the original β:α ratio resulted in a new index which became known as biological index (BIX). The BIX takes into account the broadening of the humic portion of the emission spectrum, caused by the presence of the peak β (Huguet et al. 2009). As demonstrated on Table 5, BIX consists in the ratio of the emitted fluorescence intensity at 380 nm divided by the fluorescence intensity at 430 nm, when these are excited at 310 nm. In Table 7, intervals of BIX values are associated with their DOM characteristics, namely their autochtonous component.

Table 7 – Intervals of BIX values and their associated DOM characteristics – (adapted with permission (Huguet et al. 2009), License Number: 4434880980266).

BIX values	DOM characteristics
0.6-0.7	Low autochtonous component
0.7-0.8	Intermediate autochtonous component
0.8-1.0	Strong authochtonous component
>1	Biological or aquatic bacterial origin

2.2.6.4 Use of peak ratios for dissolved organic matter characterization

Among all the fluorescent peak ratios published, the most commonly reported are C:T, A:T, C:A and the C:M ratio. Similar to β:α and BIX, C:T and A:T serve as indicators of the relative amount of humic-like DOM relative to fresh-like DOM. Considering that both peaks C and A are associated with humic-like DOM, the higher the values of C:T and C:A ratios, the higher the proportion of degraded material.

Some studies focused on the measurements of initial C:T and A:T ratios for different types of samples, with plant and algae samples displaying ratios ranging from 0.1 to 0.3, while the soil sample ratio displayed 6.6 for C:T and 11.4 for A:T (Hansen et al. 2016). Upon biodegradation, while soil ratios increased slightly, plant and algae C:T and A:T ratios escalated to 3.2-4.9 and 2.7-4.1, respectively (Hansen et al. 2016). Photoexposure resulted in a substantial decrease of C:T and A:T ratios in all sources (Hansen et al. 2016).

Even though peaks A and C are associated with humic-like material, it has been reported that they may vary differently, prompting the notion that these peaks represent decoupled pools of DOM (Kothawala et al. 2012). Plants and algae leachates displayed a C:A ratio ranging between 0.9 and 1.1, while soil samples displayed significantly lower values, with a C:A ratio around 0.6 (Hansen et al. 2016). In the DOM fluorescing region associated with humic-like terrestrial DOM, the peak C is preferentially lost relative to peak A (Kothawala et al. 2012). This preferential retention of peak A relative to peak C in dark degradation was verified through all studied samples, regardless of water age and initial concentrations. It should be pointed out that, although peaks A and C comprise a sizeable amount of overall

fluorescence in these types of samples, the identification of structural characteristics solely associated with these two peaks is yet to be achieved.

2.2.6.5 Brief overview of specific ultraviolet absorbance

Apart from the use of fluorescence spectroscopy in an attempt to characterize DOM samples, it is understood that in UV-visible spectroscopy, the specific UV absorbance at 254 nm ($SUVA_{254}$), the absorption of light at 254 nm per unit of carbon, has proven not only to be strongly linked with the hydrophobic organic acid fraction of DOM (Spencer et al. 2012), but also as a useful indicator of DOM aromatic content (Weishaaret al. 2003) and molecular weight (Chowdhury 2013).

In surface waters, $SUVA_{254}$ values ranges between 1.0 to 6.0 L mg-C^{-1} m^{-1}; however, an increase in these values may be due to a strong terrestrial signature (Jaffé et al. 2008), or to the presence of iron, colloids and other components in the sample (Weishaaret al. 2003; Hudson et al.2007). Studies have found that the initial $SUVA_{254}$ value for peat soil leachate was 3.0 L mg-C^{-1} m^{-1}, while algal leachates displayed initial $SUVA_{254}$ values bellow 1.0 L mg-$C^{-1}m^{-1}$ (Hansen et al. 2016). The lower values associated with algae leachates support the idea that this leached DOM includes a greater amount of aliphatic compounds (a greater low molecular weight component), which do not absorb at 254 nm (Hansen et al. 2016). It should be noted that biodegradation prompts the increase of $SUVA_{254}$ values, as biodegradation tends to remove low molecular weight DOM (Pellerin et al. 2010).

3

Study area and Sampling methodologies

3.1 Thermokarst lakes and sampling sites

Samples were collected between March 2nd and March 4th 2018, in the subarctic region of Nunavik, Northern Quebec, Canada. Winter season was chosen due to the lake's higher concentrations of NOM in these lakes at this time of year due to freeze-concentration (Belzile et al. 2002), and the lack of scientific information regarding thaw lakes during winter. The sampled thermokarst lakes are located near Sasapimakwananisikw (SAS) River Valley (55º13N 77º42W), a sporadic permafrost region. Samples were collected from lake SAS-1A, lake SAS-2A, and lake SAS-1B near Kuujjuarapik-Whapmagoostui (K-W).

The SAS thaw lakes originated from the thawing of palsas, low mounds displaying circular or oval shape (Crevecoeur et al. 2015). The underlying of frozen peat layer in the ground, tends to originate a water body during the summer, freezing during winter. When the underground ice expands, the soil is forced upwards, originating a palsa. These palsas generally display high organic matter content, as they are mainly comprised of peat.

Lake SAS-2A (55º13'35.6 N, 77º41'49.1 W) located on the north side of the SAS river, at a distance of approximately 30 meters of the nearest palsa. On the south side of the SAS river, lake SAS-1A (55º13'07.7 N, 77º42'28.4 W) is located at an approximate distance of 20 meters to the nearest palsa (the same palsa associated with SAS-1B). Also, in the south side of the SAS river, lake SAS-1B (55º13'08.3 N, 77º42'29.6 W) can be found directly attached to the palsa. Figure 5 showcases the locations of the three sampled thermokarst lakes.

During winter season these regions are covered in a considerable snow layer, displaying little differences between sites; however, during the warmer seasons, the snow layer melts and reveals the specific characteristics of each of the sites.

Figure 5 - Location of the SAS-1A, SAS-2A and SAS-1B lakes in the region of Kuujjuarapik-Whapmagoostui – Obtained from Google Maps.

Lake SAS-1A displays a considerably large surface area and a relatively shallow nature, surrounding itself in a dense macrophyte population of *Carex Aquatilis*, thriving on a surface layer of recent peat (Vincent et al 2017). Lake SAS-1B has lower depth than lake SAS-1A and, as previously referred, is located directly under a palsa, thus receiving a considerably higher contribution from the palsa compared to lake SAS-1A. A schematic representation containing both lake SAS-1A and lake SAS-1B can be found in Figure 6.

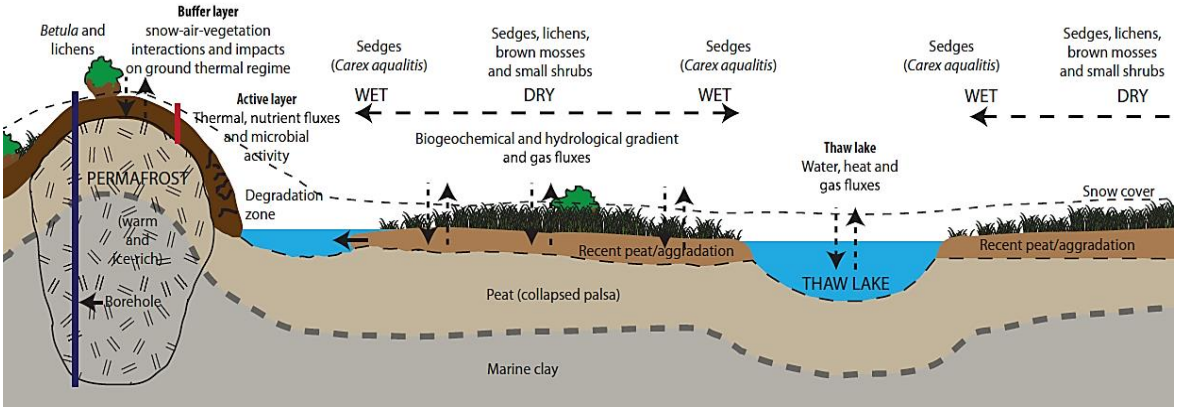

Figure 6 – Spatial variability of an approximately 100 m transect in a palsa valley (Sasapimakwananisikw River Valley, latitude 55°13′N, longitude 77°42′W), 8 km southeast of Kuujjuarapik-Whapmagoostui. The thaw lakes represented in the scheme are lake SAS-1B (left) and lake SAS-1A (Vincent et al 2017) – Reused with the knowledge of NRC Research Press © Canadian Science Publishing or its licensors.

Lake SAS-2A, although appearing to display greater depth than lake SAS-1A, has a smaller surface area, as clearly visible in Figures 5a and 5b. Similarly to lake SAS-1A, populations of *Carex Aquatilis* and other macrophytes also tend to establish themselves near this lake (Deshpande et al. 2017). It should be noted that lakes of greater depths, tend to show greater differences between surface and bottom fractions, in some cases with surface and bottom waters not mixing for long periods of time. SAS-2A has been known to comprise different relative abundances of different bacterial phyla (Crevecoeur et al. 2015). The surface area of each sampled lake was obtained by Prof. Gonçalo Vieira (IGOT, ULisboa), measuring an area of 1661 m^2 for SAS-1A, 491 m^2 for SAS-1B and 104 m^2 for SAS-2A.

Figure 7a – Photograph of lake SAS-1A during the warm season. Image provided by Prof. João Canário (2014).

Figure 7b – Photograph of lake SAS-2A during the warm season. Image provided by Prof. João Canário (2014).

Figure 7c – Photograph of lake SAS-1B during the warm season. Image provided by Prof. João Canário (2014).

The characterization of the obtained samples involved a myriad of analytical techniques, including total DOC quantification, molecular fluorescence spectroscopy, FTIR, NMR, CNHS. Considering the expected carbon content in these samples and the average recovery yield of the extraction process (of organic matter), each sample should possess at least two liters.

3.2 Overview of sampling methodologies

Sampling is a crucial part of the analytical process, as inadequate sampling techniques may prove the source of irreversible errors, compromising the validity of the final results, leading to misinformation and wrongful conclusions. The collection of liquid samples must be conducted in such a manner, that the obtained sample is representative of the original matrix. The wide variety of liquid samples undermines a universal sampling technique, therefore creating sampling techniques appropriated for each type of liquid sample is highly required in order to preserve the sample's integrity to the fullest.

The sampling strategy specifies the type of samples to be collected, as the type of sample is largely dependent on its environment. For determination of total organic carbon (TOC), dissolved oxygen and pH, the associated type of sample is usually referred to as discrete sample (Wardencki & Namiesnik 2002). Discrete samples are collected in their individual container, representing the source at the time of the collection.

The type of sampling system depends heavily on the compounds or elements to be analyzed. Some types of glass release silicon, sodium and boron, and therefore they are unsuitable when those elements are to be analyzed. In such situation, polyethylene bottles should be used instead as sampling system. In the case of samples with organic compounds, glass bottles are recommended as they do not undermine the determination of organic substances. Water samples should be taken to sealed bottles, which should be previously rinsed with sampling water, and any air bubbles should be removed under the closing system, otherwise there may be losses of volatile compounds from the water sample or gases may be dissolved in the liquid phase, altering the sample's composition. The impossibility of rinsing the bottle with sampling water before the actual collection of the sample carries the risk of generate errors; although some systems have been conceived to minimize those risks. All methods of sample collection must be conducted carefully in order to ensure that neither the collecting vessel, nor the sample storage container contaminate or alter the sample in any way (Wardencki & Namiesnik 2002).

The physicochemical properties of the sample's matrix are important in order to assess the interactions of compounds and elements with their chemical environment. These interactions are a result of the chemical properties of both the matrix and the analytes, having direct

impact on the applicability of different sample preparation techniques (Paschke 2002). Therefore, prior to sample preparation, the characterization of the initial physicochemical state of the sample must be attained. When the available sample volume restricts the measurement of the sample's physicochemical properties, one must assert (based on literature research), the most important properties to be determined. In the case of thermokarst lakes, previous studies conducted on arctic regions indicate that the main physicochemical properties to be determined are temperature, dissolved oxygen, conductivity, pH and redox potential (dos Santos 2017). The depths of sample collection are selected based on the differences observed for those physicochemical properties.

During the storage of a sample, changes in the sample composition may occur. Therefore, ensuring its integrity is fundamental to the validity of the performed analyses. However, the diversity and different rates of processes undermine the possibility of a universal method for ensuring sample stability. Changes in sample composition occur mainly through chemical reactions, physical processes, biochemical reactions and photochemical reactions (Wardencki & Namiesnik 2002). For chemical reactions, reduction and oxidation processes, as well as hydrolysis of chemical substances are common. Absorption of CO_2 from the air induces changes in pH, which in turn may produce changes in sample composition; also, in samples containing HS, the presence of chlorine may prompt the formation of halomethanes. In terms of physical changes, volatilization, diffusion and adsorption are the main processes that are likely to occur. Volatilization can be minimized by completely filling the sample collection vessel; losses by adsorption can be minimized by a rapid preservation or by eliminating the sample's exposure to the atmosphere; diffusion of organic compounds can be controlled by collecting the sample in glass containers. Samples containing organisms generally require pH control (use of extreme conditions) or low temperatures, to minimize the degradation of the sample.

3.2.1 Water sampling method

Before sampling, each container was decontaminated, first immersing the containers in a NaOH solution (0.1 M) for 1h, and then left in HNO_3 (4.0 M) overnight. Upon this, the container should be thoroughly washed with Mili-Q water.

The collection process, executed during winter, resulted in the need to drill sampling holes in the ice, in order to access the water column. Water from lakes SAS-1A and SAS-2A were sampled at two different depths: surface and lake bottom. The air temperature during collection of SAS-2A was -25.8ºC, and -19.3ºC for SAS-1A. Water from lake SAS-1B (collected at air temperature of -14.9ºC) was collected at medium depth, as the lake displayed considerably low depth. SAS water samples were collected on March 2nd, 2018.

Although conventional sampling methods suggest completely filling the containers in order to avoid loss of compounds by volatilization, the extreme conditions of the sampling environment increased the risk of freezing the water sample, causing its expansion and ultimately breaking the glass bottle, prompting sample contamination and rendering the obtained results useless. Therefore, in order to avoid such risks, the sampling bottles were not completely filled. Upon collecting the water samples, aluminum foil was used to cover the top of the bottle, to avoid contamination. The bottles were stored at 4°C until analyses.

Each of the sampled lakes displayed different depths, ice thickness and accumulation of snow over the surface ice, with each of this parameter being described in Table 8.

Table 8 – Surface, medium and bottom sampling depths for SAS-1A, SAS-1B and SAS-2A, as well as the corresponding snow depth and ice thickness of each site.

	SAS-1A	**SAS-2A**	**SAS-1B**
Snow depth	0.5 m	0.5 m	0.5 m
Ice thickness	1.0 m	1.0 m	0.5 m
Surface lake depth	just below the ice	just bellow the ice	just below the ice
Medium lake depth	1.0 m	1.5 m	0.3 m
Bottom lake depth	1.3	2.5 m	0.6 m

Each of the collected water samples was adequately labelled and a name was attributed to each of these samples. The attributed identification and corresponding water sample are expressed in Table 9.

Table 9 – Attributed identification label for each of the collected water samples based on their sampled depth and location

Identification	Sample
SAS-1A SUP	Surface water from lake SAS-1A
SAS-1A F	Bottom depth water from lake SAS-1A
SAS-2A SUP	Surface water from lake SAS-2A
SAS-2A F	Bottom depth water from lake SAS-2A
SAS-1B M	Medium depth water from lake SAS-1B

3.2.2 Method of sediment sampling

Sediment samples were collected in all the sampled lakes, upon water collection, using a sediment corer. Both SAS-2A and SAS-1B sediments appeared to display considerable peat debris at the surface and clay at deeper depths, while SAS-1A sediments were mainly peat content. The removal of the sediment corer from the bottom of the thermokarst lake is displayed in Figure 8.

Figure 8 – Sampling of sediments from the thermokarst lake bottom, obtained using a sediment corer and stored in aluminum foil.

The sediments were collected directly from the lake bottom, preserved in aluminum foil and frozen until characterization.

3.2.3 Method of soil sampling

Soil samples from SAS-2A and SAS-1A were collected near the lakes, while the soil sample from SAS-1B was collected directly from the palsa nearby the lake. Sampling was conducted using a clean stainless steel ice screw, with the samples being directly transferred with a clean aluminum rod and preserved in aluminum foil, to be stored in a freezer. The sampling process is displayed in Figure 9, where a stainless steel ice screw drills the frozen soil to retrieve a soil sample.

Figure 9 – Small metallic corer used toi retrieve a soil sample from the lake margin, with the sample then promptly stored in aluminum foil and maintained frozen.

3.3 *In situ* physicochemical parameters of thermokarst lakes

The primary objective of the measurement of physicochemical properties is to guide the collection of water samples at depths displaying significant physicochemical changes. Vertical profiles of temperature, dissolved oxygen and pH are presented below.

In the field, the physicochemical conditions bellow the ice were measured *in situ* with a Hydrolab DS5 multi-probe sensor (OTT Hydromet), including temperature (ºC), pH, conductivity (µS/cm), salinity (%), total dissolved solids (mg/l) , total dissolved gas (mm Hg), and dissolved oxygen (saturation % and mg/L). The peristaltic pump used to sample water at medium and bottom depths was a Masterflex peristaltic pump. Data obtained from the Hydrolab probe sensor is expressed in Table 10, for the different lakes and depths.

The first noticeable feature in all three thermokarst lakes is the significant difference in depth; lake SAS-2A had the greatest depth of all sampled lakes reaching 2.7 m, while lake SAS-1A and SAS-1B revealed a bottom depth of 1.3 m and 0.6 m, respectively.

Table 10 - Data obtained from the Hydrolab DS5 multi-probe sensor for the different lakes at different depths.

Depth (m)	T (ºC)	pH	Conductivity (µS/cm)	Salinity (%)	Total dissolved solids (mg/l)	Total dissolved gas (mm Hg)	Dissolved oxygen (mg/L)
SAS-2A							
2.5	2.77	5.4	115.2	0.1	0.1385	786	0.09
2.25	2.37	5.09	110.2	0.05	0.0747	773	0.07
2	1.84	5.04	88.8	0.03	0.0572	766	0.06
1.75	1.43	5	80.8	0.03	0.0515	762	0.02
1.5	0.87	4.96	83.2	0.03	0.0533	757	0.07
1.25	0.6	4.94	83.5	0.03	0.0533	754	0.27
1	0.23	4.92	83.7	0.03	0.0535	750	0.73
0.75	0.28	4.92	85.1	0.03	0.0545	748	1.21
0.5	0.25	4,.93	86.5	0.03	0.0551	746	1.48
0.25	0.18	4.95	88.7	0.03	0.0556	745	1.9
0	0.17	5.03	87	0.03	0.0559	744	2.47
SAS-1A							
1.25	0.64	6.38	156.4	0.07	0.1003	774	23.7
1.0	-0.03	6.25	156.4	0.07	0.1001	779	17.2
0.75	-0.1	6.19	156.4	0.07	0.1004	783	14.4
0.5	-0.11	6.15	156.8	0.07	0.0999	739	11.2
0.25	-0.1	6.11	156.2	0.07	0.0999	794	3
0	-0.05	6.07	155.3	0.07	0.0999	804	1.4
SAS-1B							
0.5	-0.15	6.2	160.5	0.07	0.0961	782	18.9
0.25	-0.17	5.99	156.9	0.07	0.0973	786	9.7
0	-0.17	5.95	154.1	0.07	0.0984	788	3

The first noticeable feature in all three thermokarst lakes is the significant difference in depth; lake SAS-2A had the greatest depth of all sampled lakes reaching 2.7 m, while lake SAS-1A and SAS-1B revealed a bottom depth of 1.3 m and 0.6 m, respectively.

Before asserting any comments on the obtained profiles and values for the different physicochemical parameters measured at each lake, it must be noted that the three sampled lakes had different maximum depths. Any comparisons established between the vertical profiles in these lakes must be careful to take this aspect into account.

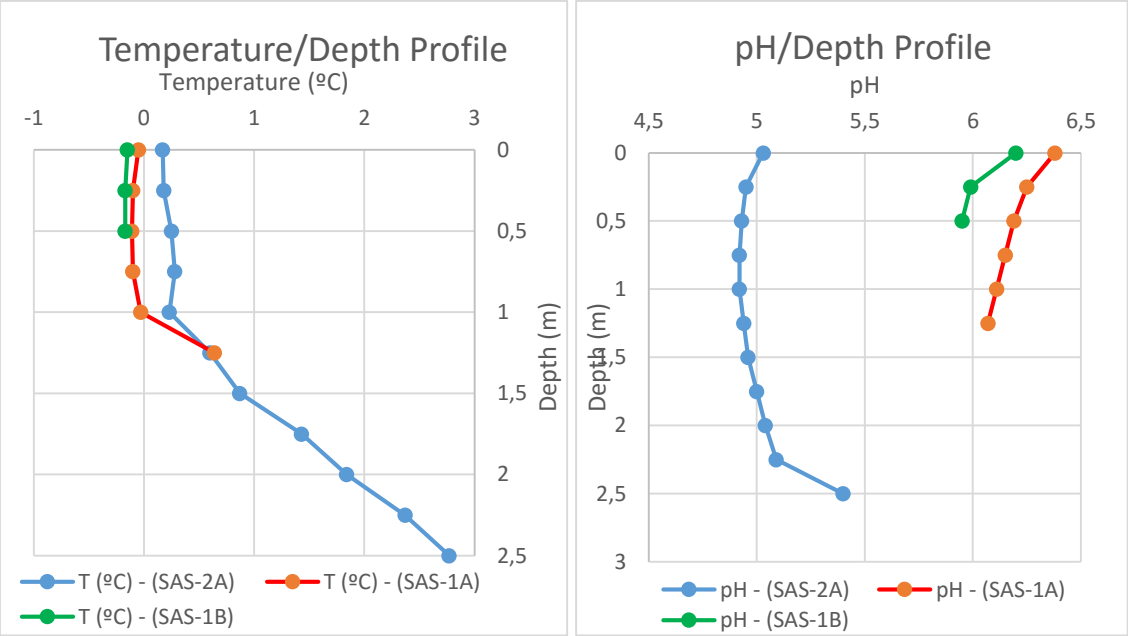

Figure 10a (left) – Temperature/depth vertical profile in all three SAS lakes. Figure 10b (right) – pH/depth vertical profile in all sampled SAS lakes (Blue line – lake SAS-2A; Red line – lake SAS-1A; Green line – lake SAS-1B).

Figure 10a displays the vertical profiles of temperature relative to depth. Due to the low depth of lake SAS-1B, no significant temperature variation is observed; however, lake SAS-1A maintains a relatively stable temperature (slightly below 0ºC) until a depth of one meter, rapidly increasing temperature for the following 25 cm. A similar trend is observed in lake SAS-2A (with a surface temperature of 0.17ºC), displaying an almost linear increase in temperature after reaching a depth of one meter.

Lakes SAS-1A and SAS-1B have a considerably higher pH when compared to lake SAS-2A, as displayed in Figure 10b. In all lakes, pH levels seem to lower during the first meter in depth; however, pH values started increasing at greater depths for lake SAS-2A.

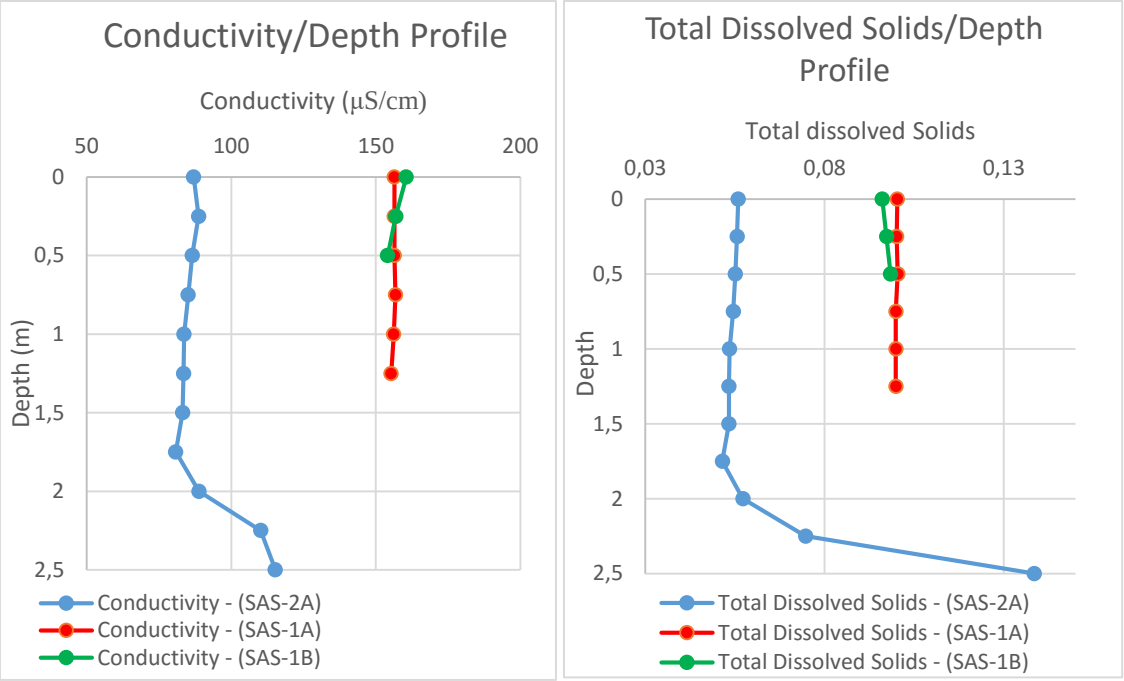

Figure 10c (left) – Conductivity/depth vertical profile in all three SAS lakes. Figure 10d (right) – Total dissolved solids/depth vertical profile in all three SAS lakes (Blue line – lake SAS-2A; Red line – lake SAS-1A; Green line – lake SAS-1B).

The trends exhibited for the vertical profiles of conductivity/depth and salinity/depth display considerable similarities. Lakes SAS-1A and SAS-1B displayed considerably higher conductivity and salinity values compared to lake SAS-2A. In both conductivity/depth and salinity/depth vertical profiles, little variation was noticed for depths below 2 m; however, below 2 m in depth, an increase in conductivity was verified for lake SAS-2A. This behavior is consistent with the idea of a higher ionic content in the bottom of deeper lakes, which would prompt a higher conductivity.

Total dissolved solids values are higher for lake SAS-1A and SAS-1B, while lake SAS-2A displays substantially lower values of total dissolved solids. Little changes in the total dissolved solids content in all lakes below 2 m deep; lake SAS-2A, at depths greater than 2 m exhibits a sizeable increase in total dissolved solids, as shown in Figure 10d. Total dissolved solids comprise the combined dissolved content of all organic and inorganic substances in a liquid whether it is in a molecular, an ionized, or a micro granular suspended form.

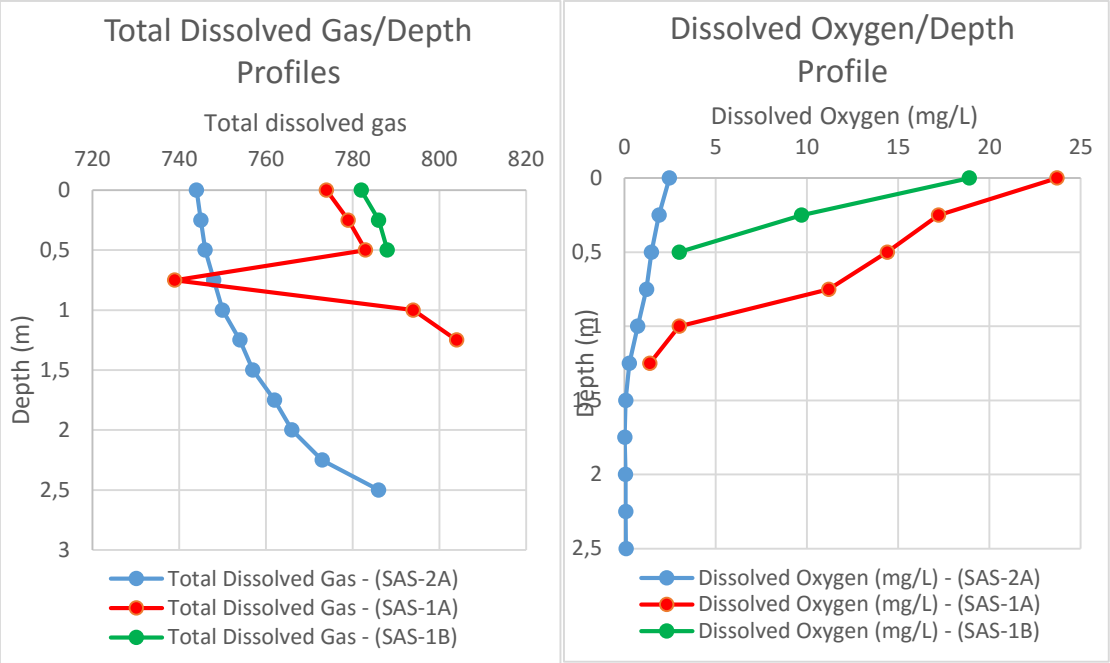

Figure 10e (left) – Total dissolved gas/depth vertical profile in all three SAS lakes. Figure 10f (right) – Dissolved oxygen/depth vertical profile in all three SAS lakes (Blue line – lake SAS-2A; Red line – lake SAS-1A; Green line – lake SAS-1B).

Figure 10e portrays the vertical profile of the variation of the total dissolved gas at different depths for all three SAS lakes. In the first 0.5 m below the surface, the total dissolved gas content in all lakes increased slightly; nevertheless, a sizeable drop was noticed at a 0.75 m depth for SAS-1A, assumed to be an erroneous measurement. The values of total dissolved gases grew increasingly higher for greater depths in lake SAS-2A. Nevertheless, lake SAS-1B appeared to display the highest values at lower depths, while SAS-1A exhibited slightly lower values.

Figure 10f exhibits the dissolved oxygen variation with depth for all sampled lakes, with lakes SAS-1A and SAS-1B displaying higher dissolved oxygen contents than lake SAS-2A. Nonetheless, these high dissolved oxygen values may be a result of the direct contact with the atmosphere upon drilling the ice, considering these values exhibit an enormous drop as the depth increases. Greater depths tend to display progressively lower dissolved oxygen values, as verified by the near anoxic conditions at the bottom of lake SAS-2A. Thawing and erosion of permafrost prompt an increase of the organic matter content in thermokarst lakes, the degradation of this organic matter requires the consumption of the existing dissolved oxygen.

4

Dissolved organic matter treatment and characterization

4.1 Filtration of the collected water samples

The water samples were pre-filtered using a 0.7µm pore filter with the aid of a water jet vacuum pump, in order to remove the portion of larger particulate matter present in the sample. Thereafter, the water sample was then filtered through a 0.45µm pore filter, the standard filter size for DOM, also with the aid of a water jet vacuum pump. The filters used during the filtration process were Whatman® Glass Microfibre Filters GF/F 0.7µm, and Durapore® Membrane Filters GF/F 0.45µm. In Figure 11a (on the left), the filtration through 0.7µm filters can be observed, whereas in Figure 11b (on the right), the previously filtered sample undergoes a new filtration using a 0.45µm filter.

Figure 11a (left) – Representation of the water sample filtration using a 0.7µm filter. Figure 11b (right) – Representation of the previously filtered water sample, undergoing a new filtration using a 0.45µm.

During the filtration process, the difference of color between different water samples became apparent, as SAS-1A SUP presented a lighter coloration compared to the other water samples, while SAS-1B M appeared to display the darkest shade of all water samples.

Both SAS-2A F and SAS-1B M displayed larger quantities of particulate matter in comparison to the remaining samples, having required two 0.7µm filters to successfully

filtrate the sample. After the 0.7μm filtration, the SAS-2A F water sample required ten 0.45μm filters to complete the 0.45μm filtration, while the remaining water samples required only five. Thus, SAS-2A F displayed a significantly higher quantity of particulate matter than the other water samples. Upon finishing the filtration process, each filter containing particulate matter was enclosed in aluminum foil, adequately labeled and stored in the freezer.

4.2 Dissolved organic carbon quantification of the dissolved organic matter samples

The determination of DOC was conducted using a wet-chemical oxidation method based on a UV-persulfate oxidation (Lopes et al. 2006). This technique is based on the oxidation of organic matter by a UV-persulfate oxidation into CO_2, which in turn will pass to a phenolphthalein solution, prompting a pH change, and a change in color. This color change will be detected through colorimetry. The use of standard solutions with known concentrations of carbon, allow to obtain a calibration curve, through which it is possible to quantify the carbon in the samples.

The UV-persulfate oxidation method was employed to quantify the organic carbon in each of the samples. The water used to prepare each reagent was bubbled with N_2 gas in order to remove all inorganic carbon prior to quantification. The DOC was measured with a Skalar (Breda, Netherlands) Sanþþ Automated Wet Chemistry Analyzer.

The DOC quantification of the DOM samples was performed after the 0.45µm filtration. The average C content of each DOM sample was calculated, as well as the standard error of the calibration curve, the detection limit, and the confidence intervals of the slope and the intercept. The presented average C content in Table 11 is the mean of two replicas of the respective sample.

Table 11 – Table containing the average C content in mg C/L for each of the DOM samples, as well as the associated standard deviation for the concentration.

Sample	Average C content (mg C/L)
DOM SAS-1A SUP	18.78 ± 1.52
DOM SAS-1A F	18.03 ± 1.52
DOM SAS-2A SUP	22.62 ± 1.52
DOM SAS-2A F	31.54 ± 1.52
DOM SAS-1B M	36.39 ± 1.52

The water sample DOM SAS-1B M displays the highest DOC content of all samples (Table 11); this considerable DOC content might be associated with its location, as lake SAS-1B is directly connected to a palsa, therefore, the NOM present in the palsa can be transferred into the lake, prompting a significant increase in its carbon content. Should this be the main source of DOM for lake SAS-1B, we expect to find a greater humic fraction compared to the other sampled lakes. However, SAS-1A displayed the lowest DOC content of the three lakes, with the surface sample containing a slightly higher DOC content than the bottom, the exact opposite of what happens in SAS-2A. Considering that the DOC content in the surface of lake SAS-1A is only slightly superior to the bottom, one cannot claim is a DOM input on the lake surface based solely on the small difference measured at different depths.

These samples were analyzed under UV-Visible spectroscopy to obtain the $SUVA_{254}$ values, which used with the DOC values expressed in Table 11, allowed to calculate the molar attenuation coefficient (ε). The table containing the $SUVA_{254}$ values and the corresponding molar attenuation coefficients for the different DOM SAS samples can be found in Section 1.3 of the Annex.

4.3 Solid-phase extraction of the dissolved organic matter

In order to characterize the organic matter present in the recovered water samples, it is vital to extract the organic matter, separating it from the inorganic component also comprised in the water samples. Prior to solid-phase extraction, 20 mL of each sample were withdrawn and used for DOC quantification, while the remainder of the filtered samples were acidified to pH 2.5 with HCl (37%) in order to increase extraction efficiency for phenols and organic acids. The acidified sample undergoes a solid-phase extraction using PPL resin, a styrene divinyl benzene polymer, as a sorbent (Dittmar et al. 2008).

The PPL resin's washing process consisted in three cycles of 20 mL of methanol, followed by three cycles of 100 mL of Milli-Q water, and returning to three cycles of 20 mL of methanol, with each cycle having the duration of 30 minutes (under magnetic stirring). Upon these cycles, the PPL resin was left in 20 mL of methanol for at least 4 hours, after which, the resin would be passed through 50 mL of Milli-Q water, followed by 50 mL of methanol and finally, 100 mL of HCl (0.01 M). Each cartridge had been rinsed with methanol in order to activate the PPL resin.

The supernatant liquid obtained upon centrifuging the sample was passed through the PPL) resin with the help of a vacuum pump, in order to fixate its organic matter content. Not more than 2 mmol of DOC or 10 L of sample were passed through 1 g of resin. Upon passing the totality of the supernatant liquid of the sample through the cartridge, the majority of the organic matter should be contained in the resin, as the remaining liquid, depleted of organic content, was recovered and labeled as global effluent, later to be analyzed in an attempt to determine the amount of organic matter fixated by the resin. Prior to DOM elution, the cartridge was also rinsed with 50 mL of 0.01M HCl, in order to completely remove the salts that might have been contained in the cartridge; this solution was also collected in order to determine the amount of organic carbon that might have been lost during this process.

Upon desalination, DOM was then eluted with 50 mL of methanol, using a nitrogen atmosphere to aid the elution, maintaining it at a sustainable pace; the eluted DOM was recovered in a glass container. A portion of the sample eluate, global effluent and the desalinization solution, recovered from the cartridge, were analyzed through ultraviolet-

visible spectroscopy, to assess the presence of organic matter, while the remaining eluate was stored at -20ºC for further characterization.

4.3.1 Acidification of the dissolved organic matter samples

The DOM SAS-1A SUP sample (initially at pH 6.38) was acidified to pH 2.49 through the addition of HCl (30%) resulting in the formation of a sizeable amount of particulate matter. The first attempt at solid-phase extraction was therefore unsuccessful, as the particulate matter completely blocked the PPL resin in the cartridge, rendering the fixation process useless. This attempt resulted in the loss of 2.25 g of PPL resin and 56 mL of DOM SAS-1A SUP sample. In order to properly conduct the fixation process, it would be necessary to separate the newly formed particulate matter and the rest of the water sample.

The water sample was transferred into centrifuge tubes (50 mL each) and centrifuged for 20 minutes at 6000 rotations per minute, in an attempt to separate the particulate matter from the supernatant liquid. The supernatant liquid was recovered to a previously decontaminated glass container, while the particulate fraction was transferred (using Milli-Q water) to a glass bottle. In order to centrifuge the totality of the SAS-1A SUP sample, this cycle was repeated seven times. Figures 10a and 10b clearly display the particulate matter in the sample prior and upon being centrifuged. After centrifuging the sample, the supernatant liquid containing the remaining dissolved organic carbon is almost colorless.

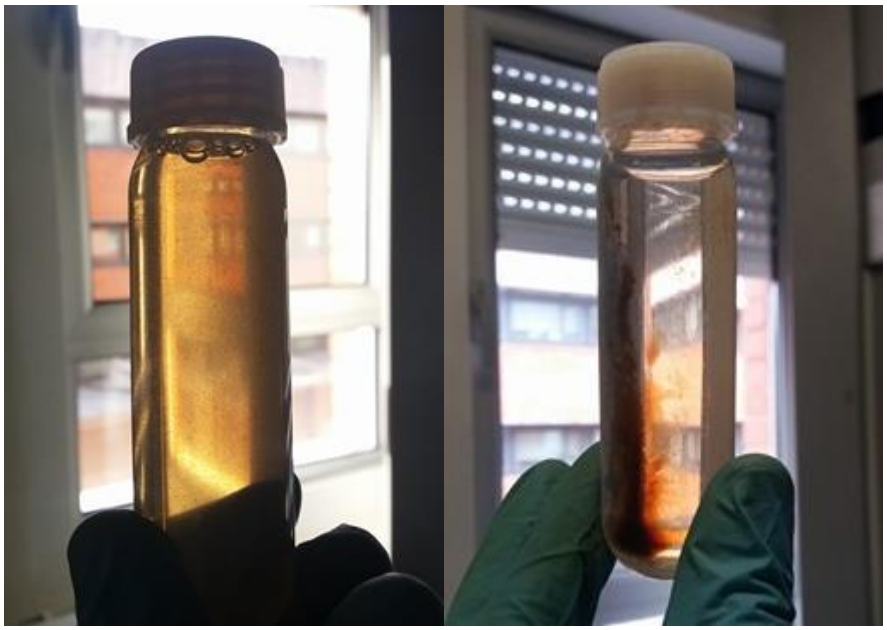

Figure 12a (left) – Acidified water sample prior to being centrifuged; Figure 12b (right) – Acidified water sample upon being centrifuged.

A total of 15 mL of supernatant liquid are to be used for DOC quantification, using UV-Visible spectroscopy and fluorescence spectroscopy, with the remainder of the sample being used for solid-phase extraction of organic matter. The bottle containing the particulate matter was frozen to preserve that portion of the sample. The expected approach towards the particulate matter, assumed to be HA, is to proceed to its desalination through dialysis, preparing the sample for further characterization. Figure 13 clearly shows the amount of particulate matter associated with the totality of the SAS-1A SUP water sample.

Figure 13 – Bottle containing the totality of the particulate fraction of SAS-1A SUP, formed upon being acidified to pH 2.5.

This precipitation phenomenon occurred in all of the collected water samples, however, the resulting supernatant liquid displayed significantly more color in SAS-2A samples than in SAS-1A samples. The DOM fraction still present in the supernatant liquid corresponds to the FA fraction of the original DOM sample, while the HA fraction precipitated upon acidification; therefore, in order to establish a clear distinction between the initial DOM present in the sample and remaining DOM upon acidification, the original filtered sample will be referred to as DOM SAS samples and the FA fraction of DOM will be referred to as FA SAS samples.

After completing the fixation of the FA SAS samples, the obtained eluates containing were frozen, upon which they would undergo lyophilization so as to remove any traces of water. The obtained lyophilized FA SAS samples' mass can be found in the Section 1.1.10 of the annex.

4.3.2 Fixation efficacy of fulvic acid samples – Specific ultraviolet absorbance

In an attempt to assess the efficacy of the fixation process, the global and desalination effluents, as well as the eluates resulting from the fixation process of each water sample, underwent UV/Visible spectroscopy. The SUVA at 254nm was obtained for each effluent eluate, and for the filtered water sample prior to fixation (used to establish comparisons) providing an indication of organic matter content and thus, allowing for the calculation of fixation percentages, desalination losses, recovery percentages, irreversible losses and non-fixated percentages. The equations associated with these factors are thoroughly explained below.

$$Fixation\ (\%) = \frac{SUVA254\ (Supernatant\ Liquid) - SUVA254\ (Global\ Effluent)}{SUVA254\ (Supernatant\ Liquid) \times Dilution\ Factor} \times 100 \quad (3)$$

A fixation percentage is the percentage of organic matter from the sample, the supernatant liquid (in this case), that is successfully fixated in the resin, with the organic matter present in the global effluent being non-fixated material. Thus, the lower the amount of carbon present in the global effluent, the more effective the fixation process. It should be noted that the equation contains no reference to the utilized volumes, as the volume of supernatant liquid that is fixated is equal to the volume obtained as global effluent.

$$Desal.losses(\%) = \frac{SUVA254\ (Desalination\ Effluent) \times V\ desalination\ effluent}{SUVA254\ (Supernatant\ Liquid) \times V\ supernatant\ liquid} \times 100 \quad (4)$$

The removal of the inorganic component during the desalination process (*Desal. losses*), is always associated with a small degree of organic matter loss from the extracted FA sample. It should be noted that considering the different volumes associated with the supernatant liquid and the desalination effluent, this factor is crucial and must be taken into account, as verified in both equation 4 and 5.

$$Recovery\ (\%) = \frac{SUVA254\ (Eluate) \times V\ eluate}{SUVA254\ (Supernatant\ Liquid) \times V\ supernatant\ liquid} \times 100 \quad (5)$$

A recovery percentage is the percentage of organic matter that is fully recovered from the resin and desalinized, referred to as eluate. The percentage of irreversible losses is quite simply the fixation percentage, without the percentage accounted for desalination losses and the recovery percentage, thus representing the percentage of organic matter that remained fixated in the resin upon the elution process. The percentage of non-fixated material is associated with the percentage of organic matter that is initially present in the supernatant liquid, but is not fixated in the resin during the fixation process.

The first results indicated poor recovery percentages of organic matter, urging the need to improve both the fixation of organic matter in the PPL resin, as well as its recovery. Table 12 showcases the first samples to undergo organic matter fixation in PPL resins. The totality of the FA SAS-1A SUP sample was fixated continuously, while the FA SAS-1A F sample was divided into two replicas.

Table 12 – Table containing the percentages associated with the recovery and loss of organic matter in the fixation process, for FA SAS-1A water samples.

Sample	**Fixation percentage (%)**	**Desalination losses (%)**	**Recovery percentage (%)**	**Irreversible loss (%)**	**Non-fixated percentage (%)**
FA SAS-1A SUP	69.92	1.80	52.43	15.69	30.08
FA SAS-1A F 1	77.69	3.03	44.91	29.74	22.31
FA SAS-1A F 2	67.54	3.42	60.91	3.21	32.45

Considering this and faced with the impossibility of using cartridges of larger capacity, we chose to fixate lower volumes (200 mL) of the supernatant liquid of the sample, in an attempt to improve the recovery percentages of the organic matter.

This alternative, although time-consuming, proved to be effective as the recovery percentages increased significantly, as described in Table 13. For FA SAS-2A SUP, FA SAS-2A F, and FA SAS-1B M however, nine replicas were conducted for each sample, with the average of losses and recovery percentages being presented in Table 13.

Table 13 – Table containing the percentages associated with the average recovery and loss of organic matter in the fixation process for FA SAS-2A SUP, FA SAS-2A F, and FA SAS-1B M water samples.

Sample	**Average fixation percentage**	**Average desalination losses**	**Average recovery percentage**	**Average irreversible loss**	**Average of non-fixated percentage**
	(%)	**(%)**	**(%)**	**(%)**	**(%)**
FA SAS-2A SUP	93.08	2.32	66.99	23.77	6.92
FA SAS-2A F	90.91	3.70	65.66	21.22	9.41
FA SAS-1B M	93.33	1.98	65.55	25.80	6.67

Comparing the observed changes expressed in Table 13, it becomes apparent that the average fixation percentage increased from the range of by approximately 20%, thus prompting a sizeable reduction in the non-fixated percentage from the initial 20-30%, to the final 6-9%. The recovery percentage also increased to an average of approximately 65%, significantly higher than the range of 44-60% verified in the SAS-1A samples.

4.3.3 Fixation efficacy of fulvic acid samples – dissolved organic carbon

In order to confirm the previously obtained fixation, desalination losses, and recovery percentages, each obtained component underwent DOC quantification. This assessment was necessary considering that the previously obtained percentages were based solely on the obtained values at $SUVA_{254}$.

The first DOC quantification was conducted with a total of three samples, SAS-1A SUP and the two replicas of SAS-1A F, comprising their supernatant liquid, global effluents, desalination effluents and eluates. The average DOC content obtained values for each of the fixation components of these samples are displayed in Table 14. The original table containing the measurements for each replica, the detection limit, the standard error and the confidence interval of the slope and intercept for all performed DOC measurements can be found in Section 1.1 of the annex.

Table 14 – The DOC quantification values of each fixation component for SAS-1A SUP and SAS-1A F samples, as well as their standard deviation.

Sample	Average C content (mg C/L)
SAS-1A SUP Eluate	283.0 ± 61.34
SAS-1A F - Replica 1 Eluate	170.5 ± 30.67
SAS-1A F - Replica 2 Eluate	193.4 ± 30.67
SAS-1A SUP – Desalination Effluent	4.0 ± 2.45
SAS-1A F - Replica 1 – Desalination Effluent	1.5 ± 1.23
SAS-1A F - Replica 2 – Desalination Effluent	10.0 ± 2.45
SAS-1A SUP Global Effluent	7.3 ± 2.45
SAS-1A F 1 - Global Effluent	11.9 ± 2.45
SAS-1A F 2 - Global Effluent	35.3 ± 2.45
SAS-1A SUP Supernatant Liquid	15.1 ± 3.07
SAS-1A F Supernatant Liquid	13.9 ± 3.07

Upon analyzing the obtained DOC values, it became apparent that the both global effluents and desalination effluents displayed abnormally higher carbon values than expected. For instance, the FA SAS-1A F 2 - Global Effluent, containing a similar volume to SAS-1A F Supernatant Liquid, displayed a significantly higher carbon content.

Taking into consideration the unexpected high carbon content in global effluents associated with the organic matter fixation process, it was theorized that during the resin washing procedure, the utilized 100 ml volume of Milli-Q water at pH 2 might be insufficient to

remove all traces of methanol in the resin, therefore prompting an increased carbon content in global effluents and desalination effluents.

4.3.3.1 Assessing the presence of methanol in fixation effluents

In an attempt to test this theory, two trials were conducted in order to assess the contribution of methanol to the carbon content measured in global and desalination effluents. The first trial consisted in three blanks (replacing the sample with Milli-Q water at pH 2), in which the resin washing method was conducted exactly as it was for the samples. However, upon passing 3 cartridge volumes of methanol, the blanks would be washed with 100 ml of Milli-Q water at pH 2 at room temperature (used for blank 1 and 2) and at 25ºC for the remaining blank (blank 3). The measured room temperature at the time of the resin wash was 20.5ºC.

The second trial would also be comprised of three blanks (blank 4, 5 and 6), in which the resin would be washed with 200 ml of Milli-Q water at pH 2 in all at room temperature (blank 4 and 6) and at 25ºC for the remaining blank (blank 5), conducting the entire washing process at a lower flow rate (as an attempt to remove a greater portion of methanol from the resin) in comparison to the first trial. While conducting the washing process, the cartridge associated with blank 6 fractured, reducing the second trial to blanks 4 and 5. The measured room temperature at the time of the resin wash was 21.5ºC.

Table 15 – Dissolved organic carbon (DOC) values associated with the global and desalination effluents, as well as the eluates, of the fixation blanks. Experiments 1, 2 and 3 were conducted in the first trial, while experiments 4 and 5 were conducted in the second trial.

Sample	**Average real C content (mg C/L)**
Fixation Blank – Global Effluent 1	13.61 ± 1.68
Fixation Blank – Global Effluent 2	9.28 ± 1.68
Fixation Blank – Global Effluent 3	6.89 ± 0.84
Fixation Blank – Global Effluent 4	8.45 ± 0.25
Fixation Blank – Global Effluent 5	3.15 ± 0.25
Fixation Blank – Dessalination Effluent 1	8.82 ± 0.08
Fixation Blank – Dessalination Effluent 2	8.80 ± 0.08
Fixation Blank – Dessalination Effluent 3	5.53 ± 0.84
Fixation Blank – Dessalination Effluent 4	0.86 ± 0.08
Fixation Blank – Dessalination Effluent 5	0.83 ± 0.08
Fixation Blank – Eluate 1	1.14 ± 0.17
Fixation Blank – Eluate 2	0.82 ± 0.08
Fixation Blank – Eluate 3	1.02 ± 0.08
Fixation Blank – Eluate 4	1.31 ± 0.25
Fixation Blank – Eluate 5	2.14 ± 0.25
H_2O MQ pH 2	0.00 ± 0.08

The obtained global and desalination effluents, as well as the eluate, were analyzed using UV-visible spectroscopy and have undergone carbon quantification through DOC. Considering that methanol does not absorb in the 200-500 nm range, it was expected that UV-visible spectroscopy would be unable to provide information regarding the amount of methanol in the global and desalination effluents. The DOC quantification however, would be suitable to detect the presence of methanol in the conducted trials. The information displayed in Table 15 displays the obtained results, clearly indicating a significantly higher carbon content for global effluents in the first trial, when compared to the global effluents of

the second trial, proving that there is methanol being passed into the global and desalination effluents. The presence of such a sizeable carbon content, could only be attributed to the presence of methanol in both global and desalination effluents. This presence of methanol in the global and desalination effluents, displayed variations between columns with different resin washing proceedings. Passing through the resin a greater volume of Milli-Q water allowed to remove a substantially greater quantity of methanol, as displayed by the carbon content difference between desalination effluents 4 and 5 (200ml of Milli-Q water used to wash the resin prior to fixation), and desalination effluents 1, 2 and 3 (100ml of Milli-Q water used to wash the resin). Thus, the washing procedure we had used during the fixation process of most of the samples was insufficient to remove traces of methanol from the resin.

Remaining only one sample that had not undergone the fixation process (FA SAS-1B M), the resin washing procedure was altered, increasing the volume of Milli-Q water to 200ml, so that the removal of methanol would be more successful. A table containing the percentages for all replicas of each sample can be found in the Section 1.1 of this work.

Table 16 – Average fixation, non-fixated, desalination and irreversible losses, and recovery percentage calculated using the obtained DOC values for each of the fixation components obtained for each sample.

DOC Values	FA SAS-1A SUP	FA SAS-1A F	FA SAS-2A SUP	FA SAS-2A F	FA SAS-1B M
Fixation (%)	51.83	-70.27	-267.43	-535.84	69.21
Desalination losses (%)	0.59	1.81	11.02	64.63	4.55
Recovery(%)	41.54	59.47	79.36	84.45	76.00
Irreversible losses (%)	9.70	-131.55	-357.81	-749.54	-11.35
Non-fixated (%)	48.17	170.27	367.43	704.92	30.79

Upon obtaining the average fixation, desalination losses, and recovery percentages of all fixation experiments of every sample, as displayed in Table 16, it became clear that the DOC results obtained with FA SAS-1B M samples had considerably less methanol than the previous samples, and thus, displaying a less atypical fixation percentage than verified in FA SAS-1A and FA SAS-2A samples. The table containing the percentages associated with each of the obtained replicas is expressed in the Section 1.2.3 of the annex.

4.3.3.2 Comparison between specific ultraviolet absorbance and dissolved organic carbon quantification of the fixation process

As previously referred, the fact that the methanol used in the resin washing process is partly retained in the resin, gives rise to a significantly higher carbon content in global and desalination effluents. Thus, when comparing the obtained percentages from DOC quantification and $SUVA_{254}$, it is crucial to realize that the fixation percentage, the non-fixated percentage, the percentage of desalination losses, and the percentage of irreversible losses are not comparable, since the presence of methanol cannot be measured using $SUVA_{254}$.

The presence of methanol is quite apparent in the atypical average fixation percentages and the average percentage of desalination losses of DOC compared to the average obtained percentages in $SUVA_{254}$, as verified in Table 17 (next page). The tables containing a direct comparison between DOC and $SUVA_{254}$ percentages of all replicas of each sample can be found in the Section 1.2.3 of the annex.

The average recovery percentages obtained from DOC and $SUVA_{254}$ did not display extreme differences as verified for the other percentages. However, with the exception of FA SAS-1A SUP, the average recovery percentages obtained from DOC quantification were higher than the average recovery percentages associated with $SUVA_{254}$. It should be noted that the DOC percentages for FA SAS-1B M are significantly closer to the percentages obtained in $SUVA_{254}$, as a result of the fixation method changes that arose from the methanol detection during the extraction process.

Table 17 – Comparison between the average fixation percentage, the average non-fixated percentage, the average percentage of desalination losses, average recovery percentage, and the average percentage of irreversible losses obtained from DOC and $SUVA_{254}$ values.

DOC	FA SAS-1A SUP	FA SAS-1A F	FA SAS-2A SUP	FA SAS-2A F	FA SAS-1B M
Fixation (%)	51.83	-70.27	-267.43	-535.84	69.21
Desalination losses (%)	0.59	1.81	11.02	64.63	4.55
Recovery (%)	41.54	59.47	79.36	84.45	76.00
irreversible losses (%)	9.70	-131.55	-357.81	-749.54	-11.35
Non-fixated (%)	48.17	170.27	367.43	704.92	30.79

$SUVA_{254}$	FA SAS-1A SUP	FA SAS-1A F	FA SAS-2A S	FA SAS-2A F	FA SAS-1B M
Fixation (%)	69.92	72.62	93.08	90.91	93.33
Desalination losses (%)	1.80	3.23	2.32	3.70	1.98
Recovery (%)	52.43	52.91	66.99	65.66	65.55
irreversible losses (%)	15.69	16.47	23.77	21.22	25.80
Non-fixated (%)	30.08	27.38	6.92	9.41	6.67

4.4 Fluorescence spectroscopy of dissolved organic matter and fulvic acid samples

The fluorescence spectra were recorded on a JASCO spectrophotometer, model FP-6500; the obtained EEMs involved scanning and recording of individual emission spectra (250-600 nm) with sequential increments of 10 nm for the excitation wavelength (225-450 nm). The peaks were recorded at a scan speed of 1000 nm/min using emission and excitation band widths of 5 nm. It should be noted that every DOM SAS and FA SAS sample was diluted by a factor of 10, using Milli-Q water.

Scatter signals on EEM spectra are generally large and pose a challenge for a clearer peak identification in the obtained EEM spectra. All fluorescence EEMs were processed via MATLAB (Matlab R2015a), isolating not only the water Raman scatter, but also the first- and second-order Rayleigh scattering, removing them from the original EEM spectra. Figure 14a and 14b showcase the EEM fluorescence spectra for DOM SAS-2A SUP with the water Raman scattering as well as the first- and second-order Rayleigh scattering bands (Figure 14a), and without these scattering bands (Figure 14b).

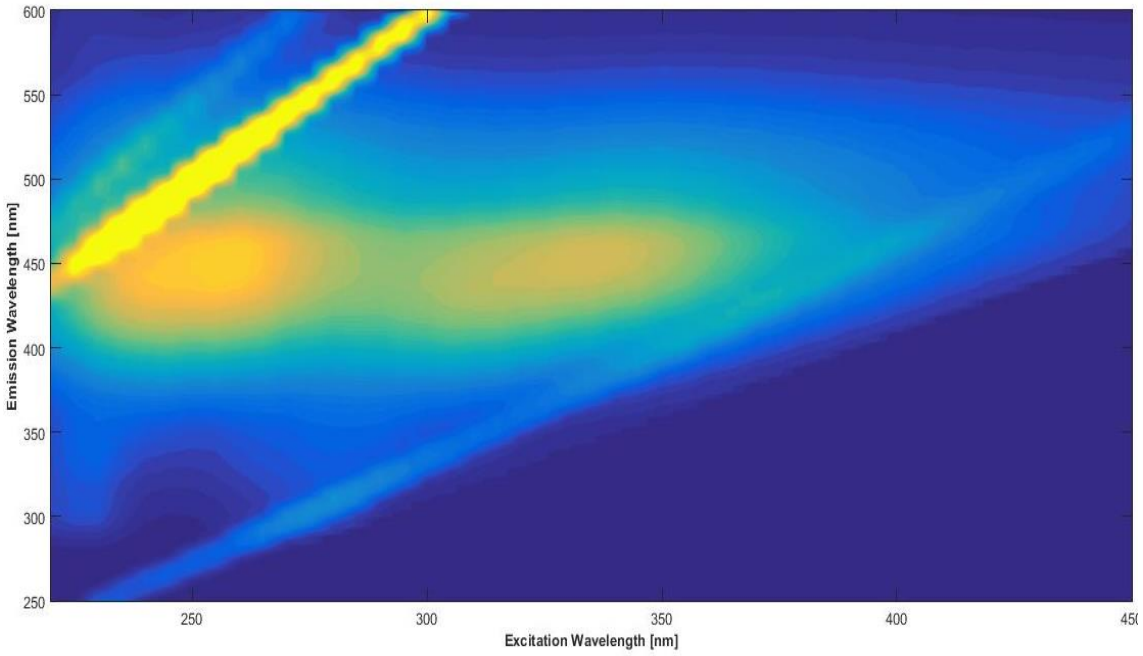

Figure 14a – Two-dimensional EEM of DOM SAS-2A SUP, containing the water Raman scattering band as well as the first- and second-order Rayleigh scattering bands.

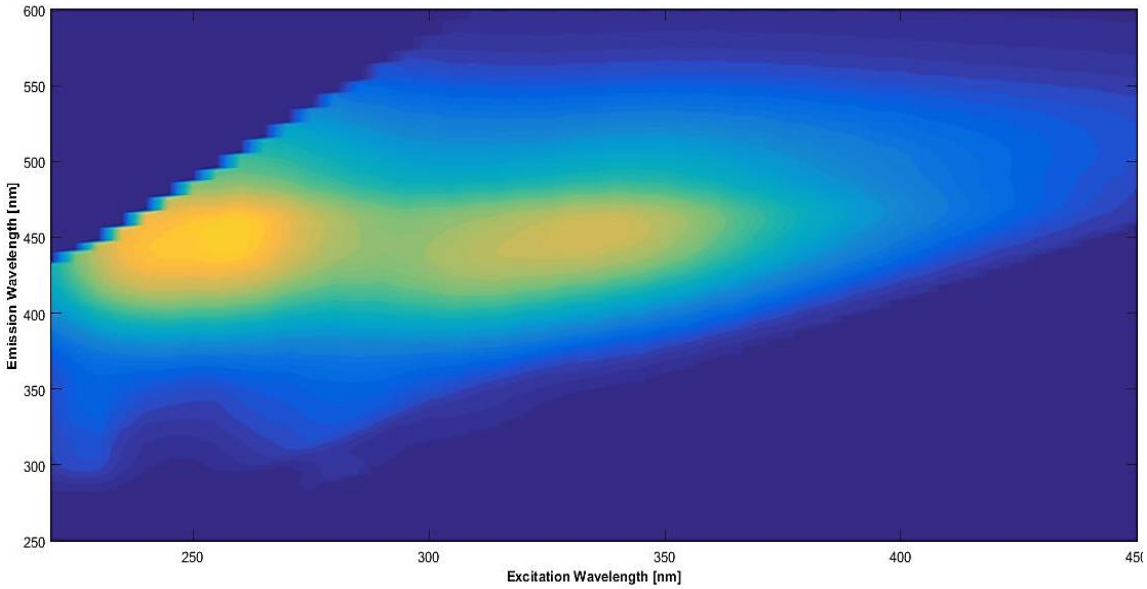

Figure 14b – Two-dimensional EEM of DOM SAS-2A SUP upon removing the Raman and Rayleigh scattering bands.

4.4.1 Fluorescence excitation-emission matrices of dissolved organic matter samples

The EEM fluorescence spectra was obtained for all of the DOM samples, using a dilution factor of 10, exposing mainly two primary peaks in all samples, peak A and peak C. These peaks are consistently associated with humic-like substances, as one would expect in samples obtained from thermokarst lakes. In the obtained matrix it is also possible to observe two peaks of lower intensity, peak T and peak B, usually associated with "fresh" DOM. The specific locations of each of the observed peaks in the DOM sample EEMs were obtained and used to comprise Table 18.

Considering the data displayed in Table 18, none of the specific peak locations seemed to differ significantly from different DOM samples; this is an important notion, as there are a number of factors that may prompt significant change in the specific location of a designated fluorescence peak.

Table 18 – Specific locations of peak A, C, T and B in the obtained EEMs for DOM SAS lake samples.

Sample	Peak A	Peak C	Peak T	Peak B
DOM SAS-1A SUP	255 Ex. λ/	335 Ex. λ/	280 Ex. λ/	280 Ex. λ/ 2
	444 em. Λ	450 em. λ	338 em. λ	96 em. Λ
DOM SAS-1A F	255 Ex. λ/	335 Ex. λ/	280 Ex. λ/	280 Ex. λ/
	444 em. Λ	452 em. λ	322 em. λ	304 em. Λ
DOM SAS-2A SUP	260 Ex. λ/	335 Ex. λ/	280 Ex. λ/	280 Ex. λ/
	454 em. Λ	452 em. λ	324 em. λ	296 em. Λ
DOM SAS-2A F	260 Ex. λ/	335 Ex. λ/	280 Ex. λ/	285 Ex. λ/
	448 em. Λ	448 em. λ	326 em. λ	302 em. Λ
DOM SAS-1B M	255 Ex. λ/	335 Ex. λ/	285 Ex. λ/	290 Ex. λ/
	444 em. Λ	448 em. λ	342 em. λ	294 em. Λ

As previously referred, the use of peak ratios and indexes can further provide insight, into the nature of DOM samples when relying on fluorescence spectroscopy. Thus, having located the different peaks comprised in the EEMs of the different DOM samples, a set of peak ratios and indexes, previously explained in the introduction part, were calculated with the purpose of characterizing the different DOM samples, as well as gaining insight regarding their source and origin.

Table 19 – Calculated ratios and indexes, previously introduced and explained, associated with the different DOM samples under study.

	DOM SAS-1A SUP	DOM SAS-1A F	DOM SAS-2A SUP	DOM SAS-2A F	DOM SAS-1B M
C:A ratio	0.80	0.80	0.85	0.84	0.83
C:T ratio	2.81	7.12	6.54	8.24	4.71
A:T ratio	3.54	8.94	7.72	9.76	5.70
BIX	0.46	0.41	0.35	0.43	0.38
β:α	0.42	0.40	0.35	0.43	0.37
HIX (Equation 1)	6.54	11.3	14.55	15.23	15.53
HIX (Equation 2)	0.87	0.92	0.94	0.94	0.94
FI	1.52	1.50	1.44	1.60	1.43

Analyzing the C:T and A:T peak ratios, it became apparent that DOM SAS-1A F, DOM SAS-2A SUP and DOM SAS-2A F display similar values, with a range interval suggesting a considerable humic content, as it would be expected. However, even though DOM SAS-1B M displayed lower values than these three samples, the lowest C:T and A:T peak ratios resulted from DOM SAS-1A SUP. DOM SAS-1A SUP presented a C:T and a A:T ratio of 2.812 and 3.538, respectively; values considerably inferior to those observed even in the same lake (DOM SAS-1A F), suggesting the presence of a sizeable quantity of "fresh" DOM, in the surface portion of the SAS-1A lake. The C:A ratio displays slight change throughout the different DOM samples, with SAS-1A lake values displaying the lowest values, possibly suggesting a slightly inferior proportion of degraded material when compared to SAS-2A and SAS-1B lakes.

The obtained EEMs have not undergone any sort of in-depth fluorescence data correction, so the fluorescence index (FI) used was the same as McKnight (McKnight et al. 2001) used on uncorrected emission spectra. The obtained values for FI all display little variation, ranging between 1.4 and 1.6, reinforcing the idea that all DOM samples displayed mainly

plant/terrestrial derived. Considering that the DOM samples come from thermokarst lakes, and their organic matter content mainly arises from the degraded permafrost, the obtained FI values and their suggestion is not unexpected.

It must be noted that the calculated HIX values in this work are merely an approximation to HIX Equation 1 (Zsolnay et al. 1999) and Equation 2 (Ohno 2002). In the obtained EEMs, the excitation wavelength interval is 5 nm, and the emission wavelength interval is 2 nm; HIX should be obtained at an excitation wavelength of 254 nm, in an emission interval of both 300-345 nm and 435-480 nm (Cox et al. 2000). Therefore, in the obtained EEMs, there is no measurement for an excitation wavelength at 254 nm, and emission wavelengths are always even numbers. An attempt to perform an approximation to the HIX value was obtained at an excitation wavelength of 255 nm, for an emission interval of both 300-346 nm and 434-480 nm.

The approximation HIX values obtained for DOM SAS-1A samples are lower than the in the other samples, with DOM SAS-1A SUP showcasing nearly half the HIX approximation value of DOM SAS-1A F. A presence of such a low HIX approximation value reinforces the notion that DOM SAS-1A SUP might have a considerable “fresh” DOM contribution.

Although BIX and the β:α index were not particularly appropriate for DOM samples from this nature, considering the absence of a noticeable M peak, these indexes were calculated just as a safeguard, meant to assess whether the results suggest a very low marine autochtonous component. Considering that the obtained values are well below 0.6, the results are consistent with the expected values.

The obtained data from the fluorescence scan has undergone data treatment, so as to remove the second order Rayleigh scatter line, in order to make the fluorescence peaks in the EEMs more noticeable and differentiated. Using the obtained intensity matrices, two different sets of graphic representations of the EEM were obtained: A two-dimensional contour plot and a three-dimensional surface plot, allowing for a clearer peak identification. The obtained 2D and 3D EEMs obtained for each DOM sample are expressed from Figure 15a to Figure 15e, aligning the most noticeable peaks visible in the graphic representation. It should be noted that the intensities of each plot were adjusted in order to better display the existing peaks.

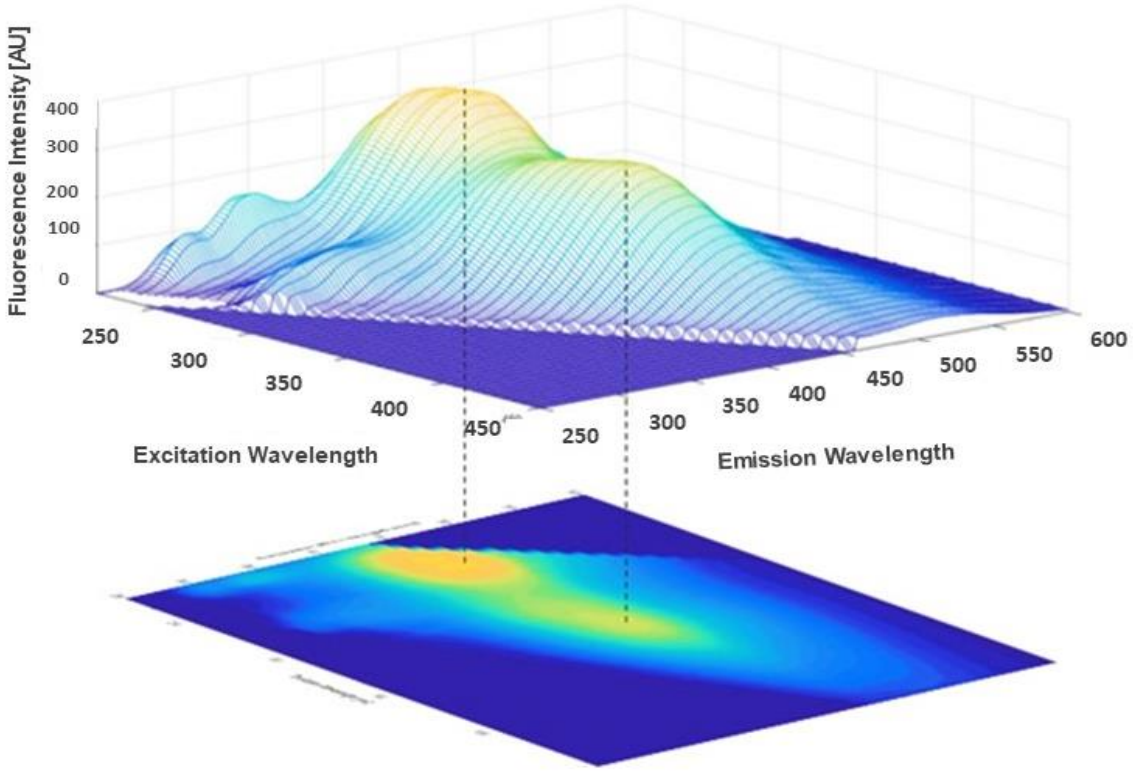

Figure 15a – Two-dimensional and three-dimensional graphic representation of the obtained EEMs for DOM SAS-1A F.

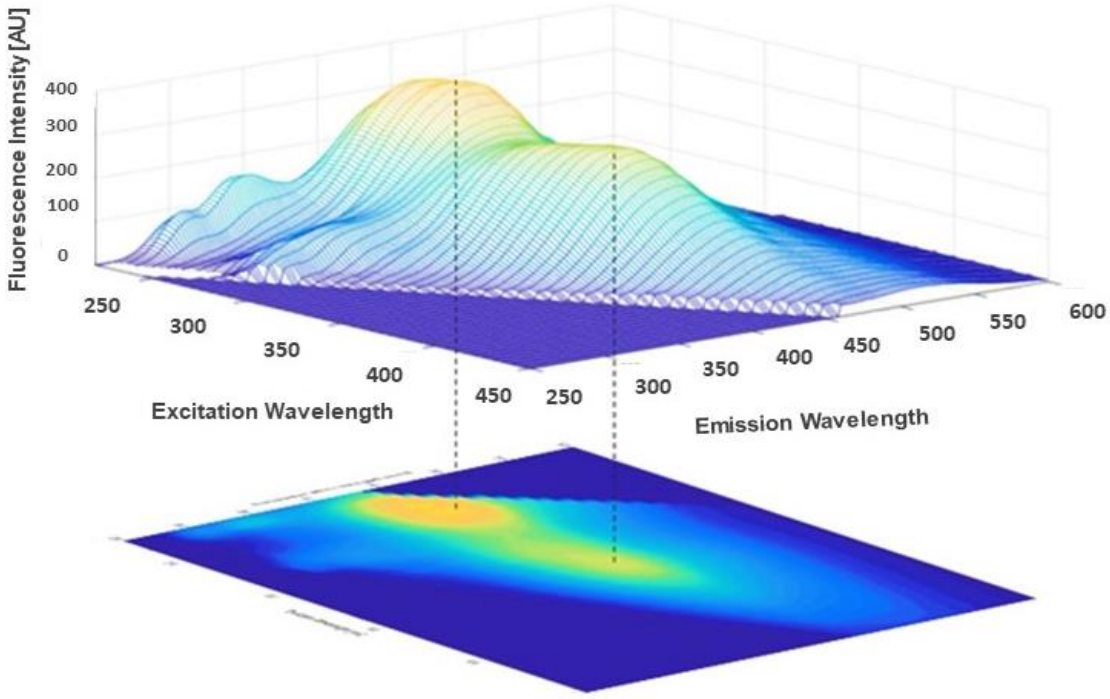

Figure 15b – Two-dimensional and three-dimensional graphic representation of the obtained EEMs for DOM SAS-1A SUP.

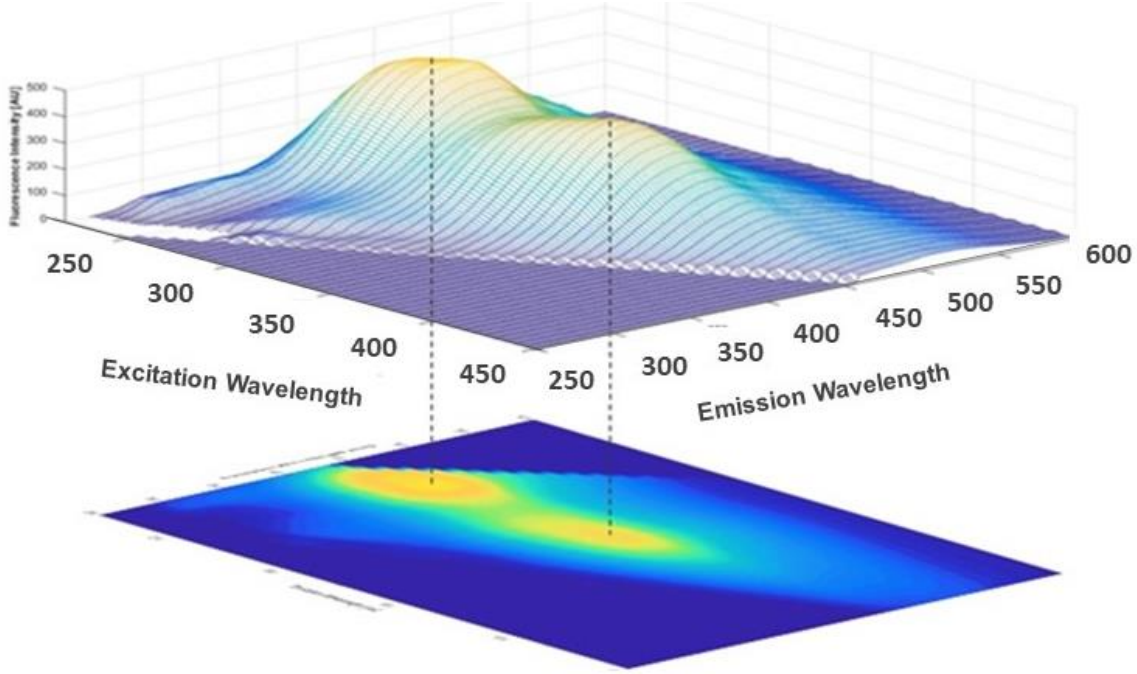

Figure 15c – Two-dimensional and three-dimensional graphic representation of the obtained EEMs for DOM SAS-2A F.

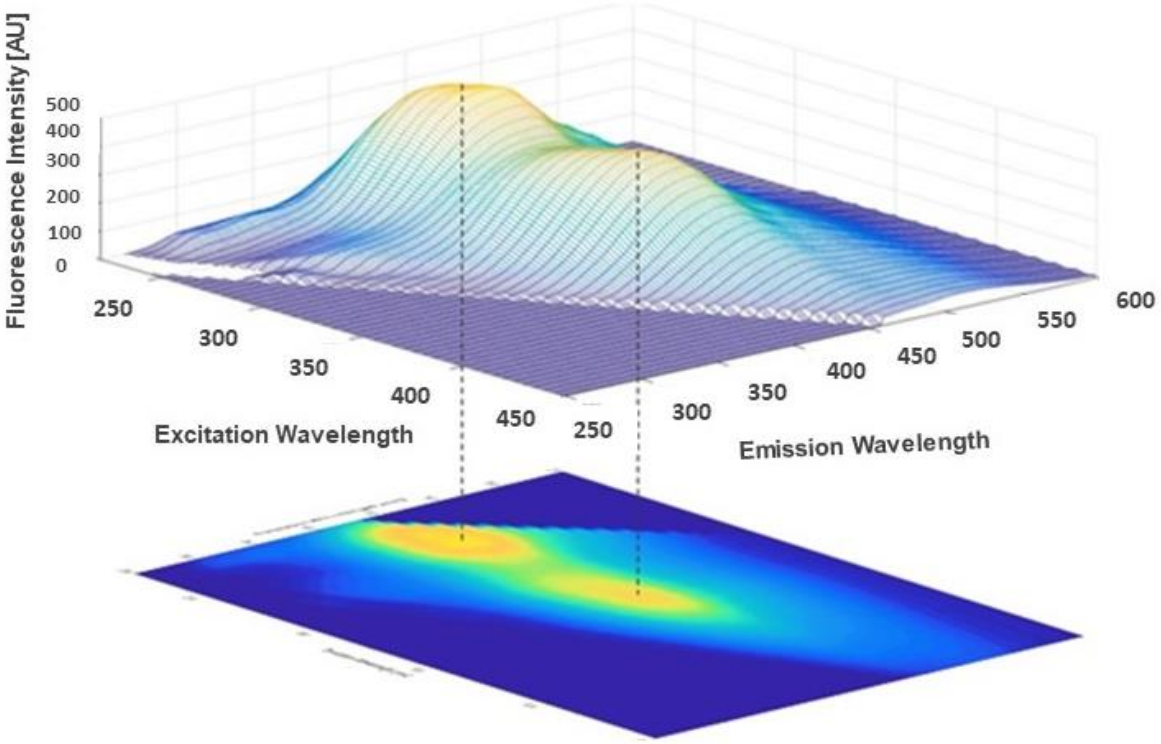

Figure 15d – Two-dimensional and three-dimensional graphic representation of the obtained EEMs for DOM SAS-2A SUP.

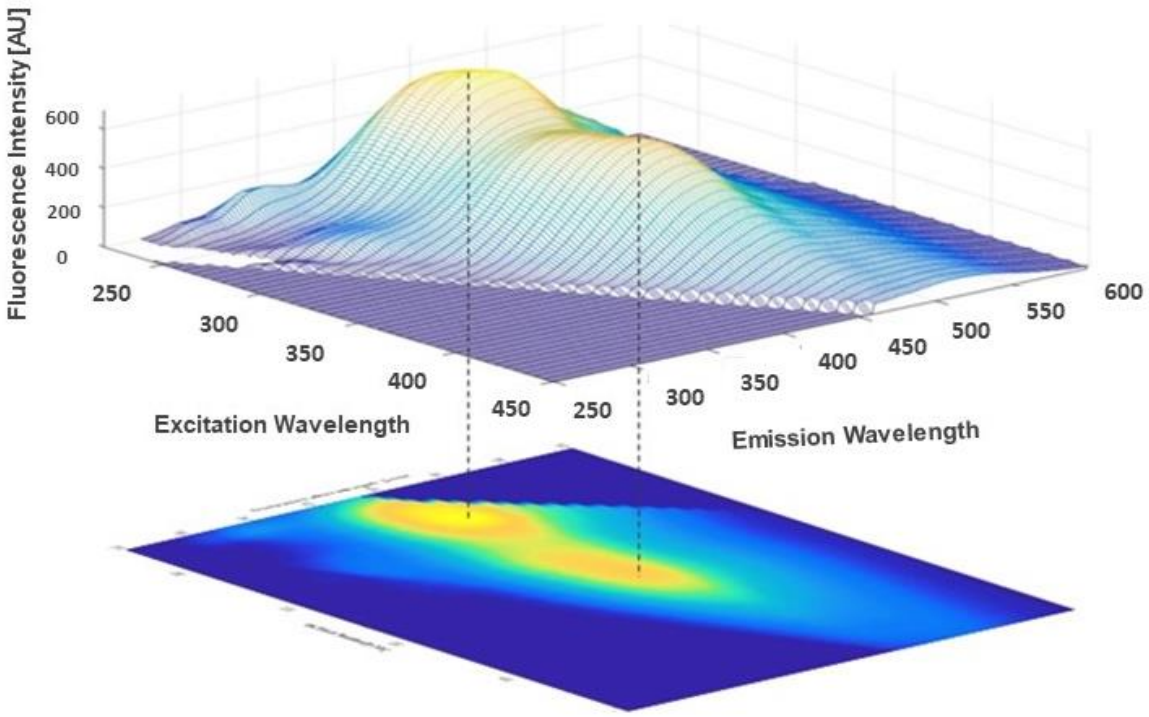

Figure 15e – Two-dimensional and three-dimensional graphic representation of the obtained EEMs for DOM SAS-1B M.

4.4.2 Fluorescence excitation-emission matrices of fulvic acid samples

As previously stated, the acidification of the DOM sample prior to extraction, prompted the precipitation of the HA portion of the sample. Upon the removal of the particulate HAs present in the sample, the remaining DOM was assumed to be the FA component.

Therefore, each of the FAs resulting from each DOM sample was analyzed once again using fluorescence spectroscopy and the resulting EEMs were compared to the original DOM sample EEMs, in order to assess whether there are significant changes. The main peaks comprised in the obtained EEMs for the FA SAS samples were detected, and their locations were expressed in Table 20. It should be noted that peak B was not noticeable in all FA SAS sample EEMs.

Table 20 – Specific locations of peak A, C, T and B in the obtained EEMs for FA SAS samples.

Sample	Peak A	Peak C	Peak T	Peak B
FA SAS-1A SUP	255 Ex. λ/ 440 em. λ	335 Ex. λ/ 448 em. λ	255 Ex. λ/ 358 em. λ	280 Ex. λ/ 296 em. Λ
FA SAS-1A F	245 Ex. λ/ 438 em. λ	330 Ex. λ/ 460 em. λ	275 Ex. λ/ 316 em. λ	-
FA SAS-2A SUP	255 Ex. λ/ 456 em. λ	335 Ex. λ/ 452 em. λ	275 Ex. λ/ 316 em. Λ	-
FA SAS-2A F	250 Ex. λ/ 438 em. λ	330 Ex. λ/ 448 em. λ	275 Ex. λ/ 316 em. λ	-
FA SAS-1B M	250 Ex. λ/ 448 em. λ	335 Ex. λ/ 454 em. λ	275 Ex. λ/ 316 em. λ	-

In the EEMs of FA SAS-1A and FA SAS-2A samples, the locations of peak A and C displayed little variation between DOM samples and FA samples, with slight shifts in the emission wavelengths, and slight variations in the excitation wavelength. However, peak T in the EEM of FA SAS-1A SUP appeared to be located at considerably lower excitation wavelength (a variation of 25 nm in comparison to the DOM sample) and displaying an emission wavelength shift from 338 nm to 358 nm; this red shift can be associated with changes to the molecular structure of the "fresh" DOM, during the acidification process used to separate the HA and the FA fractions. The remaining FA samples did not display such a considerable variation in the location of peak T in comparison to DOM samples. The presence of peak B was only noticeable in FA SAS-1A SUP, not being noticed in the remaining FA SAS samples' EEMs.

Table 21 – Calculated ratios and indexes, previously introduced and explained, associated with the different FA samples.

	FA SAS-1A SUP	FA SAS-1A F	FA SAS-2A SUP	FA SAS-2A F	FA SAS-1B M
C:A ratio	0.88	0.89	0.87	0.94	0.90
C:T ratio	0.74	5.70	9.69	6.95	12.96
A:T ratio	0.83	3.66	11.09	7.41	14.34
BIX	0.55	0.52	0.49	0.49	0.39
HIX (Equation 1)	1.83	7.20	18.54	10.59	18.30
HIX (Equation 2)	0.65	0.88	0.95	0.91	0.95
FI	1.61	1.68	1.39	1.64	1.49

The C:A peak ratios have clearly shown an increase in all FA SAS samples in comparison with the respective DOM SAS sample; considering that higher degradation is associated with lower C:A ratios, the increase in C:A peak ratio values on FA fractions suggests these fractions contain less degraded matter than the original DOM sample.

Both C:T and A:T peak ratios in FA SAS samples have lowered for FA SAS-1A SUP, FA SAS-1A F and FA SAS-2A F, suggesting that upon separating HA and FA from the original DOM sample, the majority of the "fresh" DOM was comprised in the FA fraction. It should be noted that the only A:T and C:T peak ratio bellow 1.0 is associated with FA SAS-1A SUP, strengthening the notion of a "fresh" DOM input at the surface of lake SAS-1A.

The HIX approximation of FA samples compared to the original DOM samples, similarly to C:T and A:T peaks, has displayed lower values for FA SAS-1A SUP, FA SAS-1A F and FA SAS-2A F, prompting the idea that these FA samples contain a lower relative humic content; FA SAS-2A SUP and FA SAS-1B M however have an increased HIX approximation value compared to their original DOM values, associated with a higher relative humic content.

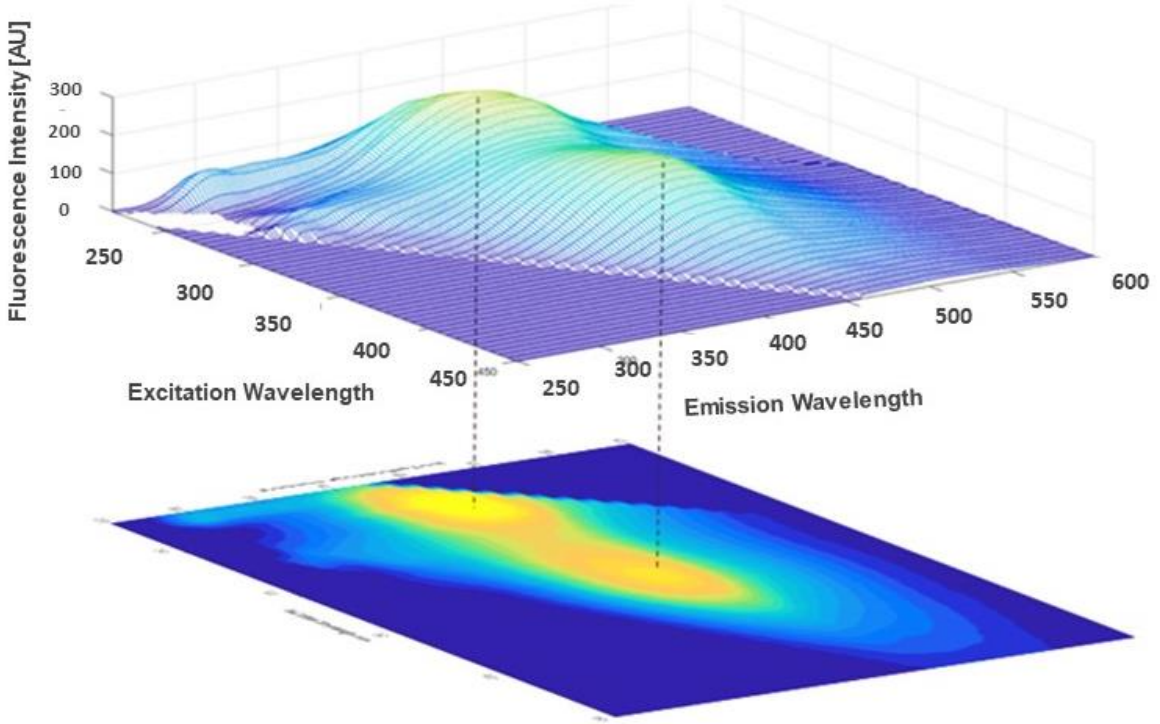

Figure 16a – Two-dimensional and three-dimensional graphic representation of the obtained EEMs for FA SAS-1A F.

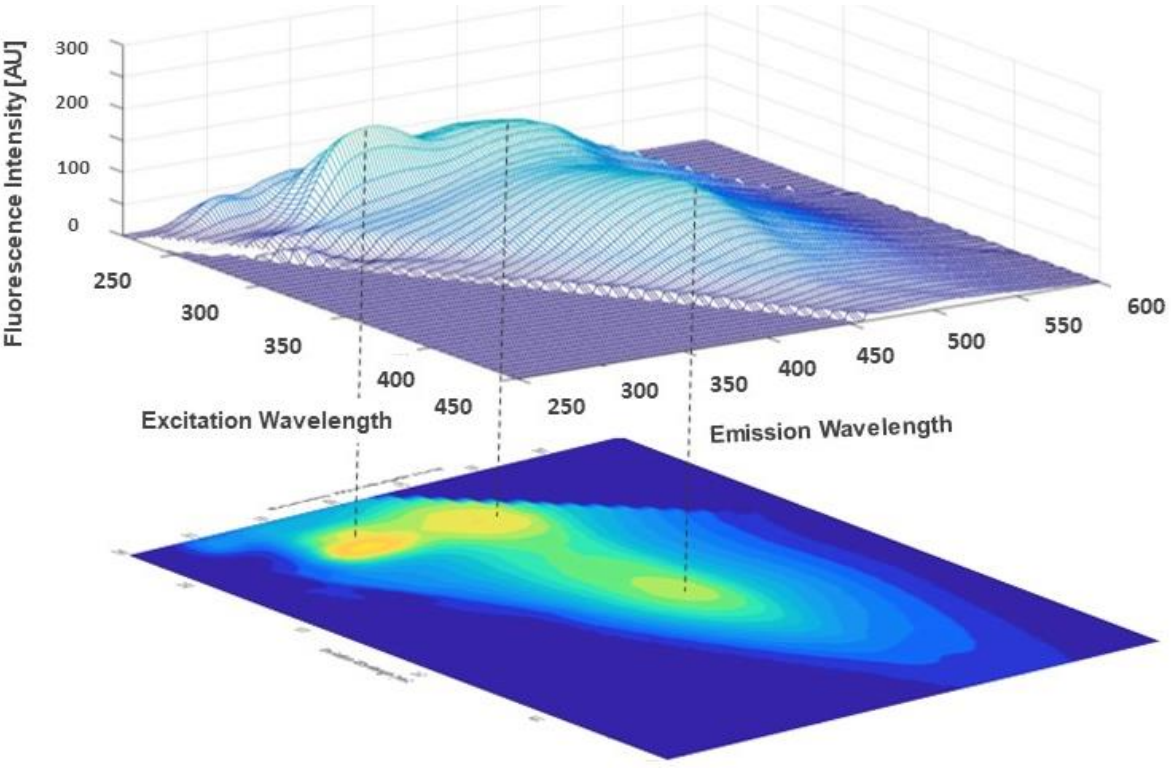

Figure 16b – Two-dimensional and three-dimensional graphic representation of the obtained EEMs for FA SAS-1A SUP.

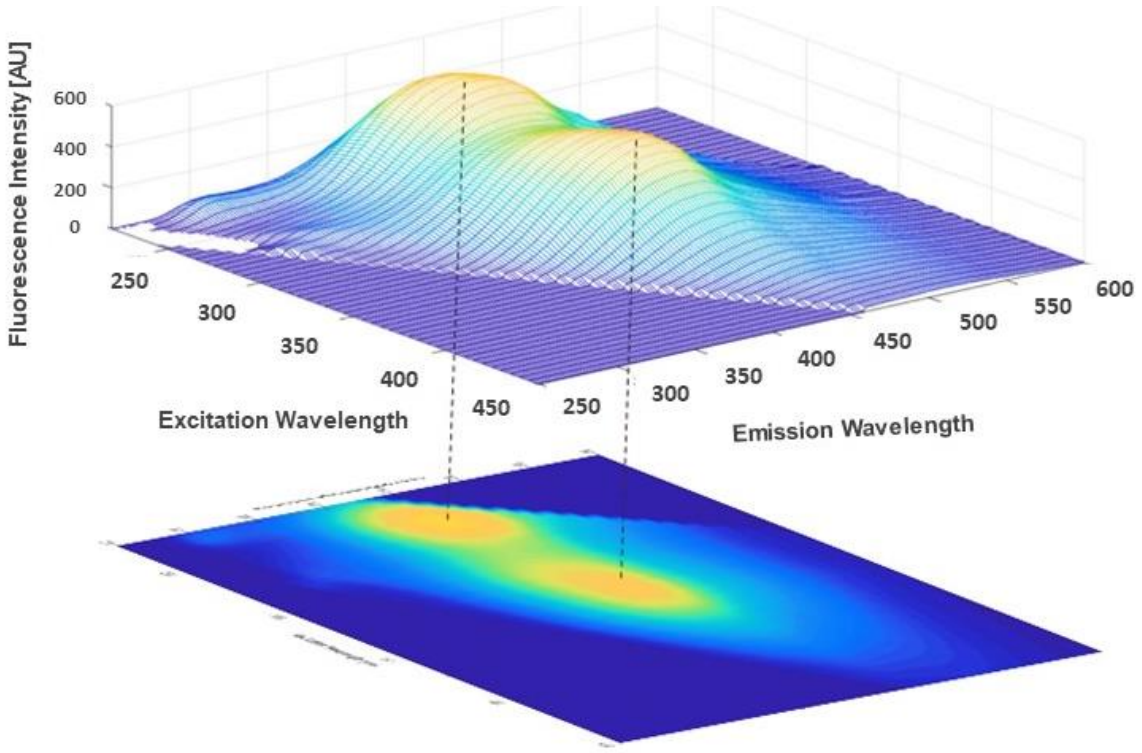

Figure 16c – Two-dimensional and three-dimensional graphic representation of the obtained EEMs for FA SAS-2A F.

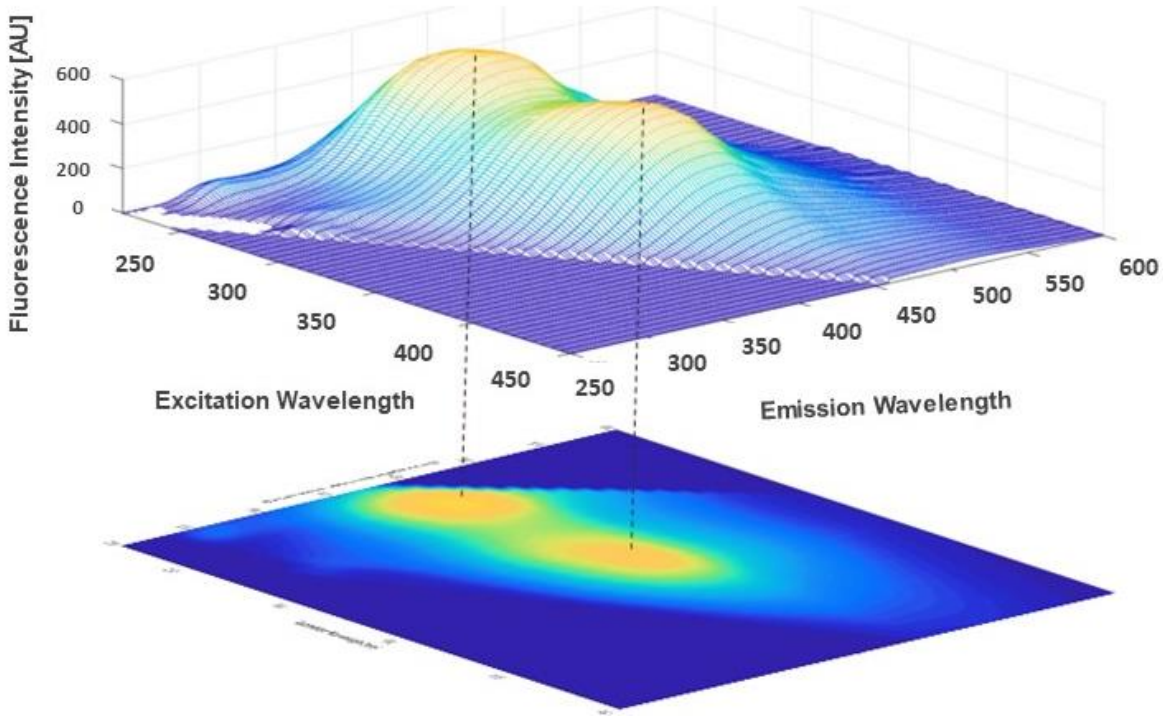

Figure 16d – Two-dimensional and three-dimensional graphic representation of the obtained EEMs for FA SAS-2A SUP.

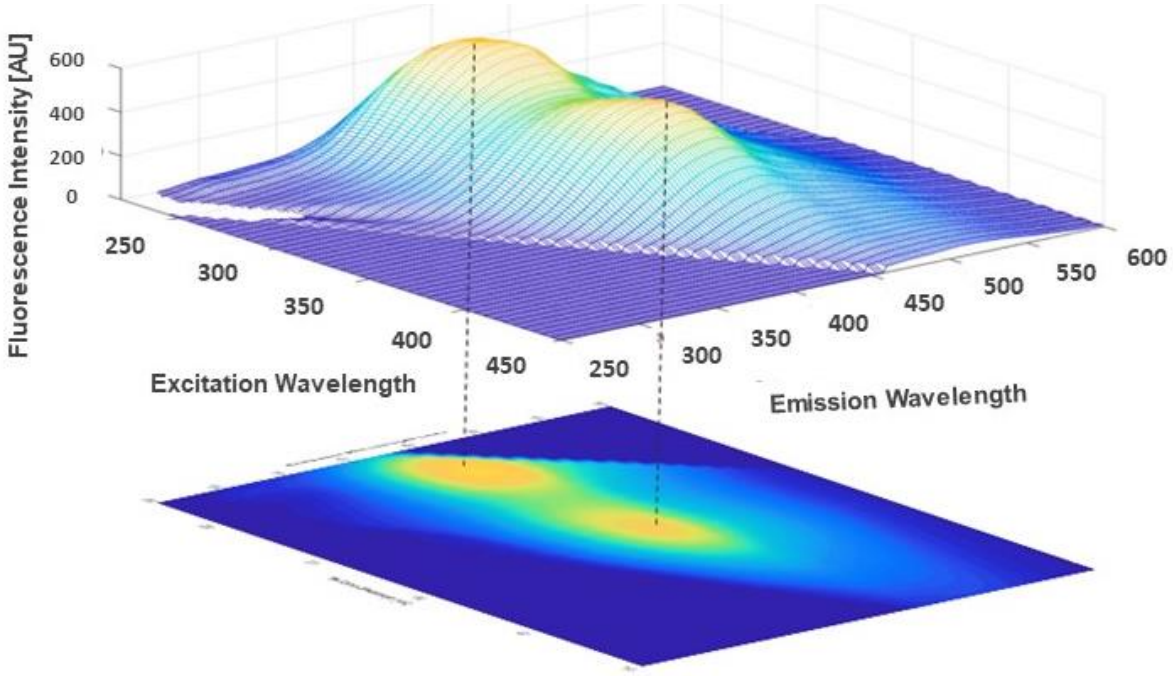

Figure 16e – Two-dimensional and three-dimensional graphic representation of the obtained EEMs for FA SAS-1B.

Obtained FI values for FA SAS samples revealed higher values for all FA SAS samples in comparison with the DOM SAS samples, except in the case of FA SAS-2A SUP. FA SAS-2A SUP displayed a lower FI than DOM SAS-2A SUP, thus reinforcing the notion of a strong terrestrial origin. As shown in Figure 16b, the EEMs obtained for FA SAS-1A SUP sample clearly express peak T with the highest relative intensity, even higher than peak A and C; EEMs from FA SAS-1A F however, reveal a considerably lower relative intensity for peak T.

It was theorized that the origin of this "fresh" DOM presence in the surface of lake SAS-1A, is directly related to its surrounding environment. As previously referred, during the warm season the SAS valley region becomes rich in macrophytes, namely *Carex Aquatilis*, populating the surrounding area of the thermokarst lakes (Matveev et al. 2016; Deshpande et al. 2017). Lake SAS-1A is a relatively shallow lake with a wide surface area; in comparison, lake SAS-2A possesses greater lake depth, however, its surface area is considerably smaller than lake SAS-1A. Throughout the warmer seasons, *Carex Aquatilis* populates both SAS-1A and SAS-2A regions. During winter, the extreme environmental conditions are not suitable for the existence of macrophytes, prompting the collapse of the *Carex Aquatilis* population. Considering this, an organic matter input of these plants into the

thermokarst lakes is to be expected, leading to an increase in the labile organic matter content within the lake. The greater surface area in lake SAS-1A in comparison to lake SAS-2A, may prompt a greater contact surface with the existing macrophytes, resulting in an increased organic input into the lake, thus explaining the intense “fresh” DOM fluorescence peak in the EEM at FA SAS-1A SUP in comparison to FA SAS-2A samples. Considering that lake SAS-1B is located directly attached to a palsa, its environment is considerably different than lake SAS-1A, despite their great geographical proximity.

As previously referred, lake SAS-2A showed the greatest depth of all sampled lakes, having a considerably lower surface area than lake SAS-1. The increased depth of this lake prompts significant differences between surface and bottom samples, namely in the relative abundance of existing microbial communities (Crevecoeur et al. 2015); these changes at different depths may explain the differences exhibited in the C:T, A:T peak ratios and HIX approximation values for FA SAS-2A SUP and FA SAS-2A F. Also, throughout the various depths of lake SAS-2A, both lateral transferences and upward diffusions of organic matter are to be expected, and considering that the surface and bottom portions of the lake tend not to be mixed, greater differences might be expected.

4.5 Fourier-transform infrared resonance spectroscopy analysis of fulvic acid samples

All FTIR-ATR spectra were acquired on a Bruker IFS 55, equipped with a Golden Gate single reflection diamond ATR system in the 4000-500 cm^{-1} region, and are expressed in Figure 17. The spectra resolution was 4 cm^{-1} (with an interval of 1 cm^{-1}) and 64 scans were averaged.

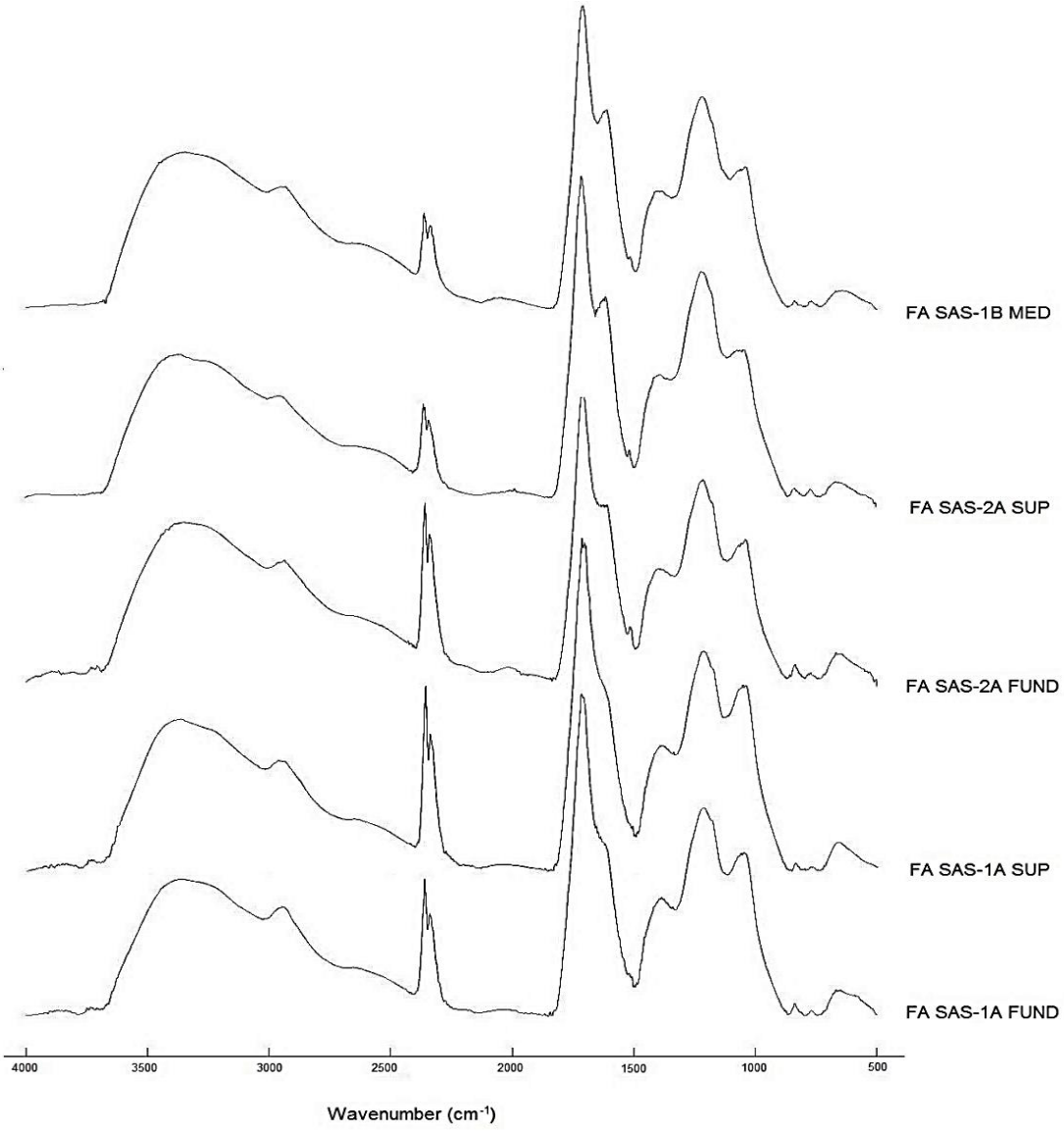

Figure 17 – The FTIR-ATR spectra of all lyophilized FA SAS samples.

The obtained spectra were scanned between 4000 and 400 cm^{-1} and showed considerable similarities between all FA SAS samples. The 3500-3000 cm^{-1} band, usually assigned to H-bonded OH stretching of phenol, hydroxyl and carboxyl groups; the 2960 cm^{-1} band corresponding to the asymmetric CH stretching of CH_2 (Stevenson & Goh 1971). All spectra display two peaks around 2360 and 2340 cm^{-1} associated with the presence of CO_2 at the time of the analysis (Charpentier et al. 2009). The band at 1717 cm^{-1} is commonly associated with the -C=O stretching of COOH (Santos and Duarte 1998), however aldehydic and ketonic C=O groups may also prompt absorption near this wavenumber (Stevenson & Goh 1971). The previously referred 1717 cm^{-1} band appeared to display a "shoulder" at approximately 1626 cm^{-1}, caused by the aromatic -C=C stretching and the asymmetric $–COO^-$ stretching. At 1392 cm^{-1}, the existence of the band is due to OH phenolic deformation and $–COO^-$ stretching of the phenolic OH (and COO^- antisymmetric stretching), or C-H deformation in CH_2 and CH_3 groups (Stevenson & Goh 1971). The strong band located at 1219 cm^{-1} is directly related to the C=O band of 1717 cm-1, being associated with C-O stretching and OH deformation of COOH groups (with possible contributions from other groups as aryl ethers) (Sillanpää 2014; Stevenson & Goh 1971). In the 1050 cm-1 region, the band is due to the C-O stretching of polysaccharides or polysaccharide-like substances (Stevenson & Goh 1971). The bands located at 826 cm^{-1} and lower wavenumbers, are considered to be a result of the aromatic CH out-of-plane bending (Sillanpää 2014).

Despite the overall similarities that all five samples display between themselves, there are however, noticeable differences in the region of 1800-900 cm^{-1}. The relative intensity of the band at 1626 cm^{-1}, attributed to the aromatic -C=C stretching and the asymmetric $–COO^-$ stretching (Sillanpää 2014) is lower in the FA SAS-1A samples than in the FA SAS-2A and FA SAS-1B samples, prompting the notion that FA SAS-1A samples contain a lower content in aromatic groups compared to the other samples. In FA SAS-1A samples, the 1600-1660 cm^{-1} band displays a shoulder-like appearance rather than the well-defined band displayed in FA SAS-2A and FA SAS-1B samples. Considering the 1600-1660 cm^{-1} region is also associated with $–COO^-$ stretching, the possibility of a higher carboxylate content in FA SAS-1B and FA SAS-2A samples, could also explaining the difference in the spectra; however, this notion is disregarded as there is neither a significant difference between samples in the 1717 cm^{-1} region (associated with C=O stretching of COOH), nor in the 1392 cm^{-1} region (also associated with $–COO^-$ stretching) (Gondar et al. 2005).

There is also the presence of a reasonably well-defined band with low relative intensity at 1515 cm^{-1} in the FTIR spectra of FA SAS-2A and FA SAS-1B samples, assigned to an aromatic C=C stretching, and characteristic of lignin derived structures (Santos et al. 2000). Considering the fact that this wavenumber region displays few additional bands, it presents itself as an important region to analyze when it comes to searching for lignin derived structures (Duarte et al. 2005). The presence of this band presents the idea that FA SAS-1A samples contain a lower content in in lignin derived structures when compared to FA SAS-1B and FA SAS-2A samples, thus reinforcing the notion of a higher aromatic content in FA SAS-1B and FA SAS-2A samples.

The spectra display very little change between FA samples of the same lake at different depths; the only noticeable difference is the 1626 cm^{-1} band in the FA SAS-2A samples, with FA SAS-2A SUP (surface sample) presenting itself as a well-defined band, while the FA SAS-2A F (sampled at a greater depth) displays the 1626 cm^{-1} band almost as a "shoulder" of the 1717 cm^{-1} band.

4.6 Nuclear magnetic resonance spectroscopy analysis of the fulvic acid samples

All of the NMR spectra were acquired using a Bruker Avance-500 spectrometer operating at 500.13 MHz for ^{1}H and 125.77 MHz for ^{13}C and equipped with a liquid nitrogen cooling CryoProbe Prodigy^{TM}. The lyophilized FA SAS samples were dissolved in D_2O in 5 mm NMR tubes, prior to NMR spectroscopy. The resulting ^{1}H NMR spectra for all FA SAS samples are shown in Figure 18.

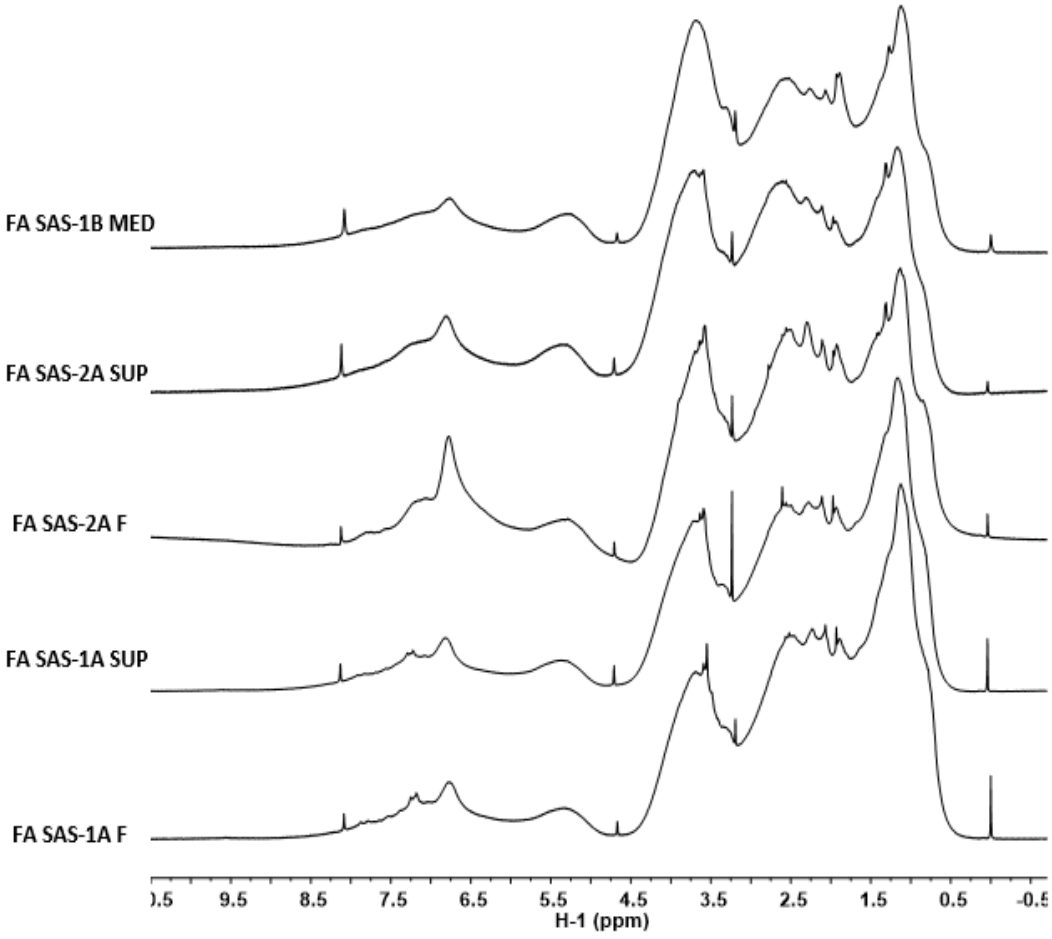

Figure 18 – Obtained liquid-state ^{1}H NMR spectra for all FA SAS samples (D_2O as solvent).

The ^{1}H NMR spectra of FA SAS samples, similarly to other ^{1}H NMR spectra, exhibit distinct regions associated with specific components and functional groups are known to resonate.

The region between 0.6 and 1.6 ppm is generally attributed to a group of aliphatic DOM components derived from linear terpenoids, however it may also contain resonances arising from other aliphatic functionalities, as the case of methyl groups. Some studies used 2D NMR experiments, namely HMBC and HMQC, to establish that the obtained signals located in this specific region are attributed to the product of the degradation of long-chain aliphatic compounds (Lam et al. 2007). Upon analyzing all ^{1}H NMR spectra it became clear that among these samples, FA SAS-1A samples showcase the highest peak in the 0.6 and 1.6 ppm region. FA SAS-2A SUP, FA SAS-2A F and FA SAS-1B M, apart from the main aliphatic peak also display a slight peak noticeable at *ca*. 1.25 ppm. In both FA SAS-1A and FA SAS-2A, the samples from the lake bottom display higher intensity in the 0.6 to 1.6 region than their corresponding surface samples.

The spectral region defined between 1.6 and 3.2 ppm in the ^{1}H NMR spectra of the FA SAS samples is usually associated with carboxyl-rich alicyclic molecules (CRAMs). The CRAM are a complex mixture of carboxylated and fused alicyclic structures, with a carboxyl C to aliphatic C ratio ranging from 1:2 to 1:7. Based on NMR and FT-ICR-MS experiments, it was proposed that CRAM is a result of the degradation of cyclic terpenoid biomolecules (Hertkorn et al. 2006). The CRAM region has been known to comprise a significantly high percentage of the total composition of DOM samples (Lam et al. 2007).

The spectral region at which carbohydrates and peptides resonate is located between 3.2 and 4.5 ppm, clearly noticeable in the ^{1}H NMR spectra of FA SAS samples. Considering the high complexity of DOM samples and the resulting resonance overlapping from peptide and carbohydrate moieties, the identification of specific molecules proves itself challenging (Mitchell, Simpson, Soong, et al. 2013). From the ^{1}H NMR spectra it became apparent that among FA SAS samples, the relative intensity displayed in the 3.2 to 4.5 ppm spectral region displays significant changes. The FA SAS-1A samples seem to showcase the lowest relative intensity in the carbohydrate and peptide region of the ^{1}H NMR spectra, while FA SAS-1B displays a slightly higher relative intensity than FA SAS-2A samples. In the region located between 4.5 and 6.5 ppm, there is one broad peak between 5 and 6 ppm, possibly arising mainly from double bonds and anomeric protons in carbohydrates (Lam & Simpson 2008).

The specific spectral region between 6.5 and 8.4 is mainly associated with aromatic and phenolic compounds as well as amides. Aromatic molecules present in DOM are generally

associated with lignin monomers and aromatic amino acids (Mitchell, Simpson, Soong, et al. 2013). At approximately 6.75 ppm in the obtained ^{1}H NMR spectra, there is a clearly noticeable peak generally associated with the presence of lignin (Woods et al. 2012); this lignin peak displays greater intensity in the FA SAS-2A F sample than in the remaining samples, suggesting a higher lignin content in the bottom of lake SAS-2A. In every one of the ^{1}H NMR spectra of the FA SAS samples, the abundance of the aromatic component relative to the aliphatic component is low; this lack of abundance of the aromatic component was not unexpected, as several studies of ^{1}H NMR focused on DOM characterization have showcased low aromatic abundance (Woods et al. 2011; Woods et al. 2012; Santos et al. 2012).

Due to the highly complex nature of the FA SAS samples, the 1D ^{1}H NMR spectra displayed severe peak overlap, thus hindering the possibility of obtaining profound structural information regarding the samples. As an attempt to gain further structural insight into the FA SAS samples, an ^{1}H-^{13}C HSQC NMR experiment was conducted for FA SAS-1A SUP and FA SAS-2A SUP samples.

The ^{1}H-^{13}C HSQC NMR spectrum of FA SAS-1A SUP is shown in Figure 19, where 7 distinct regions were clearly noticeable. Region I, spanning from approximately δ^{1}H = 0.5-1.5 ppm and δ^{13}C = 10-30 ppm, can be attributed to purely aliphatic groups. Region 2, located in the chemical shift range of *ca*. δ^{1}H = 1.5-3.5 ppm and δ^{13}C = 30-45 ppm, is associated with the CRAM fraction of the sample, consisting mainly of functionalized aliphatic groups like R_1-CH, where R_1 is an aromatic carbon, a COOH group, a NH group or a C=O group (Matos et al. 2017). Region 3, situated in a chemical shift range of *ca*. δ^{1}H = 3.0-4.0 ppm and δ^{13}C = 50-65 ppm, comprises a clearly noticeable cross peak at δ^{1}H = 3.25-3.80 and *ca*. δ^{13}C = 50, which can be assigned to aromatic methoxyl (Ar-O-CH_3) (Simpson 2001), suggesting the presence of ethers and esters.

A groups of cross peaks associated with CHOH fragments is generally found in region 4, at a chemical shift of *ca*. δ^{1}H = 3.25-4.5 ppm and δ^{13}C = 65-80 ppm, normally attributed to carbohydrates (Hertkorn et al., 2002). Although a small peak was observed in the ^{1}H NMR spectra at *ca*. 5.5 ppm, it should be noted that in the spectral region of *ca*. δ^{1}H = 4.5-6 ppm and δ^{13}C = 80-110 ppm, the obtained HSQC spectra displayed no signals, suggesting a low abundance of anomeric carbons associated with carbohydrates. Region 5 is in the aromatic

region of the HSQC NMR spectra, situated between *ca.* $\delta^{1}H$ = 6.25-7.5 ppm and $\delta^{13}C$ = 115-135 ppm. In this region, two main groups of cross peaks are clearly visible, most likely representing oxygenated aromatic systems.

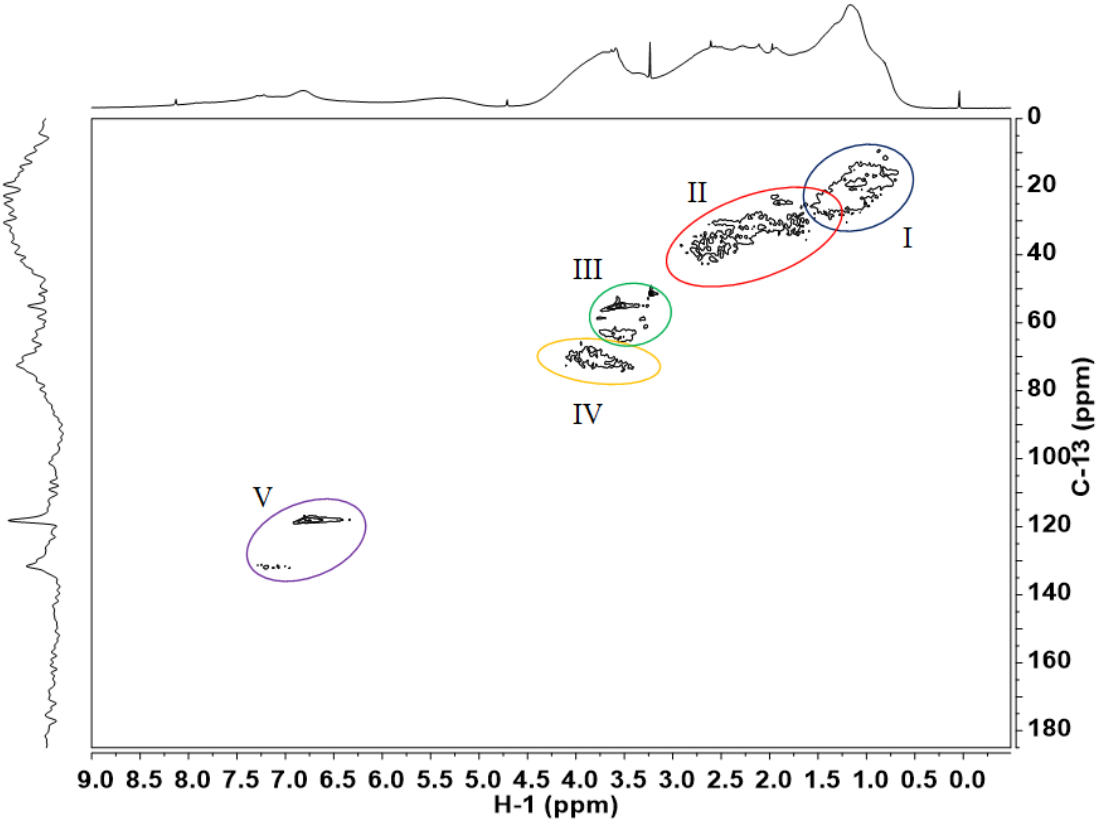

Figure 19 – Obtained liquid-state ^{1}H-^{13}C HSQC NMR spectrum of FA SAS-1A SUP, divided into five specific spectral regions (D_2O as solvent).

As previously referred, the high complexity of the FA SAS samples hindered the structural characterization process, as the obtained ^{1}H-^{13}C HSQC NMR and ^{1}H-^{1}H COSY NMR spectra are difficult to fully interpret. Nevertheless, the retrieved spectra still provided crucial information to further advance the samples' structural characterization. The retrieved ^{1}H-^{13}C HSQC NMR spectra for FA SAS-1A F, FA SAS-2A SUP and FA SAS-2A F are expressed in Figure 20, Figure 21 and Figure 22 respectively.

Comparing the obtained ^{1}H-^{13}C HSQC NMR spectra of FA SAS-1A SUP and FA SAS-1A F, region 2 appears to be more dispersed in FA SAS-1A SUP than in FA SAS-1A F, possibly indicating a greater variety of CRAM in FA SAS-1A SUP. Region 4 however, displays the

opposite behavior as it occupies a greater area of the HSQC spectra in FA SAS-1A F than in FA SAS-1A SUP. It should be noted that any assertions made need to take into account the immense complexity of these samples.

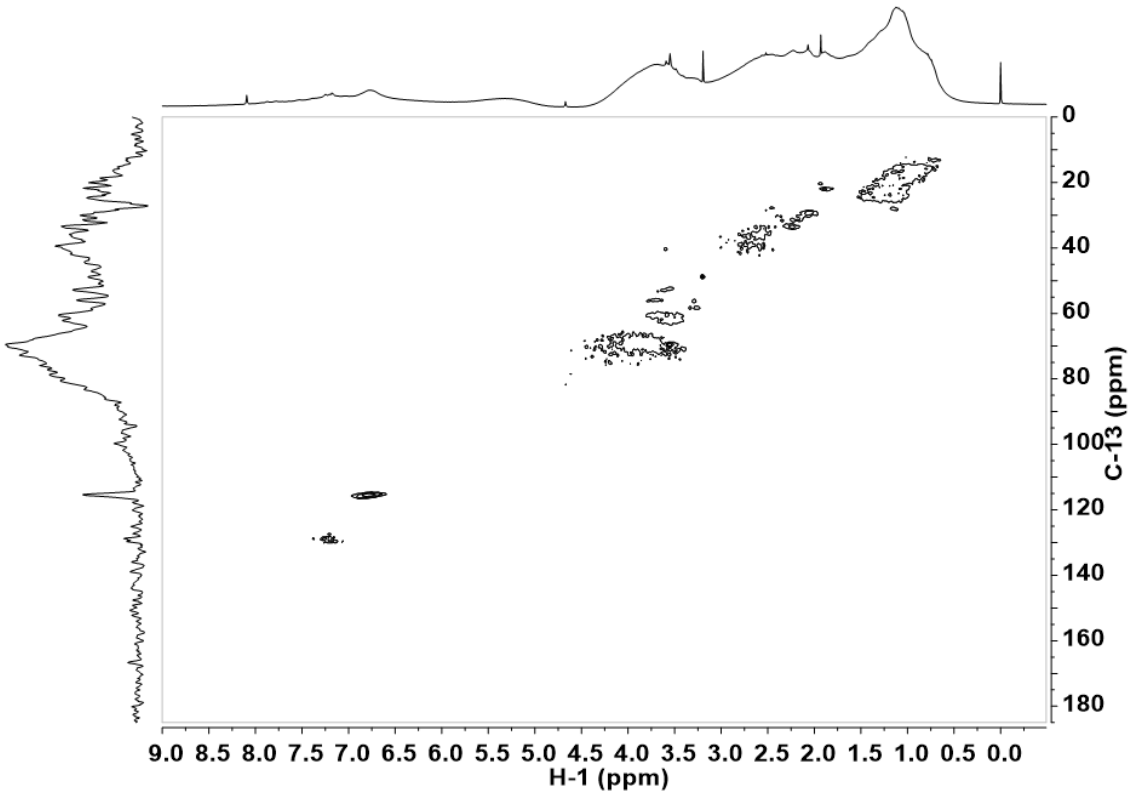

Figure 20 – Obtained liquid-state ^{1}H-^{13}C HSQC NMR spectrum of FA SAS-1A F (D_2O as solvent).

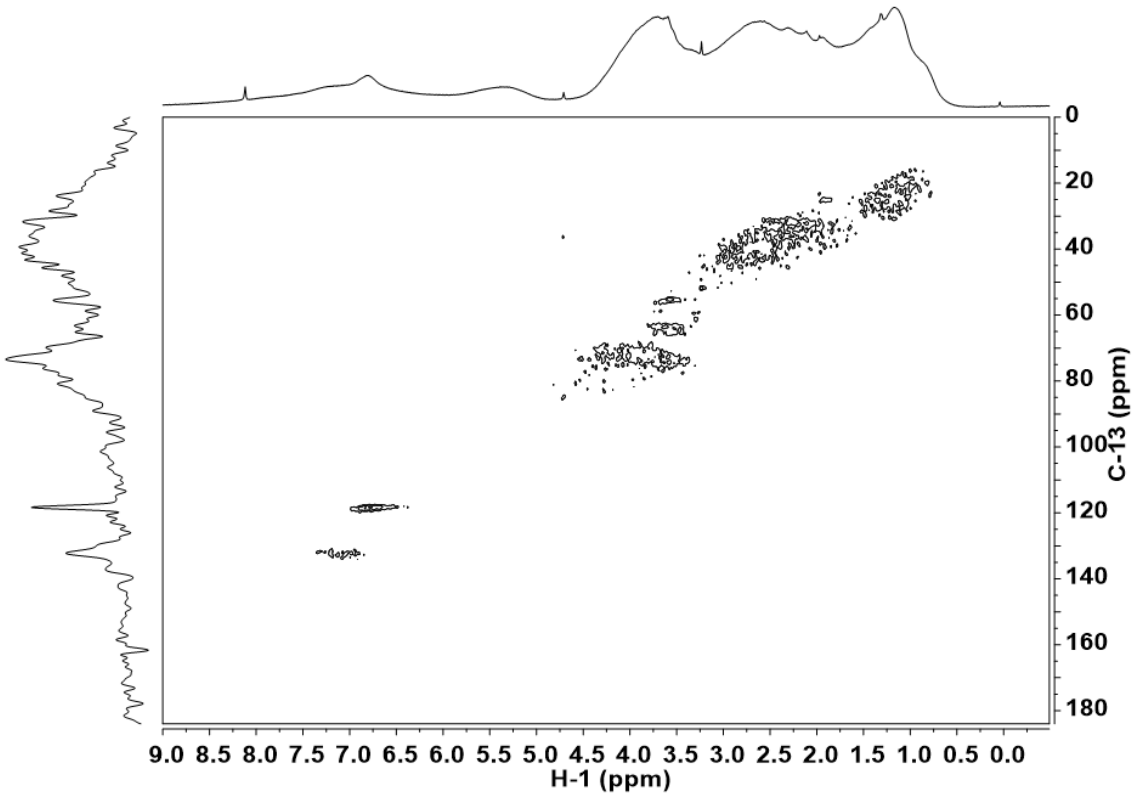

Figure 21 – Obtained liquid-state ^{1}H-^{13}C HSQC NMR spectrum of FA SAS-2A SUP (D_2O as solvent).

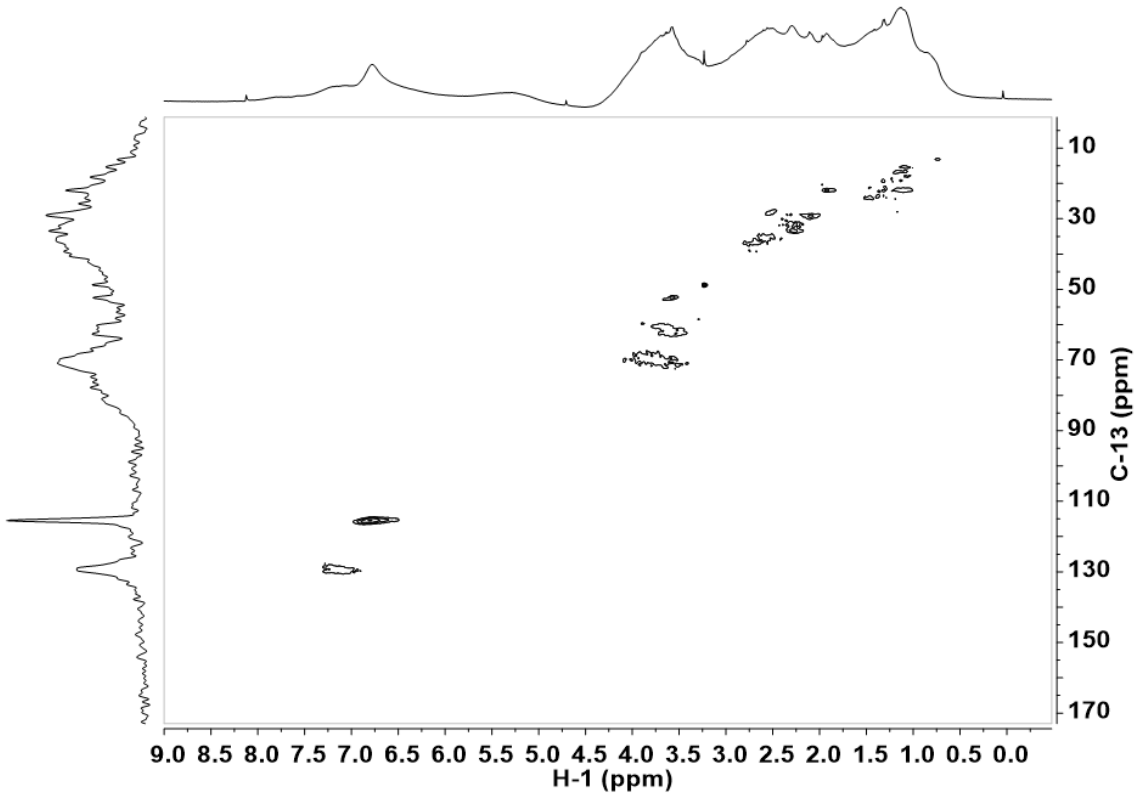

Figure 22 – Obtained liquid-state ^{1}H-^{13}C HSQC NMR spectrum of FA SAS-2A F (D_2O as solvent).

The ^{1}H-^{13}C HSQC NMR spectra of FA SAS-2A SUP seems to display a greater dispersion area of peaks relative to regions 1, 2, 3, and 4, mainly associated with aliphatic, CRAM, and carbohydrates. Nevertheless, FA SAS-2A F appears to display higher intensity peaks in the aromatic region, suggesting a higher aromatic content in comparison to FA SAS-2A SUP.

Comparisons between FA SAS samples from different lakes were also established, based on the depth at which they were sampled. Considering this, the ^{1}H-^{13}C HSQC NMR spectra of FA SAS-1A SUP seems to display a greater content in region 1, while FA SAS-2A SUP displays a greater content in regions 2, 3, 4 and 5, and occupies a greater spectral area in regions 2 and 4; this prompts the notion that FA SAS-1A SUP contains higher unsubstituted methyl aliphatic content, while FA SAS-2A SUP possibly contains greater CRAM, carbohydrate and aromatic content. The ^{1}H-^{13}C HSQC NMR spectra of FA SAS-1A F shows a greater area distribution and intensity in region 1 and 4 than in FA SAS-2A F, while region 5 displayed greater intensity in FA SAS-2A F than in FA SAS-1A F, suggesting that FA SAS-2A F comprises a greater aromatic content while FA SAS-1A F contains a greater aliphatic component.

The majority of the obtained ^{1}H-^{1}H COSY NMR for FA SAS samples displayed inconclusive data, as a result of the complexity of the samples. Nevertheless, these spectra were thoroughly analyzed, in an attempt to obtain further structural information. The ^{1}H-^{1}H COSY NMR spectrum of FA SAS-2A F displayed the best resolution and is therefore expressed in Figure 23.

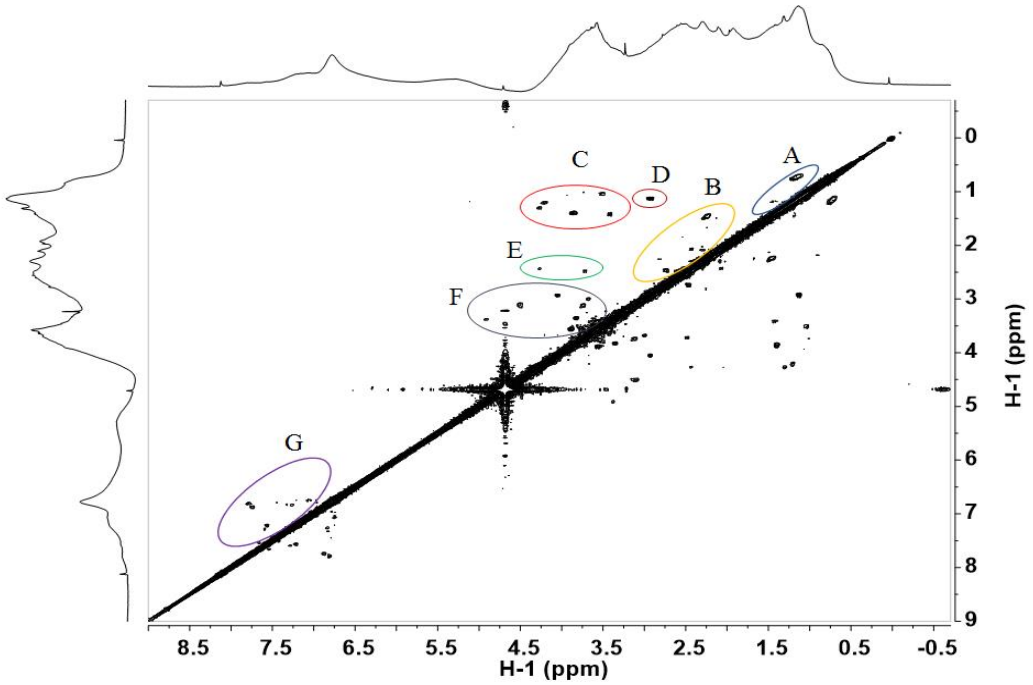

Figure 23 - Obtained liquid-state ^{1}H-^{1}H COSY NMR spectrum of FA SAS-2A F (D_2O as solvent).

The ^{1}H-^{1}H COSY NMR spectrum of FA SAS-2A F clearly showed distinct proton coupling patterns used to divide the spectrum into seven distinct types of coupling, allowing us to infer about the structural nature of the FA sample. Table 22 showcases the different identified spectral regions and the coupling involved in each of them.

Table 22 – Differentiated regions in the ^{1}H-^{1}H COSY NMR spectrum and their respective type of proton coupling.

Region	**Proton coupling**
Region A	Aliphatic protons coupled with aliphatic protons
Region B	Functionalized aliphatic protons coupled with functionalized aliphatic protons (CRAM)
Region C	Aliphatic protons coupled with protons in carbohydrates
Region D	Aliphatic protons coupled with functionalized aliphatic protons (CRAM)
Region E	Functionalized aliphatic protons (CRAM) coupled with protons in carbohydrates
Region F	Protons in carbohydrates coupled with protons in carbohydrates, and possibly coupled with protons in anomeric carbons
Region G	Aromatic protons coupled with aromatic protons

Upon analyzing the ^{1}H-^{1}H COSY NMR spectrum of FA SAS-2A F, regions G, F, C and B appear to display greater peak diversity when compared to regions A, D and E. In the ^{1}H-^{13}C HSQC NMR spectrum of FA SAS-2A F (Figure 22), the carbohydrate region, the CRAM region and the aliphatic region all displayed considerable structural diversity, implying a wide range of compounds present in these regions. The obtained ^{1}H-^{1}H COSY NMR data now confirms this, showcasing greater diversity of proton couplings in these regions, as well as in the aromatic section. As shown in Figure 23, the various coupling of aliphatic protons to protons from CRAM and carbohydrates, reinforces the notion of the existence of aliphatic chains branched with heteroatom-containing substituents, suggesting the presence of CH_3-COR, CH_3-NR_2, and CH_3-OR structures, where R is an alkyl group or simply an hydrogen atom. The obtained ^{1}H-^{1}H COSY NMR spectra for FA SAS-1A SUP, FA SAS-1A F and FA SAS-1A SUP are displayed in Section 2 of the annex.

4.7 Elemental analysis of the fulvic acid samples

The elemental CHNS analysis of FA SAS samples, data shown in Table 23, was conducted on an elemental analyzer Truspec 630-200-200. The elemental detection of carbon, hydrogen and sulphur was conducted using infrared absorption, while the elemental detection of nitrogen was conducted using thermal conductivity. It should be noted that the combustion furnace temperature was 1075ºC and the afterburner temperature was 850ºC. The elemental analysis data displayed in Table 23 does not account for the water content and the ash percentage.

Table 23 - Average value of three replicas for elemental composition, sample mass, and atomic ratios for FA SAS-1A, FA SAS-1B and FA SAS-2A samples. The complete table containing the data for each replica can be found in the Appendix.

Sample	Weight (mg)	C (%)	H (%)	N (%)	H:C	N:C
FA SAS-1A SUP	1.937	46.99	4.977	1.407	1.258	0.026
FA SAS-1A F	1.802	48.40	4.923	1.299	1.209	0.023
FA SAS-2A SUP	1.967	44.34	4.153	1.189	1.113	0.023
FA SAS-2A F	2.008	46.36	4.204	1.398	1.078	0.026
FA SAS-1B M	1.990	48.19	3.918	1.352	0.966	0.024

The values obtained for all FA SAS samples are within the same range of those obtained for SRFA (Duarte et al. 2007), Toolik lake FA, Island lake FA, and Campsite lake FA (Cory et al. 2007). However, FA from Toolik lake, Island lake and Campsite lake (as seen in Table 1) showcased slightly higher carbon and hydrogen percentages than the FA SAS samples; nevertheless, FA SAS samples displayed a slightly higher nitrogen percentage than Toolik lake, Island lake and Campsite lake. In comparison with SRFA, the carbon content was lower in FA SAS samples, while the hydrogen percentage obtained for SRFA was similar to that of FA SAS samples; the nitrogen percentage displayed in FA SAS samples was higher than in Suwannee River FA.

Although the amount of information that can be drawn from the elemental composition data is limited, the use of atomic ratios (such as H:C and N:C) can provide some qualitative

information about the samples. The atomic H:C ratio values of the FA SAS samples increased by the following order: FA SAS-1A SUP > FA SAS-1A F > FA SAS-2A SUP > FA SAS-2A F > FA SAS-1B, suggesting a higher aliphatic character of FA SAS-1A samples compared to the remaining FA SAS-2A and FA SAS-1B samples. This feature appears to be consistent with the results obtained in ^{1}H NMR spectroscopy. Compared to FA from Toolik lake, Island lake and Campsite lake, the H:C ratio of both FA SAS-1A and FA SAS-2A samples displayed values from the same range, slightly higher in FA SAS-1A samples and slightly lower in FA SAS-2A samples. The H:C ratio of FA SAS-1B M was the lowest, displaying a slightly lower value than of SRFA, suggesting FA SAS-1B M contains greater humic content.

The atomic N:C ratio for FA SAS-1A samples is also expressed in Table 23. All of the FA SAS samples revealed an atomic N:C ratio higher than the obtained values for Toolik lake FA, Island lake FA, Campsite lake FA (Cory et al. 2007), and SRFA (Duarte et al. 2007). Thawing of permafrost and consequent the release of its components, significantly increases the nitrogen content in thermokarst lakes (Deshpande et al. 2016), thus explaining the considerably higher N:C ratios exhibited in the FA SAS samples in comparison to the N:C ratios obtained by Cory (Cory et al. 2007) in Toolik lake, Island lake and Campsite lake.

4.8 Conclusions

The successful application of various analytical characterization techniques has provided insight into the composition of the different FA fractions of DOM in water samples from different subarctic thermokarst lakes, despite their extreme structural complexity. The obtained information from different analytical techniques seem to support the notion of a greater aliphatic content in FA SAS-1A samples, and lower aromatic and carbohydrate moieties in comparison to FA SAS-2A and FA SAS-1B samples. The EEM fluorescence spectra also detected the presence of "fresh" DOM in FA SAS-1A samples, likely resulting from a greater organic matter input from *Carex Aquatilis* populations during the warm season. If this "fresh" DOM in FA SAS-1A SUP samples is associated with labile organic matter, its degradation may result in an increased CO_2 and CH_4 release into the atmosphere in lake SAS-1A. Although all samples revealed considerable N:C ratios, possibly arising from the stored nitrogen in the thawing permafrost, the great proximity of lake SAS-1B to the palsa has resulted in a greater humification degree for FA SAS-1B M, as reported in the elemental analysis and fluorescence spectroscopy. FA SAS-2A samples display certain differences among themselves, as not only a greater "fresh" DOM content is detected, but the NMR spectra seem to suggest an increase in aromatic content in FA SAS-2A F.

The peatland theremokarst lakes sampled in this study are highly complex systems, subject to a wide variety of variables contributed to the differences exhibited in these samples. The HA fraction, the collected soil, and sediment samples should be analyzed, as the structural information of their NOM might help to better understand thermokarst systems.

5

Final Remarks

This dissertation enabled the structural characterization of the FA fraction of DOM in thermokarst lakes, providing insight into some of the variables that affect the chemical composition of these lake systems. The review of existing NOM structural characterization studies revealed a significant lack of research performed on NOM originating from permafrost thaw lakes, despite the considerable environmental impact these thermokarst systems create, namely in the release of vast quantities of methane into the atmosphere.

The research work presented in this dissertation tapped into that gap and aimed to provide insight into the chemical nature of these samples, identifying variations with depth and for different lakes. The use of various characterization techniques was vital to gain further understanding of the differences between samples as well as their cause, prompting a more profound study of the specific environment in which these thaw lakes are inserted.

The results obtained from this research work suggest different origins for DOM in thermokarst lakes, including contributions from thawing permafrost, from microbial origin, and from macrophytes that populate the region during the warm seasons. The depth, morphology, and proximity to palsas of each lake, also play a significant role in their DOM content. A structural characterization study involving the HA fraction of DOM, the soils collected from the lake margins, as well as the sediments sampled at lake bottom, is required to gain further understanding of these complex systems.

6

References

Aiken, G. & Leenheer, J., 2006. Isolation and Chemical Characterization of Dissolved and Colloidal Organic Matter. *Chemistry and Ecology*, 8(3), pp.135–151.

Andrew, E.R., 1971. The Narrowing of NMR Spectra of Solids by High-speed Specimen Rotation and the Resolution of Chemical Shift and Spin Multiplet Structures for Solids. *Progress in Nuclear Magnetic Resonance Spectroscopy*, 8(1), pp.1–39.

Baker, A., Bolton, L., Newson, M. & Spencer, R.G.M, 2008. Spectrophotometric properties of surface water dissolved organic matter in an afforested upland peat catchment. *Hydrological Processes*, 22, pp.2325–2336.

Belzile, C., Gibson, J.A.E. & Vincent, W.F., 2002. Colored dissolved organic matter and dissolved organic carbon exclusion from lake ice: Implications for irradiance transmission and carbon cycling. *Limnology and Oceanography*, 47(5), pp.1283–1293.

Bortiatynski, J.M., Hatcher, P.G. & Knicker, H., 1996. NMR techniques (C, N, and H) in studies of humic substances. *Humic and Fulvic Acids*, 651(7), pp.57–77.

Bouchard, F., Macdonald L.A., Turner, K. W., Thienpont, J.R., Medeiros, A.S., Biskaborn, B.K., Korosi, J., Hall, R., Pienitz, R. & Wolfe, B., 2016. Paleolimnology of thermokarst lakes : a window. *Arctic Science*, pp.1–27.

Brown, J., O.J. Ferrians, Jr., J.A. Heginbottom, & E.S.M., 1997. Circum-Arctic map of permafrost and ground-ice conditions. *U.S. Geological Survey*.

Burn, C.R., 2002. Tundra lakes and permafrost, Richards Island, western Arctic coast, Canada. *Canadian Journal of Earth Sciences*, 39(9), p.1441.

Burn, C.R. & Smith, C.A.S., 1988. Observations of the “Thermal Offset” in Near-Surface Mean Annual Ground Temperatures at Several Sites near Mayo, Yukon Territory, Canada. *Arctic*, 41(2), pp.99–104.

Cardoza, L.A., Korir, A.K., Otto, W.H., Wurrey, C.J. & Larive, C.K., 2004. Applications of NMR spectroscopy in environmental science. *Progress in Nuclear Magnetic Resonance Spectroscopy*, 45(3-4), pp.209–238.

Charpentier, F., Bureau, B., Troles, J., Boussard-Plédel, C., Michel-Le Pierrès K., Smektala, F. & Adam, J.L., 2009. Infrared monitoring of underground CO2 storage using

chalcogenide glass fibers. Optical Materials, 31(3), pp.496–500.

Chowdhury, S., 2013. Trihalomethanes in drinking water: Effect of natural organic matter distribution. *Water*, 39(1), pp.1–8.

Coble, P.G., Spencer, R.G.M., Baker, A. & Reynolds, D., 2014. Aquatic Organic Matter Fluorescence. In *Aquatic Organic Matter Fluorescence*. New York: Cambridge University Press, pp. 75–124.

Coble, P.G., Green, S., Blough, N.V. & Gagosian, R.B., 1990. Characterization of dissolved organic matter in the Black Sea by fluorescence spectroscopy. *Nature*, 348, pp.432–435.

Coble, P.G., 1996. Characterization of marine and terrestrial DOM in seawater using excitation-emission matrix spectroscopy. *Marine Chemistry*, 51(4), pp.325–346.

Coble, P.G., Castillo, C.E. Del & Avril, B., 1998. Distribution and optical properties of CDOM in the Arabian Sea during the 1995 Southwest Monsoon. *Deep-Sea Research II*, 45, pp.2195–2223.

Cook, R.L., 2004. Coupling NMR to NOM. *Analytical and Bioanalytical Chemistry*, 378(6), pp.1484–1503.

Cory, R.M., McKnight, D.M., Chin, Y. P., Miller, P. & Jaros, C. L., 2007. Chemical characteristics of fulvic acids from Arctic surface waters: Microbial contributions and photochemical transformations. *Journal of Geophysical Research: Biogeosciences*, 112(4), pp.1–14.

Cory, R.M., McNeill, K., Cotner, J.B., Amado, A.M., Purcell, J.M. & Marshall, A. G., 2010. Singlet oxygen in the coupled photo- and biochemical oxidation of dissolved organic matter. *Environmental Science & Technology*, 44(10), pp.3683–3689.

Cox, L., Celis, R., Hermosin, M.C., Cornejo, J., Zsolnay, A., & Zeller.K., 2000. Effect of organic amendments on herbicide sorption as related to the nature of the dissolved organic matter. *Environmental Science and Technology*, 34(21), pp.4600–4605.

Crevecoeur, S., Vincent, W.F., Comte, J., & Lovejoy, C., 2015. Bacterial community structure across environmental gradients in permafrost thaw ponds: Methanotroph-rich

ecosystems. *Frontiers in Microbiology*, pp.1–15.

Czudek, T. & Demek, J., 1970. Thermokarst in Siberia and Its Influence Relief on the Development of Lowland. *Quaternary Research*, 120, pp.103–120.

Deshpande, B.N., Crevecoeur, S., Matveev, A. & Vincent, W.F., 2016. Bacterial production in subarctic peatland lakes enriched by thawing permafrost. *Biogeosciences*, 13(15), pp.4411–4427.

Deshpande, B.N., Maps, F., Matveev, A. & Vincent, W.F., 2017. Oxygen depletion in subarctic peatland thaw lakes 1. *Arctic Science*, 428, pp.406–428.

Dittmar, T., Koch, B., Hertkorn, N. & Kattner, G., 2008. A simple and efficient method for the solid-phase extraction of dissolved organic matter (SPE-DOM) from seawater. *Limnology and Oceanography: Methods*, 6(6), pp.230–235.

Dittmar, T. & Paeng, J., 2009. A heat-induced molecular signature in marine dissolved organic matter. *Nature Geoscience*, 2(3), pp.175–179.

Downing, B.D., Boss, E., Bergamaschi, B.A., Fleck, J.A., Lionberger, M.A., Ganju, N.K., Schoellhamer, D.H. & Fujii, R., 2009. Quantifying fluxes and characterizing compositional changes of dissolved organic matter in aquatic systems in situ using combined acoustic and optical measurements. *Limnology and Oceanography: Methods*, 7(1), pp.119–131.

Duarte, R.M.B.O., Santos, E.B.H., Pio, C.A. & Duarte, A.C., 2007. Comparison of structural features of water-soluble organic matter from atmospheric aerosols with those of aquatic humic substances. *Atmospheric Environment*, 41, pp.8100–8113.

Duarte, R.M.B.O., Pio, C.A. & Duarte, A.C., 2005. Spectroscopic study of the water-soluble organic matter isolated from atmospheric aerosols collected under different atmospheric conditions. *Analytica Chimica Acta*, 530(1), pp.7–14.

Van Everdingen, R., 2005. Multi-language glossary of permafrost and related ground-ice terms. *National Snow and Ice Data Center/World Data Center for Glaciology, Boulder*, p.186.

Ferraro, J.R. & Krishnan, K., 1990. *Practical Fourier Transform Infrared Spectroscopy:*

Industrial and Laboratory Chemical Analysis, Academic Press Limited.

Fleck, J.A., Gill, G., Bergamaschi, B.A., Kraus, T.E.C., Downing, B.D. & Alpers, C.N., 2014. Concurrent photolytic degradation of aqueous methylmercury and dissolved organic matter. *Science of the Total Environment*, 484(1), pp.263–275.

French, H.M., Heginbottom, J.A., Johnston, G.H., Ladanvi, B., Sego, D.C. & Van Everdinger, R.O., 1988. *Glossary of Permafrost and Related Ground-Ice Terms*, National Research Council of Canada.

Gondar, D., Lopez, R., Fiol, S., Antelo, J.M. & Arce, F., 2005. Characterization and acid-base properties of fulvic and humic acids isolated from two horizons of an ombrotrophic peat bog. *Geoderma*, 126(3-4), pp.367–374.

Green, S.A., Morel, F.M.M. & Blough, N., 1992. Investigation of the electrostatic properties of humic substances by fluorescence quenching. *Environ. Sci. Technol.*, 26(2), pp.294–302.

Grosse, G., Romanovsky, V., Jorgenson, T., Anthony, K.W., Brown, J. & Overduin, P.P., 2011. Vulnerability and feedbacks of permafrost to climate change. *Eos*, 92(9), pp.73–74.

Hansen, A.M., Kraus, T.E.C., Pellerin, B.A., Fleck, J.A., Downing, B.D. & Bergamaschi, B.A., 2016. Optical properties of dissolved organic matter (DOM): Effects of biological and photolytic degradation. *Limnology and Oceanography*, 61(3), pp.1015–1032.

Hatcher, P.G., 2004. The CHNs of organic geochemistry: Characterization of molecularly uncharacterized non-living organic matter. *Marine Chemistry*, 92(1-4 SPEC. ISS.), pp.5–8.

Hayes, M.H.B., MacCarthy, P., Malcolm, R.L. & Swift, R.S., 1989. *Humic Substances II: In search of structure*, John Wiley & Sons.

Hedges, J.I., Eglinton, G., Hatcher, P.G., Kirchman, D.L., Arnosti, C., Derenne, S., Evershed, R.P., Kogel-Knaber, I., de Leeuw, J.W., Littke, R., Michaelis, W. & Rullkotter, J., 2000. The molecularly uncharacter ized component of nonliving organic matter in natural environments. *Organic Geochemistry*, 31(10), pp.945–958.

Hernes, P.J., Bergamaschi, B.A., Eckhard, R.S. & Spencer, R.G.M., 2009. Fluorescence-based proxies for lignin in freshwater dissolved organic matter. *Journal of Geophysical Research: Biogeosciences*, 114(4), pp.1–10.

Hernes, P.J., 2003. Photochemical and microbial degradation of dissolved lignin phenols: Implications for the fate of terrigenous dissolved organic matter in marine environments. *Journal of Geophysical Research*, 108(C9), p.3291.

Hertkorn, N., Benner, R., Frommberger, M., Schmitt-Kopplin, P., Witt, M., Kaiser, K., Kettrup, A. & Hedges, J.I., 2006. Characterization of a major refractory component of marine dissolved organic matter. *Geochimica et Cosmochimica Acta*, 70(12), pp.2990–3010.

Hertkorn, N., Permin, A., Perminova, I., Kovalevskii, D., Yudov, M., Petrosvan, V. & Kettrup, A., 2002. Comparative analysis of partial structures of a peat humic and fulvic acid using one- and two-dimensional nuclear magnetic resonance spectroscopy. *Journal of environmental quality*, 31(2), pp.375–87.

Hertkorn, N., Ruecker, C., Meringer, M., Gugisch, R., Frommberger, M., Perdue, E.M., Witt, M. & Schmitt-Kopplin, P., 2007. High-precision frequency measurements: Indispensable tools at the core of the molecular-level analysis of complex systems. *Analytical and Bioanalytical Chemistry*, 389(5), pp.1311–1327.

Hodgkins, S.B., Tfaily, M.M., McCalley, C.K., Logan, T.A., Crill, P.M., Saleska, S.R., Rich, V.I. & Chanton, J.P., 2014. Changes in peat chemistry associated with permafrost thaw increase greenhouse gas production. *Proceedings of the National Academy of Sciences*, 111(16), pp.5819–5824.

Hudson, N., Baker, A. & Reynolds, D., 2007. Fluorescence Analysis of Dissolved Organic Matter in Natural, Waste and Polluted Waters - A Review. *River Research and Applications*, 23(1), pp.631–649.

Hugelius, G., Strauss, J., Zubrzyncki, S., Harden, J.W., Schuur, E.A.G., Ping, C. & Schirrmeister, L., 2014. Estimated stocks of circumpolar permafrost carbon with quantified uncertainty ranges and identified data gaps. *Biogeosciences*, 11, pp.6573–6593.

Huguet, A., Vacher, L., Relexans, S., Saubusse, S., Froidefond, J.M. & Parlanti, E., 2009. Properties of fluorescent dissolved organic matter in the Gironde Estuary. *Organic Geochemistry*, 40(6), pp.706–719.

Jacobsen, N.E., 2007. *NMR Spectroscopy Explained: Simplified Theory, Applications and Examples for Organic Chemistry and Structural Biology*, Hoboken, New Jersey: John Wiley & Sons.

Jaffé, R., McKnight, D., Maie, N., Cory, R., McDowell, W.H. & Campbell, J.L., 2008. Spatial and temporal variations in DOM composition in ecosystems: The importance of long-term monitoring of optical properties. *Journal of Geophysical Research: Biogeosciences*, 113(4), pp.1–15.

Jeffries, M.O., Zhang, T., Frey, K. & Kozlenko, N., 1999. Estimating late-winter heat flow to the atmosphere from the lake-dominated Alaskan North Slope. *Journal of Glaciology*, 45(150), pp.315–324.

Kalbitz, K., Geyer, S. & Geyer, W., 2000. A comparative characterization of dissolved organic matter by means of original aqueous samples and isolated humic substances. *Chemosphere*, 40(12), pp.1305–1312.

Klapper, L., McKnight, D., Fulton, J.R., Blunt-Harris, E.L., Nevin, K.P., Lovley, D.R. & Hatcher, P.G., 2002. Fulvic acid oxidation state detection using fluorescence spectroscopy. *Environmental science & technology*, 36(14), pp.3170–3175.

Kokelj, S. V & Jorgenson, M.T., 2013. Advances in Thermokarst Research. , 119(2012), pp.108–119.

Kothawala, D.N., von Wachenfeldt, E., Koehler, B. & Tranvik, L.J., 2012. Selective loss and preservation of lake water dissolved organic matter fluorescence during long-term dark incubations. *Science of the Total Environment*, 433, pp.238–246.

Kowalczuk, P., Tilstone, G.H., Zablocka, M., Rottgers, R. & Thomas, R., 2013. Composition of dissolved organic matter along an Atlantic Meridional Transect from fluorescence spectroscopy and Parallel Factor Analysis. *Marine Chemistry*, 157, pp.170–184.

Kubista, M., Sjoback, R., Eriksson, S. & Albinsson, B., 1994. Experimental correction for the inner-filter effect in fluorescence spectra. *The Analyst*, 119(3), pp.417–419.

Lakowicz, J.R., 2006. *Principles of Fluorescence Spectroscopy* 3rd editio., New York: Springer Science+ Business Media.

Lam, B., Baer, A., Alaee, M., Lefebvre, B., Moser, A., Williams, A. & Simpson, A.J., 2007. Major structural components in freshwater dissolved organic matter. *Environ. Sci. Technol.*, 41(24), pp.8240–8247.

Lam, B. & Simpson, A.J., 2008. Direct 1H NMR spectroscopy of dissolved organic matter in natural waters. *The Analyst*, 133(2), pp.263–269.

Lead, J.R., Wilkinson, K.J., Balnois, E., Cutak, B.J., Larive, C.K., Assemi, S. & Beckett, R., 2000. Diffusion Coefficients and Polydispersities of the Suwannee River Fulvic Acid: Comparison of Fluorescence Correlation Spectroscopy, Pulsed-Field Gradient Nuclear Magnetic Resonance, and Flow Field-Flow Fractionation. *Environmental Science & Technology*, 34, pp.3508–3513.

Ling, F. & Zhang, T., 2003. Numerical simulation of permafrost thermal regime and talik development under shallow thaw lakes on the Alaskan Arctic Coastal Plain. *Journal of Geophysical Research*, 108(D16), p.4511.

Lopes, C.B., Abreu, S., Válega, M., Duarte, R.M.B.O., Pereira, M.E. & Duarte, A. C., 2006. The Assembling and Application of an Automated Segmented Flow Analyzer for the Determination of Dissolved Organic Carbon Based on UV-Persulphate Oxidation. *Analytical Letters*, 39(9), pp.1979–1992.

Matos, J.T.V., Duarte, R.M.B.O, Lopes, S.P., Silva, A.M.S. & Duarte, A.C., 2017. Persistence of urban organic aerosols composition: Decoding their structural complexity and seasonal variability. *Environmental Pollution*, 231, pp.281–290.

Matveev, A., Laurion, I., Deshpande, B.N., Bhiry, N. & Vincent, W.F., 2016. High methane emissions from thermokarst lakes in subarctic peatlands. *Limnology and Oceanography*, 61, pp.S150–S164.

McKnight, D.M., Andrews, E.D., Spaulding, S.A. & Aiken, G.R., 1994. Aquatic fulvic acids in algal-rich antarctic ponds. *Limnology and Oceanography*, 39(8), pp.1972–1979.

McKnight, D.M., Boyer, E.W., Westerhoff, P.K., Doran, P.T., Kulbe, T. & Anderson, D.T., 2001. Spectroflourometric characterization of dissolved organic matter for indication

of precursor organic material and aromaticity. *Limnology and Oceanography*, 46(1), pp.38–48.

Mikita, M.A., Steelink, C. & Wershaw, R.L., 1981. Carbon- 13 Enriched Nuclear Magnetic Resonance Method for the Determination of Hydroxyl Functionality in Humic Substances. *Analytical Chemistry*, 53(11), pp.1715–1717.

Miller, J. and Miller, J., 2010. *Statistics and Chemometrics for Analytical Chemistry* 6th ed., Essex.

Mitchell, P.J., Simpson, A.J., Soong, R., Oren, A., Chefetz, B. & Simpson, M.J., 2013. Solution-state NMR investigation of the sorptive fractionation of dissolved organic matter by alkaline mineral soils. *Environmental Chemistry*, 10(4), pp.333–340.

Mitchell, P.J., Simpson, A.J. & Simpson, M.J., 2013. Dissolved Organic Matter. *eMagRes*, 2, pp.503–516.

Murphy, K.R., Stedmon, C.A., Waite, T.D. & Ruiz, G.M., 2008. Distinguishing between terrestrial and autochthonous organic matter sources in marine environments using fluorescence spectroscopy. *Marine Chemistry*, 108, pp.40–58.

Ohno, T., 2002. Fluorescence inner-filtering correction for determining the humification index of dissolved organic matter. *Environmental Science and Technology*, 36(4), pp.742–746.

Parlanti, E., Worz, K., Geoffroy, L. & Lamotte, M., 2000. Dissolved organic matter fluorescence spectroscopy as a tool to estimate biological activity in a coastal zone submitted to anthropogenic inputs. *Organic Geochemistry*, 31(12), pp.1765–1781.

Paschke, A., 2002. Physicochemical properties of aqueous and solid environmental matrices. In *Sampling and Sample Preparation in Field and Laboratory*. Elsevier B.V., pp. 219–239.

Pedersen, J.A., Simpson, M.A., Bockheim, J.G. & Kumar, K., 2011. Characterization of soil organic carbon in drained thaw-lake basins of Arctic Alaska using NMR and FTIR photoacoustic spectroscopy. *Organic Geochemistry*, 42(8), pp.947–954.

Pellerin, B.A., Hernes, P.J., Saraceno, J.F., Spencer, R.G.M. & Bergamaschi, B.A., 2010.

Microbial Degradation of Plant Leachate Alters Lignin Phenols and Trihalomethane Precursors. *Journal of Environment Quality*, 39(3), p.946.

Preston, C., Trofymow, J.A., Niu, J. & Fyfe, C.A., 1998. 13CPMAS-NMR spectroscopy and chemical analysis of coarse woody debris in coastal forests of Vancouver Island. *Forest Ecology and Management*, 111(1), pp.51–68.

Rinnan, Å., Booksh, K.S. & Bro, R., 2005. First order Rayleigh scatter as a separate component in the decomposition of fluorescence landscapes. *Analytica Chimica Acta*, 537(1-2), pp.349–358.

Romanovsky, V.E., Smith, S.L. & Christiansen, H.H., 2010. Permafrost Thermal State in the Polar Northern Hemisphere during the International Polar Year 2007 – 2009 : a Synthesis. *Permafrost and Periglacial Processes*, 21, pp.106–116.

dos Santos, D.A.R., 2017. *Biogeochemistry of Permafrost Thermokarst Lakes in the Canadian Subarctic*. Instituto Superior Técnico.

Santos, E.B.H., Duarte, R.M.B.O., Filipe, O.S. & Duarte, A.C., 2000. Structural characterisation of the coloured organic matter from an eucalyptus pleached Kraft pulp mill effluent. *International Journal of Environmental Analytical Chemistry*, 78(3-4), pp.333–342.

Santos, E.B.H. & Duarte, A.C., 1998. The influence of pulp and paper mill effluents on the composition of the humic fraction of aquatic organic matter. *Water Research*, 32(3), pp.597–608.

Santos, P.S.M., Santos, E.B.H. & Duarte, A.C., 2012. First spectroscopic study on the structural features of dissolved organic matter isolated from rainwater in different seasons. *Science of the Total Environment*, 426, pp.172–179.

Schuur, E.A.G., Bockheim, J., Canadell, J., Euskirchen, E., Field, C.B., Goryachkin, S.V., Hagemann, S., Kuhry, P., Lafleur, P.M., Lee, H., Mazhitova, G., Nelson, F.E., RInke, A., Romanovsky, V.E., Shiklomanov, N., Tarnocai, C., Venevsky, S., Vogel, J.G. & Zimov, S.A., 2008. Vulnerability of permafrost carbon to climate change: Implications for the global carbon cycle. *BioScience*, 58(8), pp.701–714.

Scott, D.T., McKnight, D.M., Blunt.Harris, E.L., Kolesar, S.E. & Lovley, D.R., 1998.

Quinone moieties act as electron acceptors in the reduction of humic substances by humics-reducing microorganisms. *Environmental Science and Technology*, 32(19), pp.2984–2989.

Sharp, J.H., 1993. The Dissolved Organic Carbon Controversy: An Update. *Oceanography*, 6(2), pp.45–50.

Shin, H.S., Monsallier, J.M. & Choppin, G.R., 1999. Spectroscopic and chemical characterizations of molecular size fractionated humic acid. *Talanta*, 50(3), pp.641–647.

Sillanpää, M., 2014. *Natural Organic Matter Characterization and Treatment Methods*, Elsevier.

Silverstein, R.M., Webster, F.X. & Kiemle, D.J., 2005. *Spectrometric Identification of Organic Compounds* 7th ed., John Wiley & Sons.

Simpson, A., 2001. Multidimensional solution state NMR of humic substances: A practical guide and review. *Soil Science*, 166(11), pp.795–809.

Simpson, A.J., Burdon, J., Graham, C.L., Hayes, M.H.B., Spencer, N. & Kingery, W.L., 2001. Interpretation of heteronuclear and multidimensional NMR spectroscopy of humic substances. *European Journal of Soil Science*, 52(3), pp.495–509.

Simpson, A.J., Kingery, W.L., Hayes, M.H.B., Spraul, M., Humpfer, E., Dvortsak, P., Kerssenbaum, R., Godejohann, M. & Hofmann, M., 2002. Molecular structures and associations of humic substances in the terrestrial environment. *Naturwissenschaften*, 89(2), pp.84–88.

Simpson, M.J., Otto, A. & Feng, X., 2008. Comparison of Solid-State Carbon-13 Nuclear Magnetic Resonance and Organic Matter Biomarkers for Assessing Soil Organic Matter Degradation. *Soil Science Society of America Journal*, 72(1), p.268.

Spencer, R.G.M., Butler, K.D. & Aiken, G.R., 2012. Dissolved organic carbon and chromophoric dissolved organic matter properties of rivers in the USA. *Journal of Geophysical Research: Biogeosciences*, 117(3).

Stedmon, C.A. & Markager, S., 2005a. Resolving the variability in dissolved organic matter

fluorescence in a temperate estuary and its catchment using PARAFAC analysis. *Limnology and Oceanography*, 50(2), pp.686–697.

Stedmon, C.A. & Markager, S., 2005b. Tracing the production and degradation of autochthonous fractions of dissolved organic matter using fluorescence analysis. *Limnology and Oceanography*, 50(5), pp.1415–1426.

Stedmon, C.A., Markager, S. & Bro, R., 2003. Tracing dissolved organic matter in aquatic environments using a new approach to fluorescence spectroscopy. *Marine Chemistry*, 82, pp.239–254.

Stevenson, F.J. & Goh, K.M., 1971. Infrared spectra of humic acids and related substances. *Geochimica et Cosmochimica Acta*, 35(5), pp.471–483.

Streletskiy, D., Anisimov, O. & Vasiliev, A., 2015. Permafrost Degradation. In *Snow and Ice-Related Hazards, Risks, and Disasters*. Elsevier Inc., pp. 303–344. Available at: http://dx.doi.org/10.1016/B978-0-12-394849-6.00010-X.

Tan, K.H., 2003. *Humic Matter in Soil and the Environment Principles and Controversies*, Marcel Dekker, Inc.

Tarnocai, C., Canadell, J.G., Schuur, E.A.G., Kuhry, P., Mazhitova, G. & Zimov, S., 2009. Soil organic carbon pools in the northern circumpolar permafrost region. *Global Biogeochemical Cycles*, 23, pp.1–11.

Thurman, E.M., 1985. *Organic geochemistry of natural waters*, Martinus Nijhoff/Dr W. Junk Publishers.

Tipping, E., 1994. WHAM - A chemical equilibrium model and computer code for waters, sediments, and soil incorporating a discrete site/electrostatic model of ion-binding by humic substances. *Computers & Geosciences*, 20(6), pp.973–1023.

Vincent, W.F., Lemay, M. & Allard, M., 2017. Arctic permafrost landscapes in transition: towards an integrated Earth system approach. *Arctic Science*, 3(2), pp.39–64.

Vonk, J.E., Bowden, W.B., Laurion, I., Vincent, W.F., Alekseychik, P., Amyot, M. & Billet, M.F., 2015. Reviews and syntheses : Effects of permafrost thaw on Arctic aquatic ecosystems. *Biogeosciences*, 12, pp.7129–7167.

Walter, K.M., Edwards, M.E., Grosse, G., Zimov, A. & Chapin III, F.S., 2007. Thermokarst lakes as a source of atmospheric CH4 during the last deglaciation. *Science*, 318, pp.633–636.

Wardencki, W. & Namiesnik, J., 2002. Sampling water and aqueous solutions. In *Sampling and Sample Preparation in Field and Laboratory*. Elsevier B.V., pp. 33–60.

Weishaar, J.L., Fram, M.S., Fujii, R. & Mopper, K., 2003. Evaluation of Specific Ultraviolet Absorbance as an Indicator of the Chemical Composition and Reactivity of Dissolved Organic Carbon. , pp.4702–4708.

Wilson, H.F. & Xenopoulos, M.A., 2009. Effects of agricultural land use on the composition of fluvial dissolved organic matter. *Nature Geoscience*, 2(1), pp.37–41.

Wilson, M.A., Goh, K.M., Collin, P.J. & Greenfield, L.G., 1986. Origins of humus variation. *Organic Geochemistry*, 9(5), pp.225–231.

Woods, G.C., Simpson, M.J., Koerner, P.J., Napoli, A. & Simpson, A.J., 2011. HILIC-NMR: Toward the Identification of Individual Molecular Components in Dissolved Organic Matter. *Environmental Science & Technology*, 45(9), pp.3880–3886.

Woods, G.C., Simpson, M.J. & Simpson, A.J., 2012. Oxidized sterols as a significant component of dissolved organic matter: Evidence from 2D HPLC in combination with 2D and 3D NMR spectroscopy. *Water Research*, 46(10), pp.3398–3408.

Zhang, T., 2005. Influence of seasonal snow cover on the ground thermal regime: an overview. *Reviews in Geophysics*, 43, pp.1–23.

Zimov, S.A., 1997. North Siberian Lakes: A Methane Source Fueled by Pleistocene Carbon. *Science*, 277(5327), pp.800–802.

Zsolnay, A., Baigar, E., Jimenez, M., Steinweg, B. & Saccomandi, F., 1999. Differentiating with fluorescence spectroscopy the sources of dissolved organic matter in soils subjected to drying. *Chemosphere*, 38(1), pp.45–50.

7

Annex

Section 1 – Dissolved organic carbon Quantification

The DOC quantification process was possible through the use of calibration curves obtained using standard solutions of Potassium hydrogen phthalate of known concentrations. A total of eleven DOC quantification experiments were conducted on both SAS samples and fixation blanks. Section 1.1 is solely associated to the DOC quantification experiments conducted on SAS samples, including the initial quantification upon filtration and the quantifications after the extraction process. This section contains the confidence intervals of each obtained slope and intercept, as well as the standard deviation, limit of detection and an hypothesis test to assess whether the standard calibration solution of 0 ppm of C. Section 1.2 focuses on the carbon quantification in the fixation blanks experiments, attempting to detect the presence of methanol; this section also contains the confidence intervals of each obtained slope and intercept, as well as the standard deviation, limit of detection and an hypothesis test to assess whether the standard calibration solution of 0 ppm of C.

Section 1.1

Section 1.1 is organized as displayed in Table 1.1.1.

Sections of Section 1.1	**Description**
Section 1.1.1	Initial quantification of DOM SAS water samples
Section 1.1.2	Quantification of FA SAS-1A SUP and FA SAS-1A F fixation process
Section 1.1.3	Quantification of FA SAS-2A SUP (Replicas 1. 2 and 3) fixation process
Section 1.1.4	Quantification of FA SAS-2A SUP (Replicas 4. 5 and 6) fixation process
Section 1.1.5	Quantification of FA SAS-2A SUP (Replicas 7. 8 and 9) fixation process
Section 1.1.6	Quantification of FA SAS-2A F (Replicas 1, 2,3. and 4) fixation process
Section 1.1.7	Quantification of FA SAS-2A F (Replicas 5, 6, 7, 8. and 9) fixation process
Section 1.1.8	Quantification of FA SAS-1B M (Replicas 1, 2,3. and 4) fixation process
Section 1.1.9	Quantification of FA SAS-1B M (Replicas 5, 6, 7, 8. and 9) fixation process

The DOC quantifications exhibited in Section 1.1.1 and 1.1.2 utilized a calibration curve interval ranging from 1 to 6 ppm of C. However, the importance of measuring a standard solution of 0 ppm of C came to light, thus Sections from 1.1.3 to 1.1.9 displayed a calibration curve interval ranging from 0 to 5 ppm of C. Considering this, only Sections from 1.1.3 to 1.1.9 display the hypothesis test to assess whether the 0 ppm C standard was significantly different from zero.

Section 1.1.1.

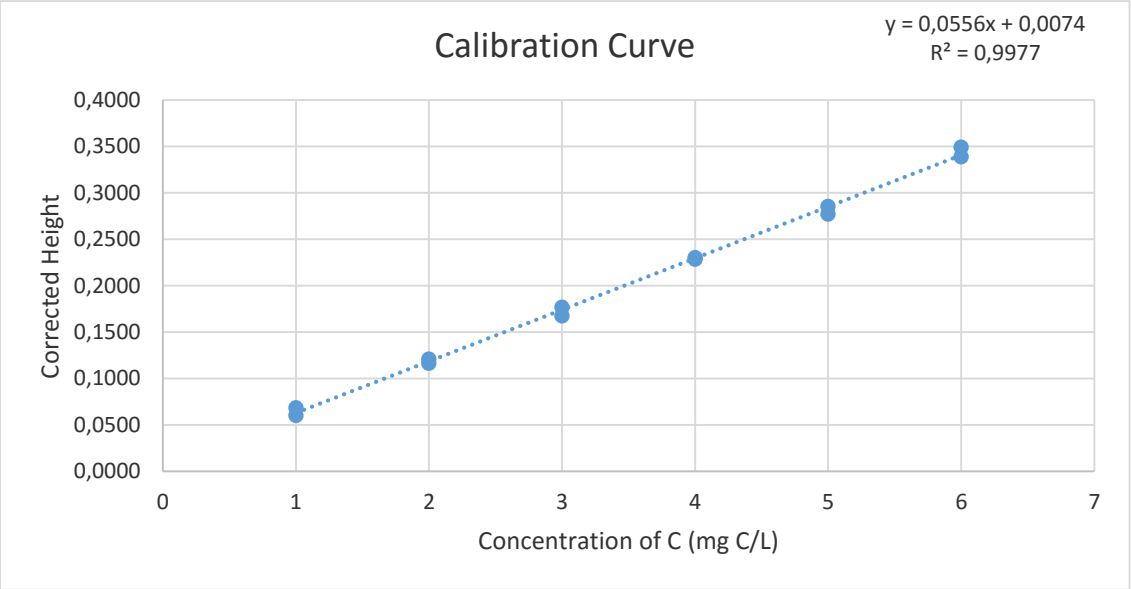

Figure 1.1.1.a – Calibration curve obtained to quantify the DOC content in the SAS water samples upon filtration. Two sets of measurements were used to construct the calibration curve.

The obtained values for DOC quantification of the filtered DOM SAS water samples are expressed in Table 11.

Table 1.1.1.1 – Table containing the slope and intercept of the calibration curve (a linear equation, type y=bx+a), as well as the confidence interval for both slope and intercept, and the obtained limit of detection (LOD).

b	**a**	**Δb**	**Δa**	**LOD (Corrected height)**
0.056	0.007	±0.002	±0.007	0.005

Table 1.1.1.2 – Table containing the dilution factor, average C content of two replicas of each sample and their respective confidence interval.

Sample	Dilution Factor	Average C content (mg C/L)	Confidence Interval (mg C/L)
DOC SAS-1A SUP	10	18.78	±1.52
DOC SAS-1A F	10	18.03	±1.52
DOC SAS-2A SUP	10	22.62	±1.52
DOC SAS-2A F	10	31.54	±1.52
DOC SAS-1B M	10	36.39	±1.52

Section 1.1.2.

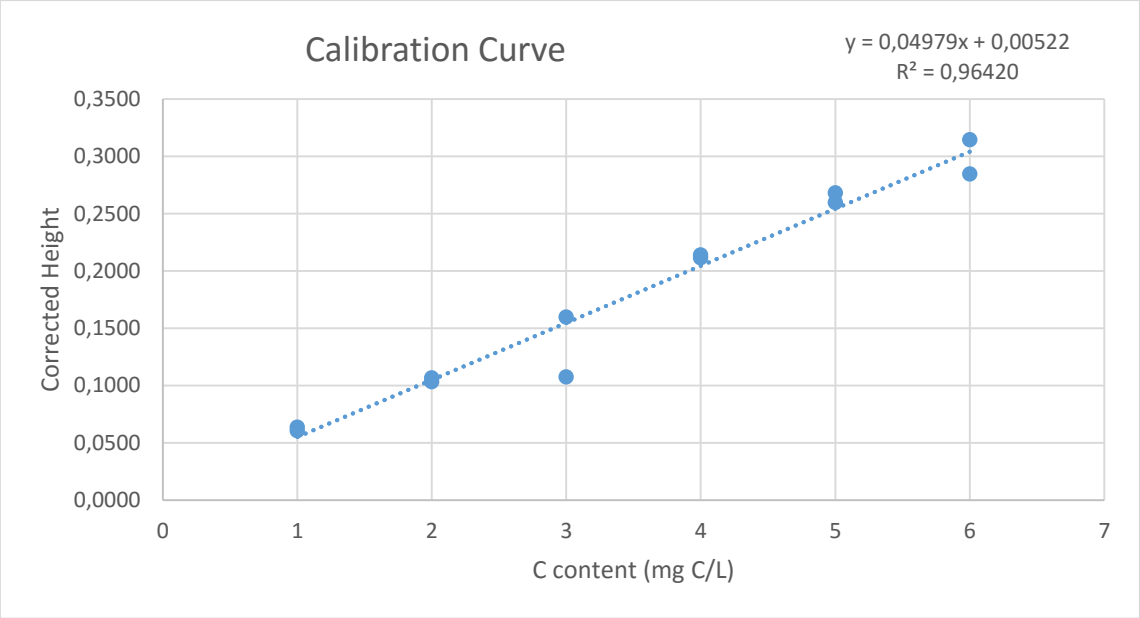

Figure 1.1.2.a – Calibration curve obtained to quantify the DOC content in the fixation process of FA SAS-1A SUP and FA SAS-1A F samples. Two sets of measurements were used to construct the calibration curve.

Table 1.1.2.1 – Table containing the slope and intercept of the calibration curve (a linear equation, type y=bx+a), as well as the confidence interval for both slope and intercept, and the obtained limit of detection (LOD) for DOC quantification of eluates and effluents resulting from the fixation of FA SAS-1A SUP and FA SAS-1A F samples.

b	a	Δb	Δa	LOD (Corrected height)
0.050	0.0052	±0.0068	±0.026	0.023

Table 1.1.2.2 – Table containing the dilution factor, average C content of two replicas of each sample and their respective confidence interval.

Sample	Dilution Factor	Average real C content (mg C/L)	Confidence Interval
SAS-1A S Eluate	100	283.03	±61.34
SAS-1A F 1 Eluate	50	170.48	±30.67
SAS-1A F 2 Eluate	50	193.44	±30.67
SAS-1A S Desalination Effluent	4	4.02	±2.45
SAS-1A F 1 Desalination Effluent	2	1.49	±1.23
SAS-1A F 2 Desalination Effluent	4	9.98	±2.45
SAS-1A S Global Effluent	4	7.29	±2.45
SAS-1A F 1 Global Effluent	4	10.51	±1.87
SAS-1A F 2 Global Effluent	4	30.89	±3.73
SAS-1A S Supernatant Liquid	5	15.14	±3.07
SAS-1A F Supernatant Liquid	5	11.70	±3.73

The results for the SAS-1A F supernatant liquid and global effluents SAS-1A F 1 and SAS-1A F 2 were obtained using the calibration curve of Section 1.1.3.

Section 1.1.3.

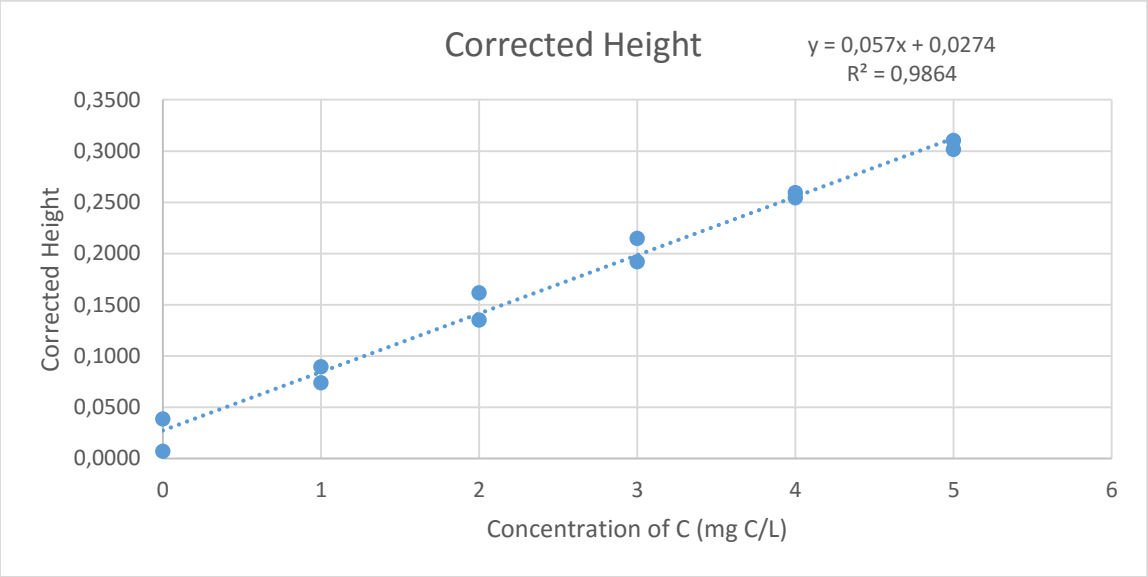

Figure 1.1.3.a – Calibration curve obtained to quantify the DOC content in the fixation process of FA SAS-2A SUP (replicas 1. 2 and 3). Two sets of measurements were used to construct the calibration curve.

Table 1.1.3.1 – Table containing the slope and intercept of the calibration curve (a linear equation, type y=bx+a), as well as the confidence interval for both slope and intercept, and the obtained limit of detection (LOD) for DOC quantification of eluates and effluents resulting from the fixation of FA SAS-2A SUP sample (replicas 1. 2 and 3).

b	**a**	**Δb**	**Δa**	**LOD (Corrected height)**
0.057	0.027	0.005	0.014	0.040

Table 1.1.3.2 – Table containing the dilution factor, average C content of two replicas of each sample and their respective confidence interval for DOC quantification of eluates and effluents resulting from the fixation of FA SAS-2A SUP sample (replicas 1. 2 and 3).

Sample	**Dilution Factor**	**Average real C content (mg C/L)**	**Confidence Interval**
SAS-2A S 1 Eluate	20	60.30	±7.47
SAS-2A S 2 Eluate	20	67.00	±7.47
SAS-2A S 3 Eluate	20	63.96	±7.47
SAS-2A S 1 Desalination Effluent	5	9.82	±1.87
SAS-2A S 2 Desalination Effluent	2	3.23	±0.75
SAS-2A S 3 Desalination Effluent	50	45.70	±18.67
SAS-SA S 1 Global Effluent	50	245.66	±18.67
SAS-2A S 2 Global Effluent	50	246.89	±18.67
SAS-2A S 3 Global Effluent	50	22.32	±18.67
SAS-2A S Supernatant Liquid	5	20.21	±1.87

Table 1.1.3.3 – Table containing the |t| two-way critical value and the obtained |t| value for the standard solutions of 0 ppm C, as well as the corresponding hypothesis test for α=0.05. H_0: the standard solution of 0 ppm C is equal to zero; H_1: the standard solution of 0 ppm C is different than zero.

Critical value of |t| (two way)	12.71
Obtained |t|	2.07

As the critical value of |t| is greater than the obtained value of |t|, we cannot reject hypothesis H_0. that states that the standard solution of 0 ppm of C is equal to zero.

Section 1.1.4.

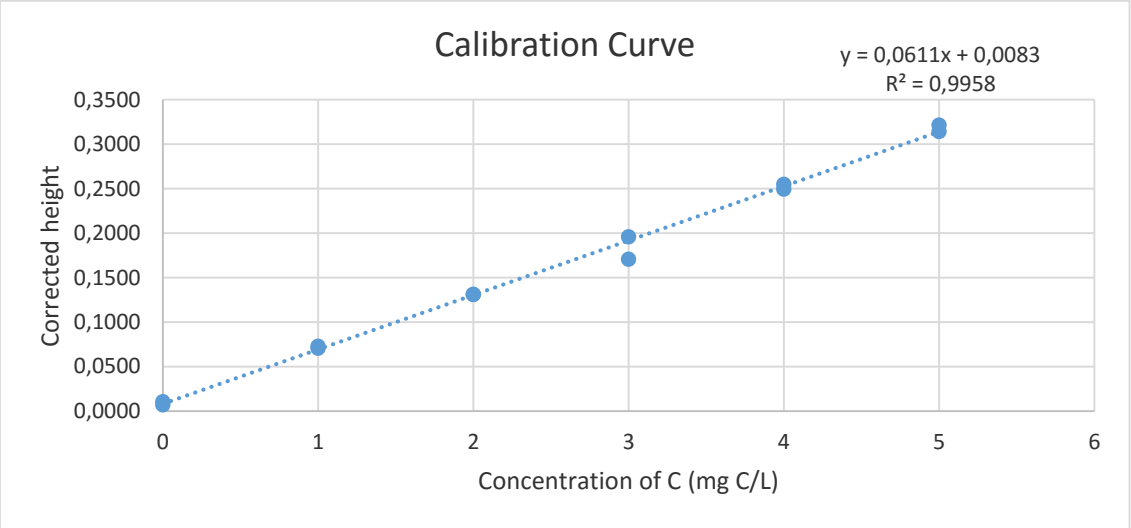

Figure 1.1.4.a – Calibration curve obtained to quantify the DOC content in the fixation process of FA SAS-2A SUP (replicas 4. 5 and 6). Two sets of measurements were used to construct the calibration curve.

Table 1.1.4.1 – Table containing the slope and intercept of the calibration curve (a linear equation, type y=bx+a), as well as the confidence interval for both slope and intercept, and the obtained limit of detection (LOD) for DOC quantification of eluates and effluents resulting from the fixation of FA SAS-2A SUP sample (replicas 4, 5 and 6).

b	**a**	**Δb**	**Δa**	**LOD (Corrected height)**
0.061	0.008	±0.003	±0.009	0.016

Table 1.1.4.2 – Table containing the dilution factor, average C content of two replicas of each sample and their respective confidence interval for DOC quantification of eluates and effluents resulting from the fixation of FA SAS-2A SUP sample (replicas 4, 5 and 6).

Sample	**Dilution Factor**	**Average real C content (mg C/L)**	**Confidence Interval**
SAS-2A SUP Global Effluent 4	5	10.16	±1.03
SAS-2A SUP Global Effluent 5	20	61.41	±4.14
SAS-2A SUP Desalination Effluent 4	1	3.06	±0.21
SAS-2A SUP Desalination Effluent 5	1	2.79	±0.21
SAS-2A SUP Desalination Effluent 6	1	3.11	±0.21
SAS-2A SUP Eluate 4	20	64.11	±4.14
SAS-2A SUP Eluate 5	20	55.89	±4.14
SAS-2A SUP Eluate 6	20	54.71	±4.14
SAS-2A SUP Global Effluent 6	5	17.59	±1.03
SAS-2A S Supernatant Liquid	5	20.21	±1.03

Table 1.1.4.3 – Table containing the |t| two-way critical value and the obtained |t| value for the standard solutions of 0 ppm C, as well as the corresponding hypothesis test for α=0.05. H_0: the standard solution of 0 ppm C is equal to zero; H_1: the standard solution of 0 ppm C is different than zero.

Critical value of |t| (two way)	12.71
Obtained |t|	6.92

As the critical value of |t| is greater than the obtained value of |t|, we cannot reject hypothesis H_0. that states that the standard solution of 0 ppm of C is equal to zero.

Section 1.1.5.

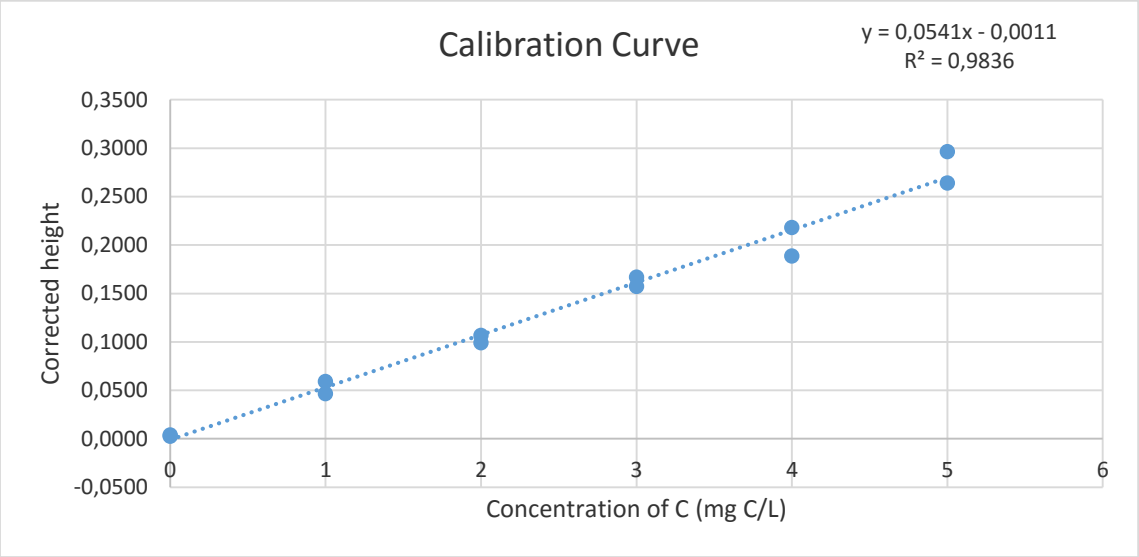

Figure 1.1.5.a – Calibration curve obtained to quantify the DOC content in the fixation process of FA SAS-2A SUP (replicas 7. 8 and 9). Two sets of measurements were used to construct the calibration curve.

Table 1.1.5.1 – Table containing the slope and intercept of the calibration curve (a linear equation, type y=bx+a), as well as the confidence interval for both slope and intercept, and the obtained limit of detection (LOD) for DOC quantification of eluates and effluents resulting from the fixation of FA SAS-2A SUP sample (replicas 7. 8 and 9).

b	**a**	**Δb**	**Δa**	**LOD (Corrected Height)**
0.054	-0.001	±0.005	±0.015	0.012

Table 1.1.5.2 – Table containing the dilution factor, average C content of two replicas of each sample and their respective confidence interval for DOC quantification of eluates and effluents resulting from the fixation of FA SAS-2A SUP sample (replicas 7, 8 and 9).

Sample	**Dilution Factor**	**Average real C content (mg C/L)**	**Confidence Interval**
SAS-2A SUP Global Effluent 7	5	5.25	±2.09
SAS-2A SUP Global Effluent 8	20	32.07	±8.35
SAS-2A SUP Global Effluent 9	20	28.23	±8.35
SAS-2A SUP Desalination Effluent 7	1	3.15	±0.42
SAS-2A SUP Desalination Effluent 8	1	3.29	±0.42
SAS-2A SUP Desalination Effluent 9	3	7.13	±1.25
SAS-2A SUP Eluate 7	50	88.73	±20.87
SAS-2A SUP Eluate 8	20	66.90	±8.35
SAS-2A SUP Eluate 9	20	77.56	±8.35
SAS-2A S Supernatant Liquid	5	20.22	±2.09

Table 1.1.5.3 – Table containing the |t| two-way critical value and the obtained |t| value for the standard solutions of 0 ppm C, as well as the corresponding hypothesis test for α=0.05. H_0: the standard solution of 0 ppm C is equal to zero; H_1: the standard solution of 0 ppm C is different than zero.

Critical value of |t| (two way)	12.71
Obtained |t|	7.07

As the critical value of |t| is greater than the obtained value of |t|, we cannot reject hypothesis H_0. that states that the standard solution of 0 ppm of C is equal to zero.

Section 1.1.6.

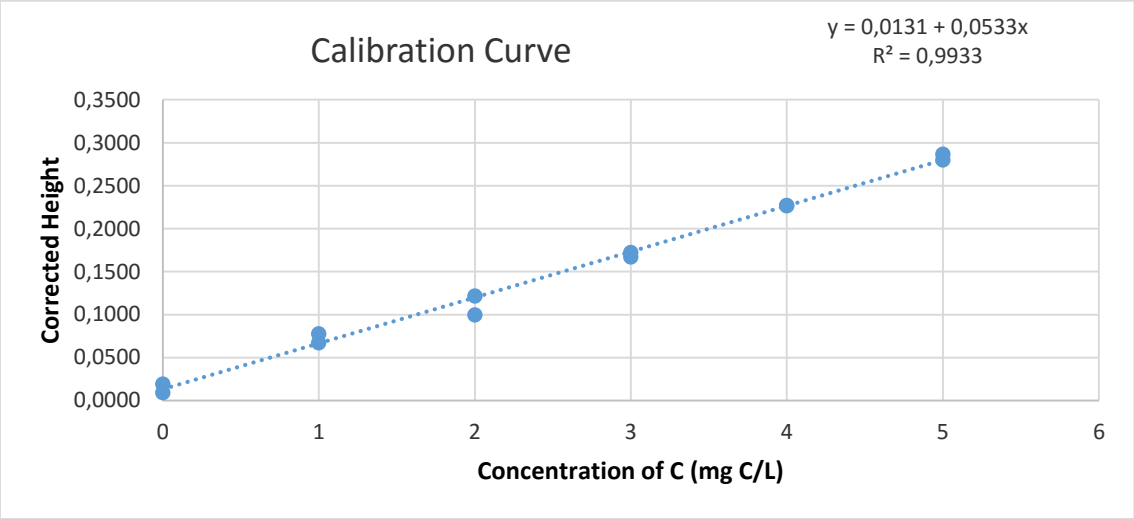

Figure 1.1.6.a – Calibration curve obtained to quantify the DOC content in the fixation process of FA SAS-2A F (replicas 1, 2, 3 and 4). Two sets of measurements were used to construct the calibration curve.

Table 1.1.6.1 – Table containing the slope and intercept of the calibration curve (a linear equation, type y=bx+a), as well as the confidence interval for both slope and intercept, and the obtained limit of detection (LOD) for DOC quantification of eluates and effluents resulting from the fixation of FA SAS-2A F sample (replicas 1, 2, 3 and 4).

b	**a**	**Δb**	**Δa**	**LOD (Corrected Height)**
0.053	0.013	±0.003	±0.009	0.019

Table 1.1.6.2 – Table containing the dilution factor, average C content of two replicas of each sample and their respective confidence interval for DOC quantification of eluates and effluents resulting from the fixation of FA SAS-2A F sample (replicas 1, 2, 3 and 4).

Sample	**Dilution Factor**	**Average real C content (mg C/L)**	**Confidence Interval**
SAS-2A F Global Effluent 1	50	271.95	±13.05
SAS-2A F Global Effluent 2	50	247.65	±13.05
SAS-2A F Global Effluent 3	10	15.91	±2.61
SAS-2A F Global Effluent 4	10	12.76	±2.61
SAS-2A F Desalination Effluent 1	50	112.43	±13.05
SAS-2A F Desalination Effluent 2	50	205.72	±13.05
SAS-2A F Desalination Effluent 3	50	77.63	±13.05
SAS-2A F Desalination Effluent 4	20	29.76	±5.22
SAS-2A F Supernatant Liquid	10	19.14	±2.61
SAS-2A F Eluate 2	20	56.75	±5.22
SAS-2A F Eluate 4	20	60.51	±5.22
SAS-2A F Eluate 1	20	59.32	±5.22
SAS-2A SUP Global Effluent 6	5	17.59	±1.30

Table 1.1.6.3 – Table containing the |t| two-way critical value and the obtained |t| value for the standard solutions of 0 ppm C, as well as the corresponding hypothesis test for α=0.05. H_0: the standard solution of 0 ppm C is equal to zero; H_1: the standard solution of 0 ppm C is different than zero.

Critical value of |t| (two way)	12.71
Obtained |t|	4.08

As the critical value of |t| is greater than the obtained value of |t|, we cannot reject hypothesis H_0. that states that the standard solution of 0 ppm of C is equal to zero.

Section 1.1.7.

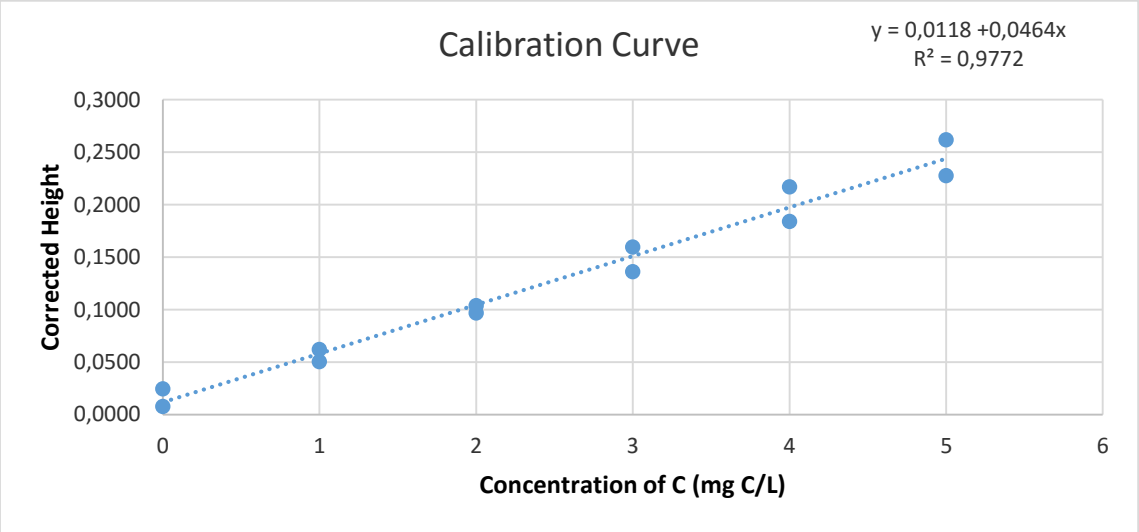

Figure 1.1.7.a – Calibration curve obtained to quantify the DOC content in the fixation process of FA SAS-2A F (replicas 5, 6, 7, 8 and 9). Two sets of measurements were used to construct the calibration curve.

Table 1.1.7.1 – Table containing the slope and intercept of the calibration curve (a linear equation, type y=bx+a), as well as the confidence interval for both slope and intercept, and the obtained limit of detection (LOD) for DOC quantification of eluates and effluents resulting from the fixation of FA SAS-2A F sample (replicas 5, 6, 7, 8 and 9).

b	**a**	**Δb**	**Δa**	**LOD (Corrected Height)**
0.046	0.012	±0.015	±0.005	0.025

Table 1.1.7.2 – Table containing the dilution factor, average C content of two replicas of each sample and their respective confidence interval for DOC quantification of eluates and effluents resulting from the fixation of FA SAS-2A F sample (replicas 5, 6, 7, 8 and 9).

Samples	**Dilution Factor**	**Average real C content (mg C/L)**	**Confidence Interval**
SAS-2A F Global Effluent 5	100	285.88	±48.62
SAS-2A F Global Effluent 6	100	224.03	±48.62
SAS-2A F Global Effluent 7	10	10.82	±4.86
SAS-2A F Global Effluent 8	10	17.19	±4.86
SAS-2A F Global Effluent 9	5	8.92	±2.43
SAS-2A F Desalination Effluent 5	20	43.19	±9.72
SAS-2A F Desalination Effluent 6	20	66.06	±9.72
SAS-2A F Desalination Effluent 7	1	3.86	±0.49
SAS-2A F Desalination Effluent 8	1	4.23	±0.49
SAS-2A F Desalination Effluent 9	1	3.47	±0.49
SAS-2A F Eluate 5	20	69.35	±9.72
SAS-2A F Eluate 6	20	72.76	±9.72
SAS-2A F Eluate 7	20	95.02	±9.72
SAS-2A F Eluate 8	20	97.28	±9.72
SAS-2A F Eluate 9	20	101.16	±9.72

Table 1.1.7.3 – Table containing the |t| two-way critical value and the obtained |t| value for the standard solutions of 0 ppm C, as well as the corresponding hypothesis test for α=0.05. H_0: the standard solution of 0 ppm C is equal to zero; H_1: the standard solution of 0 ppm C is different than zero.

Critical value of |t| (two way)	12.71
Obtained |t|	2.72

As the critical value of |t| is greater than the obtained value of |t|, we cannot reject hypothesis H_0. that states that the standard solution of 0 ppm of C is equal to zero.

Section 1.1.8.

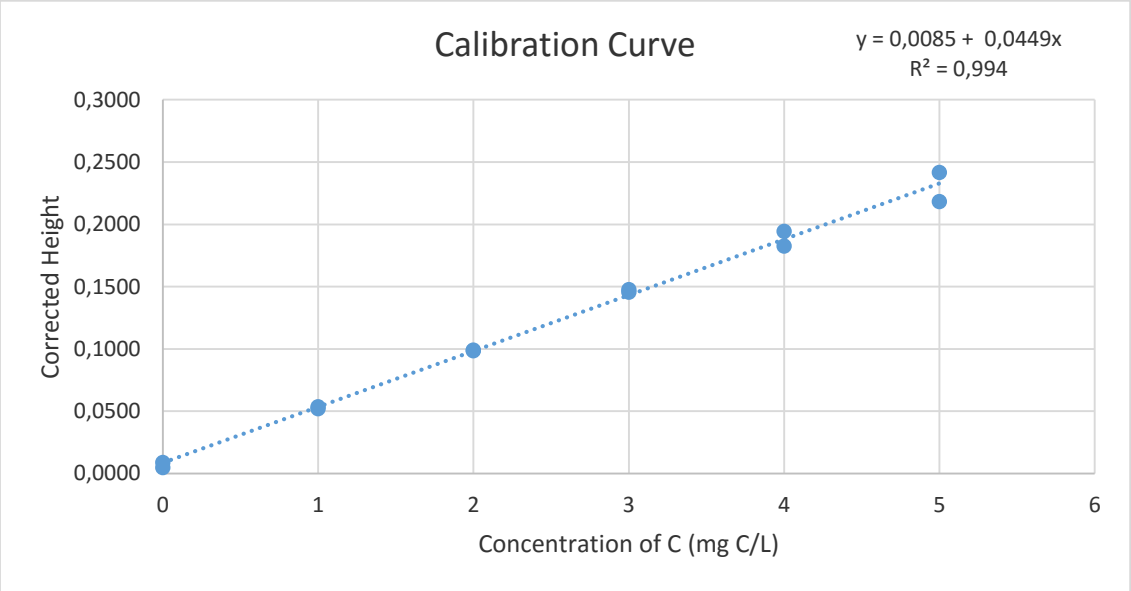

Figure 1.1.8.a – Calibration curve obtained to quantify the DOC content in the fixation process of FA SAS-1B M (replicas 1, 2, 3 and 4). Two sets of measurements were used to construct the calibration curve.

Table 1.1.8.1 – Table containing the slope and intercept of the calibration curve (a linear equation, type y=bx+a), as well as the confidence interval for both slope and intercept, and the obtained limit of detection (LOD) for DOC quantification of eluates and effluents resulting from the fixation of FA SAS-1B M sample (replicas 1, 2, 3 and 4).

b	**a**	**Δb**	**Δa**	**LOD (Corrected Height)**
0.0449	0.0085	0.0024	0.0072	0.0149

Table 1.1.8.2 – Table containing the dilution factor, average C content of two replicas of each sample and their respective confidence interval for DOC quantification of eluates and effluents resulting from the fixation of FA SAS-1B M sample (replicas 1, 2, 3 and 4).

Sample	**Dilution Factor**	**Average real C content (mg C/L)**	**Confidence Interval**
SAS-1B M Global Effluent 1	2	3.30	±0.48
SAS-1B M Global Effluent 2	1	3.50	±0.24
SAS-1B M Global Effluent 3	1	2.48	±0.24
SAS-1B M Global Effluent 4	1	1.48	±0.24
SAS-1B M Desalination Effluent 1	1	3.74	±0.24
SAS-1B M Desalination Effluent 2	1	3.50	±0.24
SAS-1B M Desalination Effluent 3	1	3.84	±0.24
SAS-1B M Desalination Effluent 4	1	7.06	±0.24
SAS-1B M Supernatant Liquid	10	23.34	±2.41
SAS-1B M Eluate 1	20	67.13	±4.82
SAS-1B M Eluate 2	20	62.92	±4.82
SAS-1B M Eluate 3	20	64.41	±4.82
SAS-1B M Eluate 4	50	98.11	±12.05

Table 1.1.8.3 – Table containing the |t| two-way critical value and the obtained |t| value for the standard solutions of 0 ppm C, as well as the corresponding hypothesis test for α=0.05. H_0: the standard solution of 0 ppm C is equal to zero; H_1: the standard solution of 0 ppm C is different than zero.

Critical value of |t| (two way)	12.71
Obtained |t|	4.80

As the critical value of |t| is greater than the obtained value of |t|, we cannot reject hypothesis H_0. that states that the standard solution of 0 ppm of C is equal to zero.

Section 1.1.9.

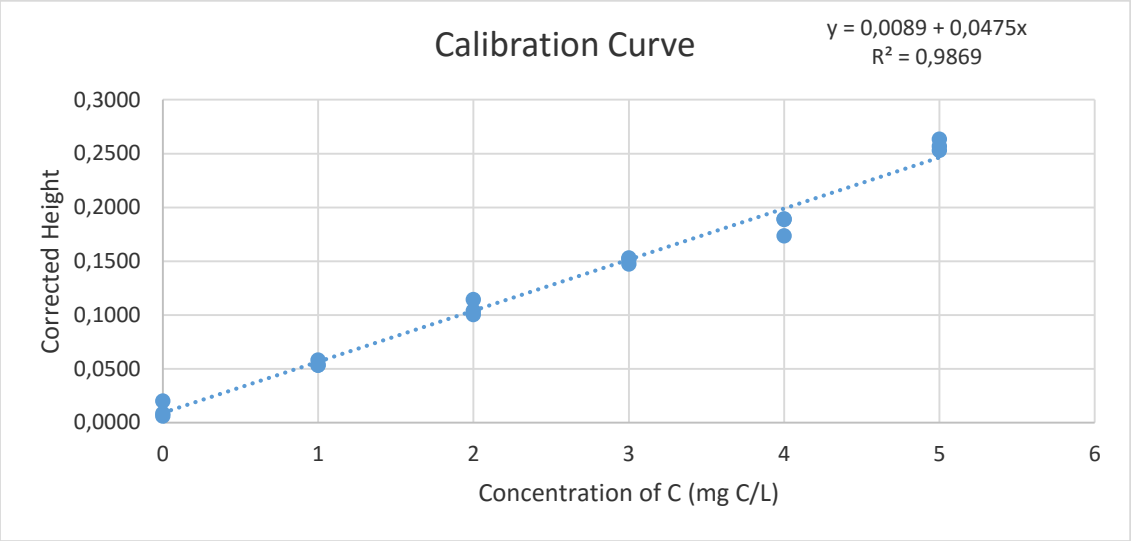

Figure 1.1.9.a – Calibration curve obtained to quantify the DOC content in the fixation process of FA SAS-1B M (replicas 5, 6, 7, 8 and 9). Three sets of measurements were used to construct the calibration curve.

Table 1.1.9.1 – Table containing the slope and intercept of the calibration curve (a linear equation, type y=bx+a), as well as the confidence interval for both slope and intercept, and the obtained limit of detection (LOD) for DOC quantification of eluates and effluents resulting from the fixation of FA SAS-1B M sample (replicas 5, 6, 7, 8 and 9).

b	**a**	**Δb**	**Δa**	**LOD (Corrected Height)**
0.048	0.009	0.003	0.009	0.020

Table 1.1.9.2 – Table containing the dilution factor, average C content of two replicas of each sample and their respective confidence interval for DOC quantification of eluates and effluents resulting from the fixation of FA SAS-2A F sample (replicas 5, 6, 7, 8 and 9).

Sample	Dilution Factor	Average real C content (mg C/L)	Confidence Interval
SAS-1B M Global Effluent 5	5	18.28	±1.65
SAS-1B M Global Effluent 6	5	16.77	±1.65
SAS-1B M Global Effluent 7	2	4.56	±0.66
SAS-1B M Global Effluent 8	2	5.32	±0.66
SAS-1B M Global Effluent 9	3	9.00	±0.99
SAS-1B M Desalination Effluent 5	3	9.38	±0.99
SAS-1B M Desalination Effluent 6	3	6.80	±0.99
SAS-1B M Desalination Effluent 7	1	2.93	±0.33
SAS-1B M Desalination Effluent 8	1	3.00	±0.33
SAS-1B M Desalination Effluent 9	1	2.91	±0.33
SAS-1B M Eluate 5	50	86.79	±16.47
SAS-1B M Eluate 6	50	94.89	±16.47
SAS-1B M Eluate 7	20	71.03	±6.59
SAS-1B M Eluate 8	20	70.74	±6.59
SAS-1B M Eluate 9	20	75.75	±6.59

Table 1.1.9.3 – Table containing the |t| two-way critical value and the obtained |t| value for the standard solutions of 0 ppm C, as well as the corresponding hypothesis test for α=0.05. H_0: the standard solution of 0 ppm C is equal to zero; H_1: the standard solution of 0 ppm C is different than zero.

Critical value of |t| (two way)	4.30
Obtained |t|	3.32

As the critical value of |t| is greater than the obtained value of |t|, we cannot reject hypothesis H_0. that states that the standard solution of 0 ppm of C is equal to zero.

Section 1.1.10.

This section focuses on the obtained masses of each FA SAS sample upon lyophilization. It should be noted that FA SAS-2A SUP, FA SAS-2A F and FA SAS-1B M were extracted using 9 fixation replicas, thus improving the FA recovery, resulting in a total eluate volume of 450 ml each. Considering this volume, only the totality of FA SAS-2A sample was lyophilized; in the case of FA SAS-2A F and FA SAS-1B M samples, 150 ml of the total 450 ml were lyophilized, thus explaining the lower obtained FA sample mass.

Table 1.1.10 – Table containing the obtained masses for the lyophilized FA SAS samples.

Sample	Mass
FA SAS-1A SUP	30.1 mg
FA SAS-1A F	33.5 mg
FA SAS-2A SUP	74.9 mg
FA SAS-2A F	26.9 mg
FA SAS-1B M	24.3 mg

Section 1.2.

Section 1.2 is divided into three subsections, where sections 1.2.1 and 1.2.2 are dedicated to the calibration curve, hypothesis testing of standard solution 0 ppm C, and confidence interval for slope and intercept, as well as for each measurement. Section 1.2.3 highlights the difference between the different calculated percentages calculated upon the extraction process, comparing results from DOC and $SUVA_{254}$.

Section 1.2.1.

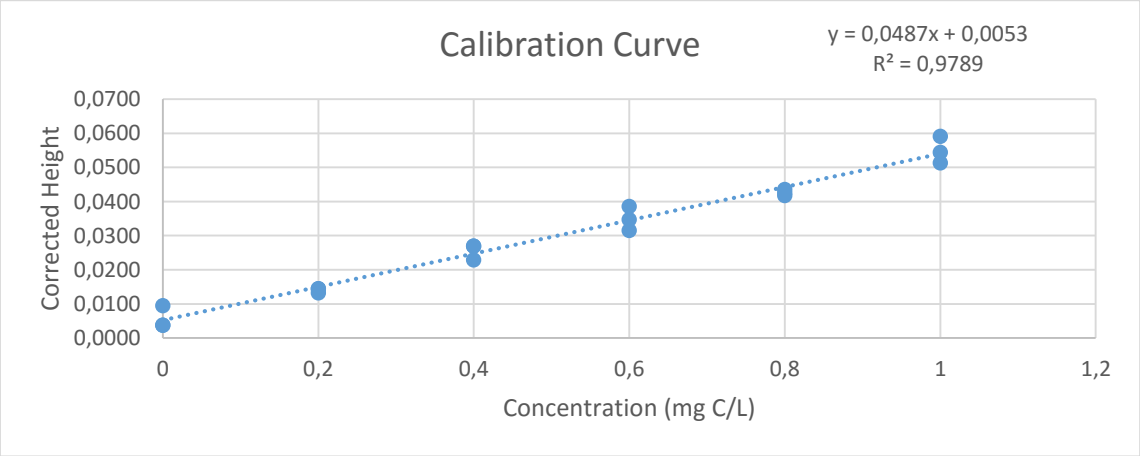

Figure 1.2.1.a – Calibration curve obtained to quantify the DOC content in the fixation blanks, as a way to assert the presence of methanol in the resulting effluents. Three sets of measurements were used to construct the calibration curve.

Table 1.2.1.1 – Table containing the slope and intercept of the calibration curve (a linear equation, type y=bx+a), as well as the confidence interval for both slope and intercept, and the obtained limit of detection (LOD) for DOC quantification of eluates and effluents resulting from the content in the fixation blank.

b	a	Δb	Δa	LOD (Corrected Height)
0.049	0.005	0.004	0.002	0.020

Table 1.2.1.2 – Table containing the dilution factor, average C content of two replicas of each sample and their respective confidence interval for DOC quantification of eluates and effluents resulting from the detection of DOC in the fixation blanks.

Sample	**Dilution Factor**	**Average real C content (mg C/L)**	**Confidence Interval**
Fixation Blank - Global Effluent 1	20	13.61	±1.68
Fixation Blank - Global Effluent 2	20	9.28	±1.68
Fixation Blank - Global Effluent 3	10	6.89	±0.84
Fixation Blank - Global Effluent 4	3	8.45	±0.25
Fixation Blank - Global Effluent 5	3	3.15	±0.25
Fixation Blank - Desalination Effluent 3	10	5.53	±0.84
Fixation Blank - Desalination Effluent 4	1	0.86	±0.08
Fixation Blank - Desalination Effluent 5	1	0.83	±0.08
Fixation Blank - Eluate 1	2	1.14	±0.17
Fixation Blank - Eluate 2	1	0.82	±0.08
Fixation Blank - Eluate 3	1	1.02	±0.08
Fixation Blank - Eluate 4	3	1.31	±0.25
Fixation Blank - Eluate 5	3	2.14	±0.25
H_2O MQ pH 2	1	0.00	±0.08

Table 1.2.1.3 – Table containing the |t| two-way critical value and the obtained |t| value for the standard solutions of 0 ppm C, as well as the corresponding hypothesis test for α=0.05. H_0: the standard solution of 0 ppm C is equal to zero; H_1: the standard solution of 0 ppm C is different than zero.

Critical value of |t| (two way)	4.30
Obtained |t|	3.67

As the critical value of |t| is greater than the obtained value of |t|, we cannot reject hypothesis H_0. that states that the standard solution of 0 ppm of C is equal to zero.

Section 1.2.2.

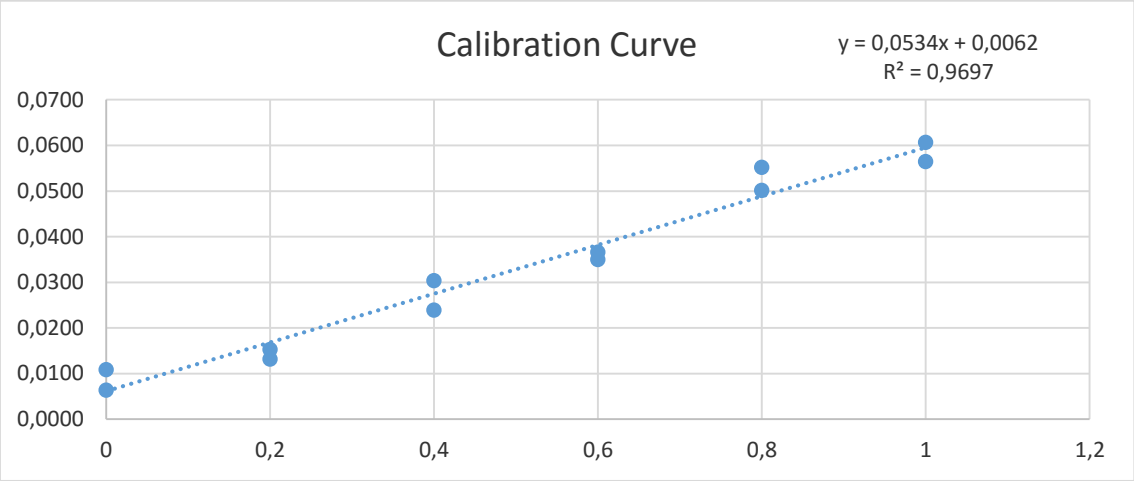

Figure 1.2.1.a – Calibration curve obtained to quantify the DOC content in the fixation blanks, as a way to assert the presence of methanol in the resulting effluents. Three sets of measurements were used to construct the calibration curve.

Table 1.2.1.1 – Table containing the slope and intercept of the calibration curve (a linear equation, type y=bx+a), as well as the confidence interval for both slope and intercept, and the obtained limit of detection (LOD) for DOC quantification of eluates and effluents resulting from the content in the fixation blank.

b	**a**	**Δb**	**Δa**	**LOD (Corrected Height)**
0.053	0.006	0.007	0.004	0.010

Table 1.2.1.2 – Table containing the dilution factor, average C content of two replicas of each sample and their respective confidence interval for DOC quantification of eluates and effluents resulting from the detection of DOC in the fixation blanks.

Sample	**Dilution Factor**	**Concentration of C (mg/L)**	**Confidence Interval**
Desalination Blank - Desalination Effluent 1	20	8.82	±2.25
Desalination Blank - Desalination Effluent 2	20	8.80	±2.25

Table 1.2.1.3 – Table containing the |t| two-way critical value and the obtained |t| value for the standard solutions of 0 ppm C, as well as the corresponding hypothesis test for α=0.05. H_0: the standard solution of 0 ppm C is equal to zero; H_1: the standard solution of 0 ppm C is different than zero.

Critical value of |t| (two way)	12.71
Obtained |t|	5.44

As the critical value of |t| is greater than the obtained value of |t|, we cannot reject hypothesis $H_{0.}$ that states that the standard solution of 0 ppm of C is equal to zero.

Section 1.2.3.

Table 1.2.3.1. – Comparison between the calculated percentages of the fixation process for DOC values and $SUVA_{254}$ values for FA SAS-1A SUP and FA SAS-1A F (2 replicas) samples.

DATA DOC	**SAS-1A SUP**	**SAS-1A F 1**	**SAS-1A F 2**
Fixation Percentage (%)	51.83	14.29	-154.83
Desalination Losses (%)	0.59	0.51	3.12
Recovery Percentage (%)	41.54	58.55	60.39
Irreversible Losses (%)	9.70	-44.77	-218.34
Non-fixated Percentage (%)	48.17	85.71	254.83
DATA $SUVA_{254}$	**SAS-1A SUP**	**SAS-1A F 1**	**SAS-1A F 2**
Fixation Percentage (%)	69.92	77.69	67.55
Desalination Losses (%)	1.80	3.03	3.42
Recovery Percentage (%)	52.43	44.91	60.91
Irreversible Losses (%)	15.69	29.74	3.21
Non-fixated Percentage (%)	30.08	22.31	32.45

Table 1.2.3.2. – Comparison between the calculated percentages of the fixation process for DOC values and $SUVA_{254}$ values for FA SAS-2A SUP (9 replicas) sample.

DATA DOC	**SAS-2A S 1**	**SAS-2A S 2**	**SAS-2A S 3**	**SAS-2A SUP 4**	**SAS-2A SUP 5**	**SAS-2A SUP 6**	**SAS-2A SUP 7**	**SAS-2A SUP 8**	**SAS-2A SUP 9**
Fixation Percentage (%)	-1115.23	-1121.31	-10.44	49.74	-203.77	12.99	74.37	-55.89	-37.35
Desalination Losses (%)	12.14	3.99	56.52	3.74	3.45	3.85	3.43	3.65	8.39
Recovery Percentage (%)	74.57	82.86	79.11	78.50	69.12	67.66	97.06	74.27	91.08
Irreversible Losses (%)	-1201.94	-1208.16	-146.06	-32.50	-276.35	-58.52	-26.12	-133.81	-136.82
Non-fixated Percentage (%)	1215.23	1221.31	110.44	50.26	303.77	87.01	25.63	155.89	137.35
DATA UV-Vis	**SAS-2A S 1**	**SAS-2A S 2**	**SAS-2A S 3**	**SAS-2A SUP 4**	**SAS-2A SUP 5**	**SAS-2A SUP 6**	**SAS-2A SUP 7**	**SAS-2A SUP 8**	**SAS-2A SUP 9**
Fixation Percentage (%)	90.08	90.35	93.45	93.27	95.18	94.90	93.54	93.54	93.45
Desalination Losses (%)	3.48	3.78	2.62	2.23	1.87	1.89	1.80	1.50	1.73
Recovery Percentage (%)	74.16	66.88	68.70	66.67	48.68	57.32	83.41	63.44	73.67
Irreversible Losses (%)	12.44	19.70	22.13	24.37	44.63	35.69	8.33	28.59	18.05
Non-fixated Percentage (%)	9.92	9.65	6.55	6.73	4.82	5.10	6.46	6.46	6.55

Table 1.2.3.3. – Comparison between the calculated percentages of the fixation process for DOC values and $SUVA_{254}$ values for FA SAS-2A F (9 replicas) sample.

DATA DOC	**SAS-2A F 1**	**SAS-2A F 2**	**SAS-2A F 3**	**SAS-2A F 4**	**SAS-2A F 5**	**SAS-2A F 6**	**SAS-2A F 7**	**SAS-2A F 8**	**SAS-2A F 9**
Fixation Percentage (%)	-1321.08	-1194.12	16.86	33.33	-1393.88	-1070.67	43.47	10.19	53.38
Desalination Losses (%)	145.42	144.00	100.41	38.87	56.42	86.29	3.60	3.69	3.02
Recovery Percentage (%)	76.73	72.69	-	79.04	90.60	95.05	88.67	84.73	88.11
Irreversible Losses (%)	-1543.23	-1410.80	-	-84.58	-1540.91	-1252.01	-48.80	-78.23	-37.75
Non-fixated Percentage (%)	1421.08	1294.12	-	66.67	1493.88	1170.67	56.53	89.81	46.62
DATA UV-Vis	**SAS-2A F 1**	**SAS-2A F 2**	**SAS-2A F 3**	**SAS-2A F 4**	**SAS-2A F 5**	**SAS-2A F 6**	**SAS-2A F 7**	**SAS-2A F 8**	**SAS-2A F 9**
Fixation Percentage (%)	92.39	92.28	93.51	90.38	90.72	89.71	90.49	89.37	89.37
Desalination Losses (%)	3.77	3.59	3.65	4.11	4.45	4.28	3.16	3.11	3.21
Recovery Percentage (%)	46.24	61.14	-	64.88	83.61	67.95	66.32	68.98	66.18
Irreversible Losses (%)	42.39	27.55	-	21.39	2.66	17.48	21.02	17.28	19.99
Non-fixated Percentage (%)	7.61	7.72	-	9.62	9.28	10.29	9.51	10.63	10.63

Table 1.2.3.4. – Comparison between the calculated percentages of the fixation process for DOC values and $SUVA_{254}$ values for FA SAS-1B M (9 replicas) sample.

DATA DOC	**SAS-1B M 1**	**SAS-1B M 2**	**SAS-1B M 3**	**SAS-1B M 4**	**SAS-1B M 5**	**SAS-1B M 6**	**SAS-1B M 7**	**SAS-1B M 8**	**SAS-1B M 9**
Fixation Percentage (%)	85.85	85.02	89.40	93.65	21.69	28.16	80.46	77.21	61.43
Desalination Losses (%)	4.01	3.75	4.12	5.82	7.73	5.60	3.31	3.38	3.28
Recovery Percentage (%)	71.90	67.39	68.99	80.83	71.51	78.19	80.09	79.75	85.40
Irreversible Losses (%)	9.94	13.88	16.29	7.00	-57.55	-55.63	-2.93	-5.93	-27.25
Non-fixated Percentage (%)	14.15	14.98	10.60	6.35	78.31	71.84	19.54	22.79	38.57
DATA UV-Vis	**SAS-1B M 1**	**SAS-1B M 2**	**SAS-1B M 3**	**SAS-1B M 4**	**SAS-1B M 5**	**SAS-1B M 6**	**SAS-1B M 7**	**SAS-1B M 8**	**SAS-1B M 9**
Fixation Percentage (%)	95.91	95.57	95.22	92.43	92.43	91.22	93.48	92.00	91.74
Desalination Losses (%)	1.93	1.96	1.85	1.72	1.69	1.76	2.22	2.27	2.45
Recovery Percentage (%)	61.09	54.35	58.70	68.06	66.22	69.40	73.00	66.36	72.77
Irreversible Losses (%)	32.89	39.26	34.67	22.65	24.53	20.06	18.26	23.37	16.52
Non-fixated Percentage (%)	4.09	4.43	4.78	7.57	7.57	8.78	6.52	8.00	8.26

Section 1.3.

The DOC content in the filtered DOM SAS samples was measured, and their SUVA 254 values were obtained. Based on their DOC concentration and their absorbance, the molar attenuation coefficients (ε) were calculated and expressed in Table 1.3.1.

Sample	**Molar attenuation coefficient (ε)**
SAS-1A SUP	0,041
SAS-1A F	0,043
SAS-2A SUP	0,053
SAS-2A F	0,047
SAS-1B M	0,045

Section 2 – Nuclear magnetic resonance spectroscopy experiments

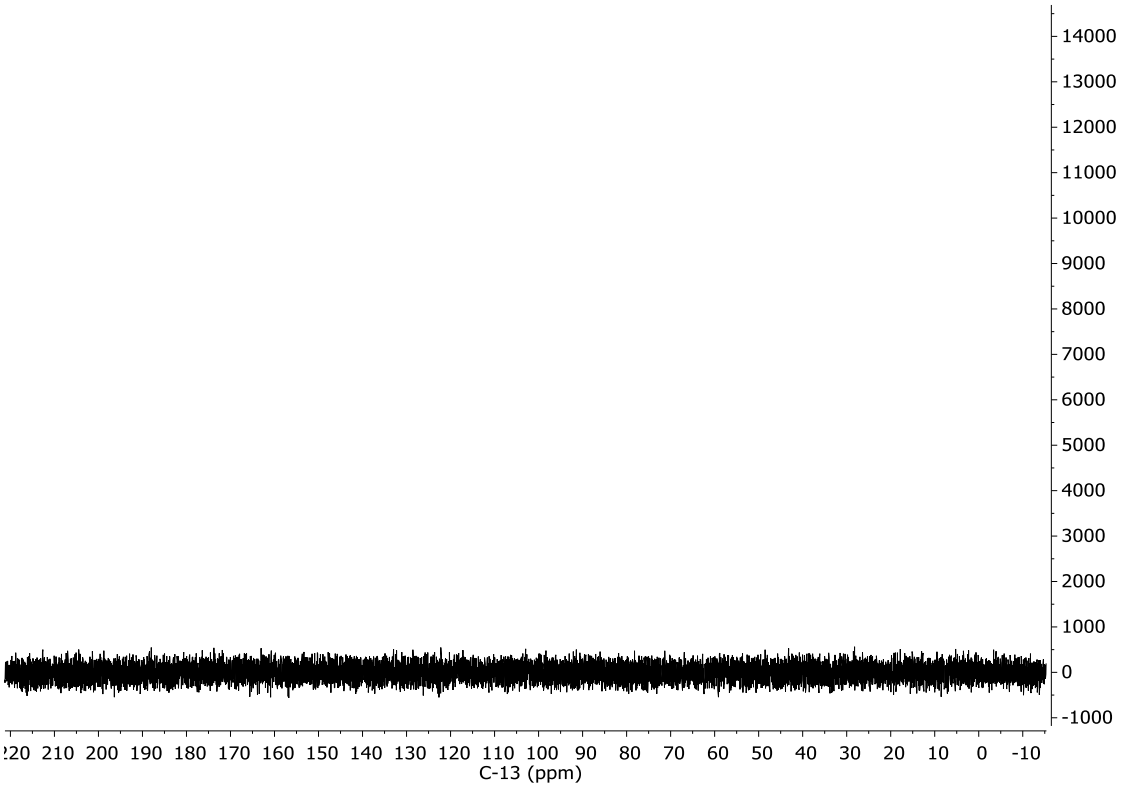

Figure 2.1 - ^{13}C liquid-state NMR spectrum of FA SAS-1A SUP (D_2O as solvent).

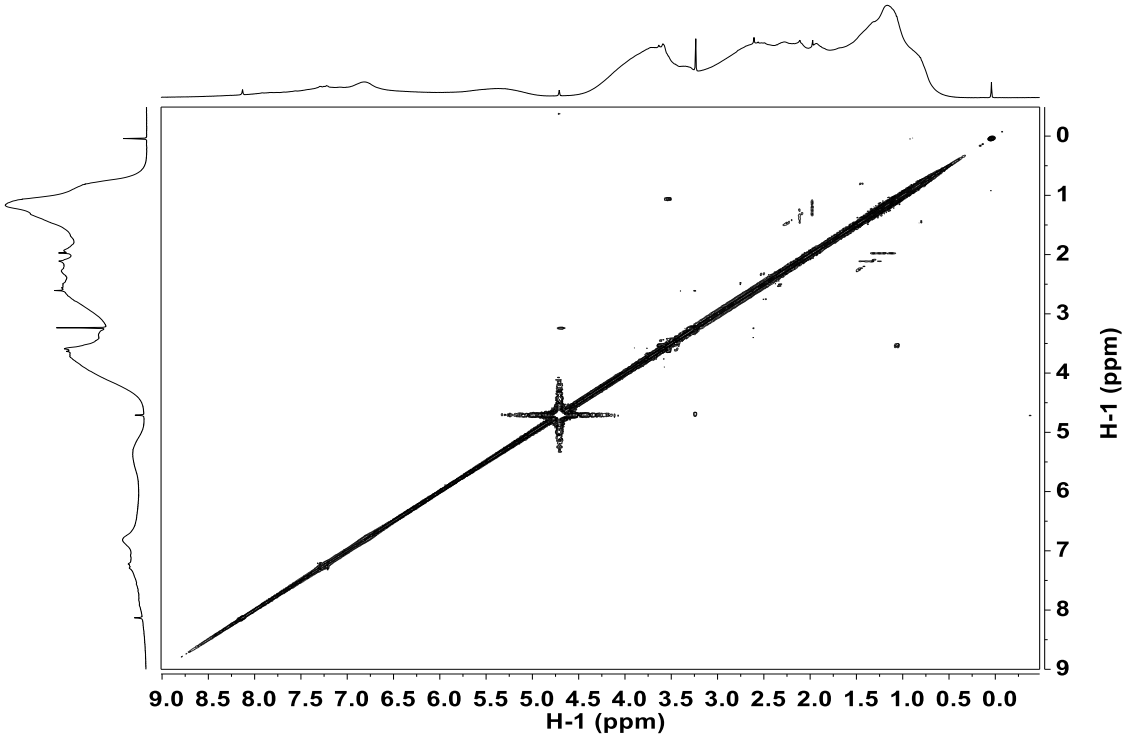

Figure 2.2 – ^{1}H-^{1}H COSY liquid-state NMR spectrum of FA SAS-1A SUP (D_2O as solvent).

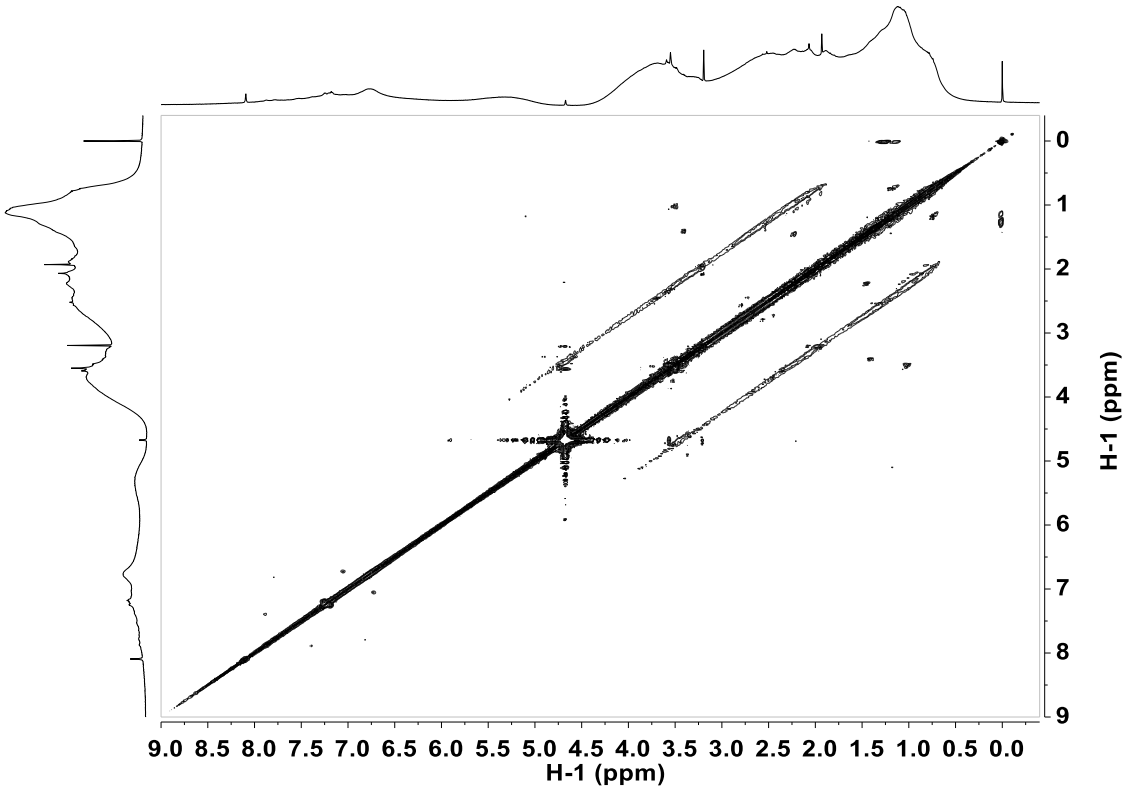

Figure 2.3 – ^{1}H-^{1}H COSY liquid-state NMR spectrum of FA SAS-1A F (D_2O as solvent).

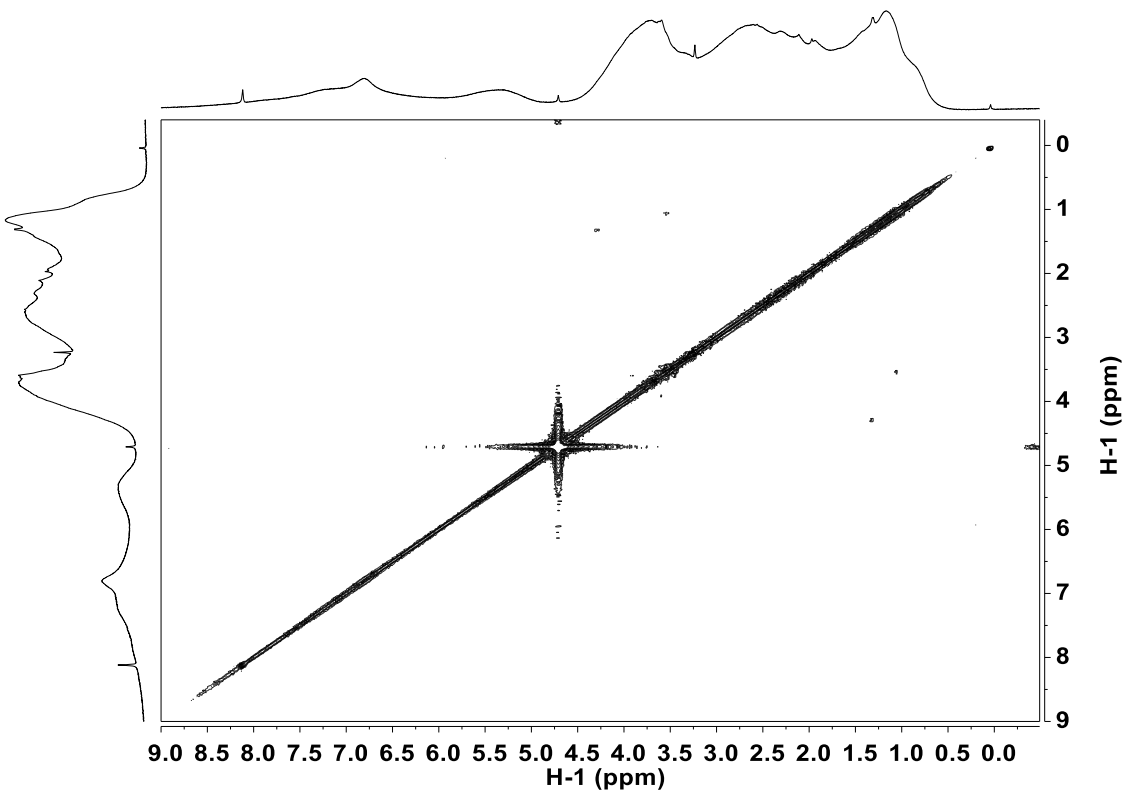

Figure 2.4 – ^{1}H-^{1}H COSY liquid-state NMR spectrum of FA SAS-2A SUP (D_2O as solvent).